Hywind Tampen Floating Offshore Wind Farm

Soundscape Analysis and Sound Source Characterisation of Operational Floating Turbines

JASCO Applied Sciences (UK) Ltd

18 September 2025

Submitted to:

Kari Mette Murvoll Jürgen Weissenberger Equinor Energy AS

Authors:

Samuel J. Welch Robin D. J. Burns C. Eric Lumsden Michael A. Wood Katie A. Kowarski S. Bruce Martin Colin P. Christie Allison L. Richardson Emily E. Maxner Colleen C. Wilson Briand J. Gaudet Eloise Callaghan

P001802-001 Document 04044 Version 2.0



Suggested citation:

Welch, S.J., R.D.J. Burns, C.E. Lumsden, M.A. Wood, K.A. Kowarski, S.B. Martin, C.P. Christie, A.L. Richardson, E.E. Maxner, C.C. Wilson, B.J. Gaudet and E. Callaghan. 2025. *Hywind Tampen Floating Offshore Wind Farm: Soundscape Analysis and Sound Source Characterisation of Operational Floating Turbines*. Document 04044, Version 2.0. Technical report by JASCO Applied Sciences for Equinor Energy AS.

The results presented herein are relevant within the specific context described in this report. They could be misinterpreted if not considered in the light of all the information contained in this report. Accordingly, if information from this report is used in documents released to the public or to regulatory bodies, such documents must clearly cite the original report, which shall be made readily available to the recipients in integral and unedited form.

Contents

Executive Summary	1
1. Introduction	3
2. Methods	5
2.1. Acoustic Data Acquisition	5
2.1.1. Deployment	5
2.1.2. Recording Parameters	7
2.1.3. Retrieval	9
2.2. Acoustic Data Management	9
3. Results	10
3.1. Total Sound Levels	10
3.2. Acoustic Analysis of Omnidirectional Noise	16
3.2.1. Rotor Speed Related Aerodynamic and Mechanical Tones	17
3.2.2. Tones Not Related to Rotor RPM	20
3.2.3. Combined Overall Omnidirectional Tonal Noise	21
3.2.4. Mooring System Noise	22
3.2.5. Cod Vocalisation Detection	25
3.2.6. Other Anthropogenic Noise	26
3.3. Comparison of Sound Levels with Ambient Conditions	30
3.3.1. Correlation With Wind Speed	30
3.3.2. Correlation With Rotor RPM	35
3.3.3. Comparison With Distance to Closest Turbine	40
3.4. Directional Analysis of Recorded Noise	42
3.4.1. Methodology and Presentation of Directional Data	42
3.4.2. Directional Acoustic Analysis	43
3.4.3. Received Levels from a Single Turbine	45
3.4.4. Turbine Sound Field Directionality	48
3.5. Marine Strategy Framework Directive Descriptor 11	49
3.6. Marine Mammal Exposure Levels	50
4. Calculation of Monopole Source Levels	53
4.1. Modelled Environmental Parameters	53
4.2. Sound Propagation Modelling	54
4.2.1. Source Considerations	55
4.2.2. Wind Speed Considerations	55
4.3. Calculated Propagation Loss	55
4.4. Backpropagated Source Levels	56
4.5. Simplified Modelled Sound Fields	58
4.5.1. Sound Pressure Level	59
4.5.2. Weighted Sound Exposure Level	60
4.5.3. Comparison with Ambient Noise	61
4.5.4. Comparison with Recorded Data	64

5. Discussion and Conclusion	67
5.1. Comparison With Hywind Scotland	69
Literature Cited	71
Appendix A. Acoustic Data Analysis Methods	A-1
Appendix B. Ambient Noise Analysis Results	B-1
Appendix C. Directional Analysis	C-1
Appendix D. Marine Mammal Impact Criteria	D-1
Appendix E. Marine Mammal Detections	E-1
Appendix F. Broadband Received Levels	F-1
Appendix G. Propagation Loss Modelling Results	G-1
Appendix H. Backpropagated Source Levels	H-1
Appendix I. Hydrophone Technical Specifications	I-1

Figures

Figure 1. Location of the Hywind Tampen offshore floating wind farm.	3
Figure 2. Concept image of a Hywind Tampen floating wind turbine (mooring system not shown	•
Figure 3. Baseplate moorings connected to the ROV: four-hydrophone directional array (left) as single omnidirectional hydrophone system (right)	nd
Figure 4. ROV camera photograph used to confirm orientation of the tetrahedral array	6
Figure 5. Map showing the AMAR deployment locations as numbered in Table 1	7
Figure 6. Photo of the tetrahedral hydrophone array set-up on a baseplate	8
Figure 7. GRAS 42 AC Pistonphone, sleeve coupler and hydrophone	9
Figure 8. Long term acoustic summary for the AMAR at Station 1 (channel D)	. 11
Figure 9. Long term acoustic summary for the AMAR at Station 2 (channel D)	
Figure 10. Long term acoustic summary for the AMAR at Station 3	
Figure 11. Long term acoustic summary for the AMAR at Station 4	
Figure 12. Power spectral density levels (bottom) and decidecade band box-and-whisker plots (top) for the AMAR at Station 1 (channel D).	. 14
Figure 13. Power spectral density levels (bottom) and decidecade band box-and-whisker plots (top) for the AMAR at Station 2 (channel D)	
Figure 14. Power spectral density levels (bottom) and decidecade band box-and-whisker plots (top) for the AMAR at Station 3.	
Figure 15. Power spectral density levels (bottom) and decidecade band box-and-whisker plots (top) for the AMAR at Station 4.	
Figure 16. Waveform and spectrogram from Station 3 showing the dominant 25 and 75 Hz tone	
Figure 17. Recording from Station 1 showing generator fundamental tone at approximately 25 with related rotational tone at approximately 75 Hz and evidence of extremely low frequence energy.	У
Figure 18. Spectrogram from Station 3 showing unstable rotational generator related tones from multiple WTGs at low rotation rates with weak, intermittent generator fundamental at 25 Hz.	
Figure 19. Spectrogram from Station 3 in 20 kn wind speed, 10.5 RPM, stability in the seconda generator tones at 75 Hz and elevated levels of the generator fundamental tone at 25.2 Hz.	-
Figure 20. Spectrogram from Station 3 showing 15 Hz fundamental tone with ascending related harmonics and coincident overlap at 75 Hz with the generator secondary tone	
Figure 21. Higher frequency tonals visible in 25 kn wind speed at Station 3	. 21
Figure 22. Relative intensity and spectral contribution of the Tampen wind farm to the soundscape (Station 1)	. 22
Figure 23. Spectrogram showing suspected mooring transients (vertical lines) from Station 1	. 23
Figure 24. Log scale spectrogram, at 40 kn wind speed, showing possible Tampen mooring transients in the presence of two echolocating sperm whales.	. 23
Figure 25. Directogram of suspected mooring noise – showing the origin of the impulses from outside the wind farm.	. 24
Figure 26. Empirical cumulative distribution functions for the one-minute kurtosis of unweighted signals at Stations 1 to 4	
Figure 27. Spectrogram and waveform showing assumed seismic survey noise at Station 1	. 27
Figure 28. Directional processing at Station 1 reveals two separate seismic surveys to the Nort and to the South.	
Figure 29. Directional processing at Station 2 reveals at least five distinct seismic sources	. 28
Figure 30. Spectrogram and waveform of suspected vessel on dynamic positioning.	. 28

Figure 31. Annotated spectrogram showing onset of high-power dynamic positioning (DP) 29
Figure 32. Spectrogram and waveform showing vessel noise at Station 1
Figure 33. Correlation between average wind speed and rotor RPM across all turbines30
Figure 34. Station 1 – Comparison of wind speed with levels in selected decidecade bands 32
Figure 35. Station 2 – Comparison of wind speed with levels in selected decidecade bands 33
Figure 36. Station 3 – Comparison of wind speed with levels in selected decidecade bands 34
Figure 37. Station 4 – Comparison of wind speed with levels in selected decidecade bands 35
Figure 38. Relationship between identified rotor related tones and rotor speed, with decidecade
(ddec) bandwidths of interest highlighted
Figure 39. Station 1 – Comparison of rotor RPM with levels in selected decidecade bands 37
Figure 40. Station 2 – Comparison of rotor RPM with levels in selected decidecade bands 38
Figure 41. Station 3 – Comparison of rotor RPM with levels in selected decidecade bands 39
Figure 42. Station 4 – Comparison of rotor RPM with levels in selected decidecade bands 40
Figure 43. Comparison of broadband received levels at each Station with distance from the
nearest wind turbine for wind speed bins from 5 for 40 kn
Figure 44. Relative positions of closest turbines to Station 1 and colour wheel orientation relative to North for directogram plots
Figure 45. Overlapping generator and rotor tonals from HY05, HY06 and HY07, all at 10.5 RPM44
Figure 46. Directogram showing different noise outputs from three WTGs, and inconsistency of
rotor rate with wind speed
Figure 47. Isolation of Very Low Frequency Noise and primary tonal sources from HY0645
Figure 48. Received SPL at Station 1 in decade bands in the direction of HY06 for various wind speed bins
Figure 49. Median power spectral densities at Station 1 from the direction of HY06 for various
wind speed bins
Figure 50. Difference in received levels between beam pointed towards HY06 and beam pointed towards HY0749
Figure 51. Distribution of one-minute decidecade SPL at Stations 1, to 4 at 63 and 125 Hz 50
Figure 52. Auditory frequency weighted daily cumulative sound exposure levels at Station 1 51
Figure 53. Auditory frequency weighted daily cumulative sound exposure levels at Station 3 51
Figure 54. Auditory frequency weighted daily cumulative sound exposure levels at Station 4 52
Figure 55. Monthly sound speed profiles at the Tampen site derived from salinity and
temperature profiles from CMEMS
Figure 56. Propagation loss in decidecade bands between HY06 and Station 1 for 5 knots wind speed
Figure 57. Propagation loss in decidecade bands between HY06 and Station 1 for 40 knots wind speed
Figure 58. Median backpropagated source levels for a single turbine based on a point source assumption using propagation loss curves averaged over the modelled source depths 57
Figure 59. 95 th percentile backpropagated source levels for a single turbine based on a point
source assumption using propagation loss curves averaged over the modelled source depths.
Figure 60. Modelled sound pressure level map for the Hywind Tampen wind farm assuming 50th percentile (median) source levels at a wind speed of 10 kn
Figure 61. Modelled sound pressure level map for the Hywind Tampen wind farm assuming 95th
percentile source levels at a wind speed of 20 kn
Figure 62. Comparison of recorded spectra at all four recording stations and a minimum, smoothed spectrum approximating the ambient noise levels in the wider Tampen area 62

Figure 63. Map showing the difference between modelled sound pressure level from the Hywind turbines and median ambient sound levels for 50th percentile (median) source levels at a wind speed of 10 kn
Figure 64. Map showing the difference between modelled sound pressure level from the Hywind turbines and median ambient sound levels for 95th percentile source levels at a wind speed of 20 kn
Figure 65. Median omnidirectional received levels in decidecade bands up to 1 kHz at all recorder stations for 10 kn wind speed
Figure 66. Median omnidirectional received levels in decidecade bands up to 1 kHz at all recorder stations for 20 kn wind speed
Figure 67. 25 Hz band levels recorded and modelled at each AMAR location
Figure 68. 80 Hz band levels recorded and modelled at each AMAR location
Figure A-1. Decidecade frequency bands (vertical lines) shown on a linear frequency scale and a logarithmic scale
Figure A-2. Sound pressure spectral density levels and the corresponding decidecade band sound pressure levels of example ambient sound shown on a logarithmic frequency scale. A-3
Figure B-1. Acoustic summary of the recorder at Station 1 for channels A (upper left), B (upper right), C (lower left), and D (lower right)B-1
Figure B-2. Decidecade band SPL and power spectral densities with percentiles for the recorder at Station 1 for channels A (upper left), B (upper right), C (lower left), and D (lower right)B-2
Figure B-1. Acoustic summary of the recorder at Station 2 for channels A (upper left), B (upper right), C (lower left), and D (lower right)B-3
Figure B-2. Decidecade band SPL and power spectral densities with percentiles for the recorder at Station 1 for channels A (upper left), B (upper right), C (lower left), and D (lower right)B-4
Figure D-1. Auditory weighting functions for the functional marine mammal hearing groups as recommended by Southall et al. (2019)
Figure E-1. Flowchart of the automated click detector/classifier processE-1
Figure E-2. Flowchart of the click train automated detector/classifier processE-2
Figure E-3. Illustration of the contour detection process
Figure E-4. Spectrogram showing sperm whale clicks in a recording from Station 1E-3
Figure E-5. Spectrogram showing killer whale echolocation clicks and whistles in a recording from Station 4E-3
Figure E-6. Spectrogram showing simultaneous sperm whale clicks, killer whale clicks, and killer whale whistles in a recording from Station 4E-4
Figure G-1. Propagation loss in decidecade bands between HY06 and Station 1 for 0 knots wind speed
Figure G-2. Propagation loss in decidecade bands between HY06 and Station 1 for 5 knots wind speed
Figure G-3. Propagation loss in decidecade bands between HY06 and Station 1 for 10 knots wind speed
Figure G-4. Propagation loss in decidecade bands between HY06 and Station 1 for 15 knots wind speed
Figure G-5. Propagation loss in decidecade bands between HY06 and Station 1 for 20 knots wind speed
Figure G-6. Propagation loss in decidecade bands between HY06 and Station 1 for 25 knots wind speed
Figure G-7. Propagation loss in decidecade bands between HY06 and Station 1 for 30 knots wind speed
~~~~··································

Figure G-8. Propagation loss in decidecade bands between HY06 and Station 1 for 35 knots wind speed
Figure G-9. Propagation loss in decidecade bands between HY06 and Station 1 for 40 knots wind speed
Tables
Table 1. AMAR deployment and retrieval dates and locations
Table 2. Distances of each of the wind turbine generators (WTGs) from the four Autonomous Multichannel Acoustic Recorders (AMARs) deployed
Table 3. Relative distances between the four hydrophones (as labelled in Figure 6) mounted on the directional monitoring systems deployed at Stations 1 and 2
Table 4. Median hourly broadband SPL in each month of deployment at Station 2
Table 5. Wind speed bins for analysis in knots and metres per second
Table 6. Distances and bearings of each of the wind turbine generators (WTGs) from the two directional Autonomous Multichannel Acoustic Recorders (AMARs) deployed42
Table 7. Geoacoustic model for Hywind Tampen54
Table 8. Backpropagated broadband source levels for the modelled wind speeds and percentiles
Table 9. Predicted received weighted 24-hour SEL at Stations 1 and 3 for the modelled wind speeds and percentiles
Table 10. Modelled maximum distances to TTS threshold levels (Southall et al. 2019) for the modelled wind speeds and percentiles61
Table 11. Differences between backpropagated broadband source levels at Hywind Tampen and Hywind Scotland for various wind speeds and percentiles70
Table A-1. Decade-band frequencies (Hz).
Table A-2. Decidecade-band frequencies (Hz)

# **Executive Summary**

JASCO Applied Sciences undertook a sound source characterisation study of the Hywind Tampen floating offshore wind farm, approximately 140 km northwest of Bergen, Norway. Four recording instruments were deployed from the DOF *Skandi Iceman* to the seabed by remotely operated vehicle in February 2024 at various positions both within and around the wind farm site. Two instruments were set up in a single-hydrophone omnidirectional configuration and two with arrays of four hydrophones to provide directional noise discrimination. Three of the four recorders (one directional system and the two omnidirectional systems) were retrieved in June 2024. The remaining directional recording system was configured with a 12-month recording schedule and was retrieved in March 2025. Recording was conducted at a 64 kHz sample rate with 24-bit resolution, and the total volume of data collected was approximately 13.3 TB.

Analysis of the recorded data was undertaken to determine the characteristics of the sound produced by the turbines at Hywind Tampen and compare this to similar sound source characterisation study of the Hywind Scotland floating system. The dominant sound emissions from the Hywind Tampen turbines are narrowband tones, principally below 200 Hz, with two notable tones at around 25 and 75 Hz being the primary contributors to the recorded sound spectra. The sources of these tones are directly related to the rotational rate of the rotor and the number of magnetic pole pairs in the generator, one directly and the other by a factor of three. Consequently, the actual frequencies generated by the rotating components of each turbine depend on the rotor RPM at any given time, where the strong tones at around 25 and 75 Hz are the frequency limits of the rotor related tones associated with the system maximum RPM. Other tones which were variously stable and unstable, continuous and intermittent were found to contribute to the spectra to a lesser extent.

Positive correlations were determined between sound levels in the frequency bands containing the 25 and 75 Hz tones and wind speed, the strength of this correlation reducing with distance from the turbines. The correlation analysis also displayed an approximate plateau of the sound levels in these bands at wind speeds above 20 kn (10.3 m/s). Similar positive correlation was observed between levels in these bands and rotor RPM, with the relationship reflecting the increase in frequency of the fundamental and triplet tones with increasing rotor RPM. Other low-level tones were also observable in the spectra, though at considerably lower intensity than those from the generator. Some of these tones were stable and intermittent, characteristic of pumps or motors under irregular operation, while others were continuous and unstable, possibly indicative of blade control systems responding to fluctuations in wind speed.

The acoustic data were manually analysed for impulses and transients caused by tension on the mooring system, which were a frequent component of the Hywind Scotland recordings. Only a handful of possible mooring transients were identified at higher wind speeds and further directional assessment found these to originate to the East of the Tampen site and they were subsequently dismissed as mooring noise. This confirmed a fundamental acoustic difference in noise signature between Hywind Scotland and Hywind Tampen, the reasons for which may be related to differences in the buoyancy of the spar structure, the mooring system, or both, rather than any difference in swell height or other environmental factors. The exact mechanism generating the transient noises at Hywind Scotland is unknown, but this mechanism appears to no longer exist in the new substructure and mooring system utilised at Hywind Tampen. A quantitative analysis of the impulsiveness of the data from all four recorders was undertaken by assessing empirical distribution function of the one-minute kurtosis, which also confirmed that kurtosis at all recorder locations was very low, indicating a nonimpulsive soundscape. Based on this, daily cumulative SELs recorded at the three shorter-term recording stations, distances ranging from 717 m to 9.35 km to the nearest turbine, were compared to non-impulsive impact criteria from Southall et al. (2019). All daily cumulative SELs recorded during this study, at these three stations, were found to lie below the thresholds for both temporary and

permanent hearing threshold shifts (i.e., hearing loss) for non-impulsive sounds for all functional hearing groups.

One recorder with directional capabilities was positioned within the wind farm in such a position to isolate the most southeasterly turbine in the array (HY06). Received levels from the direction of HY06 collected during relatively stable periods of wind were analysed for bins in 5 kn (2.6 m/s) increments from 5 to 40 kn (2.6 to 20.6 m/s) and then backpropagated to obtain statistical decidecade source levels for a single turbine operating under multiple wind speed conditions. Received levels were compared to levels from the direction of a second turbine (HY07) which, once corrected for propagation path differences, displayed no overall difference at wind speeds over 30 kn indicating no or little directionality of the sound footprint. Median broadband source levels ranged between 156.5–163.8 dB re 1  $\mu$ Pa²m², while 95th percentile broadband source levels ranged between 159.1–168.7 dB re 1  $\mu$ Pa²m². Source levels were noticeably lower for wind speeds below 20 kn (10.3 m/s), corresponding to the turbine operating at less than its maximum rotor RPM. Using the backpropagated source levels, a simple point source model was used to model the footprint of all eleven wind turbines. The largest modelled distance was 60 m for very high-frequency cetaceans (20 kn, 95th percentile) assuming an animal remains within this radius for a full 24-hour period at the depth of the greatest sound level.

The recorded spectra from the Tampen WTGs displayed very similar tonal features to the turbines at Hywind Scotland. Estimated source levels for Hywind Tampen are somewhat lower than those determined for Hywind Scotland, and this may be a consequence of the concrete Tampen substructure being less able to transfer vibrational energy combined with the lack of mooring transients elevating the overall noise signature.

## 1. Introduction

JASCO Applied Sciences (JASCO) was contracted by Equinor AS (Equinor) to undertake a sound source characterisation (SSC) study for floating wind turbine generators (WTG) at the Hywind Tampen Offshore Wind Farm (OWF), as well as soundscape analysis for the wider area. Hywind Tampen is located in the Norwegian Sea, approximately 140 km northwest of Bergen, Norway (Figure 1) and is currently the world's largest floating OWF comprising 11 horizontal axis, permanent magnet direct drive WTGs each with an 8.6 MW capacity, in a spar buoy/pillar structure. The spar substructure for each WTG is made of concrete with a maximum diameter of 18 m and a total length of 107.5 m, approximately 90 m of which is submerged. The WTGs are moored in a "honeycomb" formation via flexible lines to shared anchors with each individual turbine connected to three separate anchors.

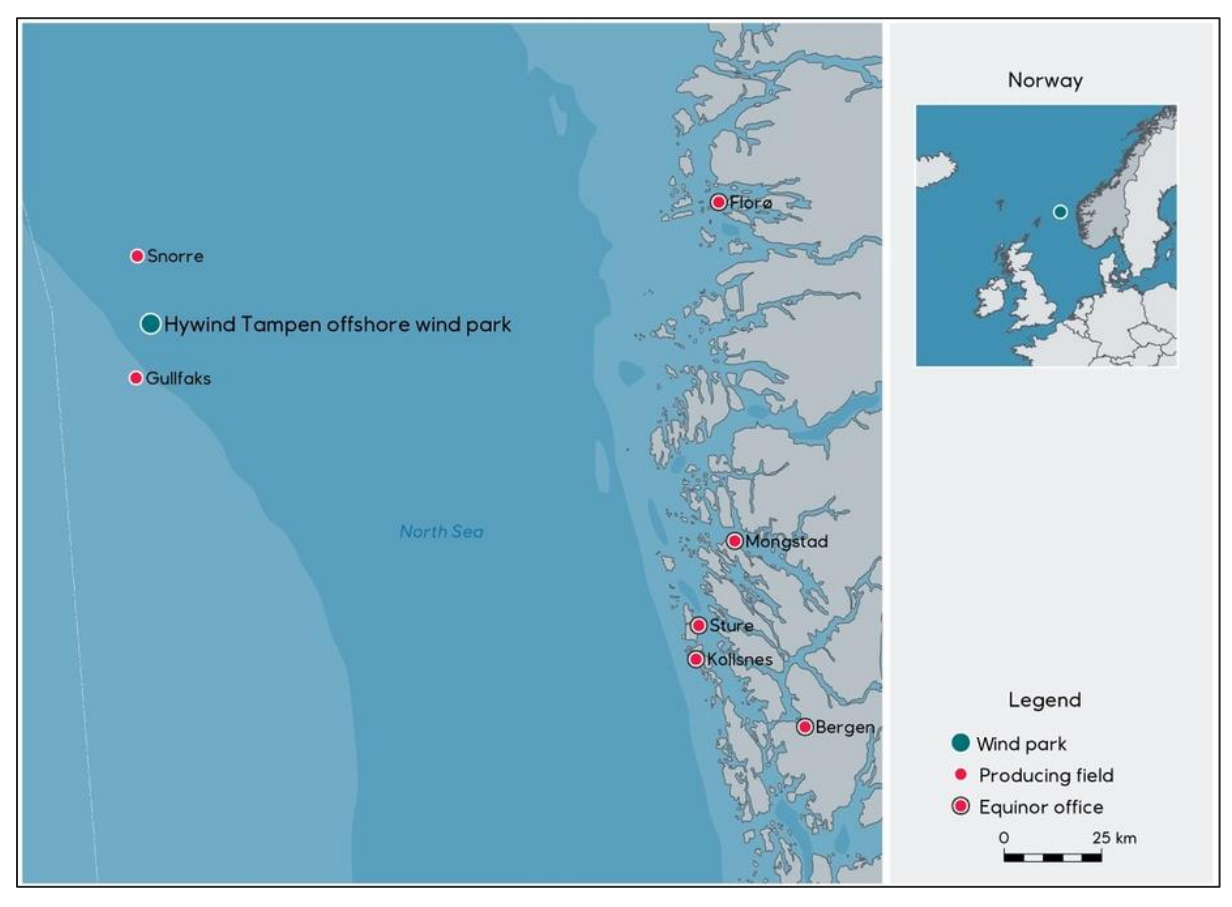


Figure 1. Location of the Hywind Tampen offshore floating wind farm.

JASCO has previously conducted similar SSC studies on both the Hywind DEMO system off the coast of Stavanger, Norway, (Martin et al. 2011) and the Hywind Scotland floating OWF off the coast of Peterhead, Scotland (Burns et al. 2022). In both studies, a number of impulsive components of the recorded sound signature were attributed to the mooring system. The principal aim of this study was to record an operational noise profile for a single Hywind Tampen system such that this data can be backpropagated to extract a source spectrum. Secondary aims were to determine whether the sounds attributed to the mooring system from the previous studies were present in this new design, and to assess the recorded acoustic data for indication of the presence of cod vocalisations.



Figure 2. Concept image of a Hywind Tampen floating wind turbine (mooring system not shown).

Four JASCO recording instruments were deployed on the seabed in February 2024 for this SSC study at various positions provided by Equinor, both within and around the wind farm site. Two instruments were set up in a single-hydrophone omnidirectional configuration and two were set up with arrays of four hydrophones to provide directional discrimination.

Three out of four recorders (one directional system and the two omnidirectional systems) were retrieved in June 2024. The remaining directional recording system was configured to record for 12 months and was retrieved in March 2025.

# 2. Methods

## 2.1. Acoustic Data Acquisition

Underwater sound was recorded with four JASCO Autonomous Multichannel Acoustic Recorders (AMARs) mounted on simple gravity baseplate moorings. Two moorings featured a single AMAR and external battery housing with a four-hydrophone directional array on a static frame (Figure 3, left), while the remaining two moorings comprised a single AMAR, external battery housing and a single omnidirectional hydrophone (Figure 3, right).

# 2.1.1. Deployment

All four moorings were deployed from the DOF *Skandi Iceman* using a Triton XLS remotely operated vehicle (ROV). The ROV grabber arm was attached to the lifting ring at the top of each mooring while the manipulator arm was used to grip further down the frame for stability (Figure 3). The ROV and baseplate were then deployed over the side of the vessel and the ROV descended to deploy each baseplate directly on the seabed. Once on the seabed, the recorder location and orientation of the tetrahedral array were documented using on the ROV compass, cameras and positioning system (Figure 4). The orientation of the directional systems is important to enable bearing alignment and accuracy. Therefore, in addition to the ROV orientation data, the vessel engine and cavitation noise from the *Skandi Iceman* was post-processed and aligned to known positions from its AIS track as it completed a circle around the deployed mooring position.





Figure 3. Baseplate moorings connected to the ROV: four-hydrophone directional array (left) and single omnidirectional hydrophone system (right).

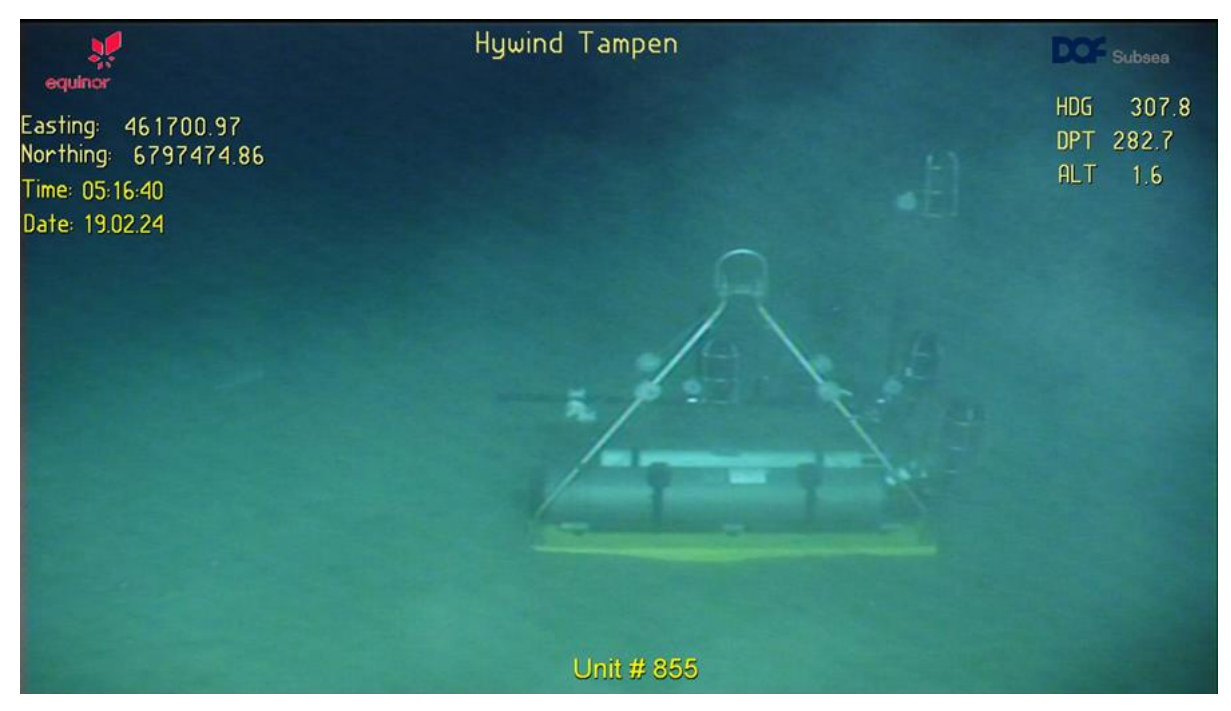


Figure 4. ROV camera photograph used to confirm orientation of the tetrahedral array.

Four deployment locations were provided by Equinor and were chosen to capture different components of the sound field as well as the sound levels at various distances from the wind farm. The deployment locations are presented in Table 1 and Figure 5, and distances from the recorders to the individual turbines are presented in Table 2. One of the directional systems was placed within the wind farm array such that a single wind turbine could be isolated by directional post-processing. The other directional system (approximately 4 km from the wind farm array) and the two omnidirectional systems (approximately 2 km and 10 km from the wind farm array) were selected to provide data relating to the aggregate noise from the whole wind farm. The farthest recorder to the southeast additionally provides an element of a control site to give an indication of ambient noise.

Table 1. AMAR deployment and retrieval dates and locations.

Station	Recorder number	Deployment UTC	Retrieval ¹	Recording duration	Latitude (°N)	Longitude (°E)	Water depth (m)	Directional?
1	855	19 Feb 2024 04:14	07 Jun 2024	3 months	61.30728	2.28337	284	Yes
2	865	19 Feb 2024 05:41	08 Mar 2025	12 months	61.30068	2.35747	288	Yes
3	860	19 Feb 2024 07:03	07 Jun 2024	3 months	61.31882	2.31368	291	No
4	863	19 Feb 2024 02:47	07 Jun 2024	3 months	61.23882	2.40395	273	No

Recorders were retrieved by vessel crew without JASCO field team present; exact retrieval times were not documented.

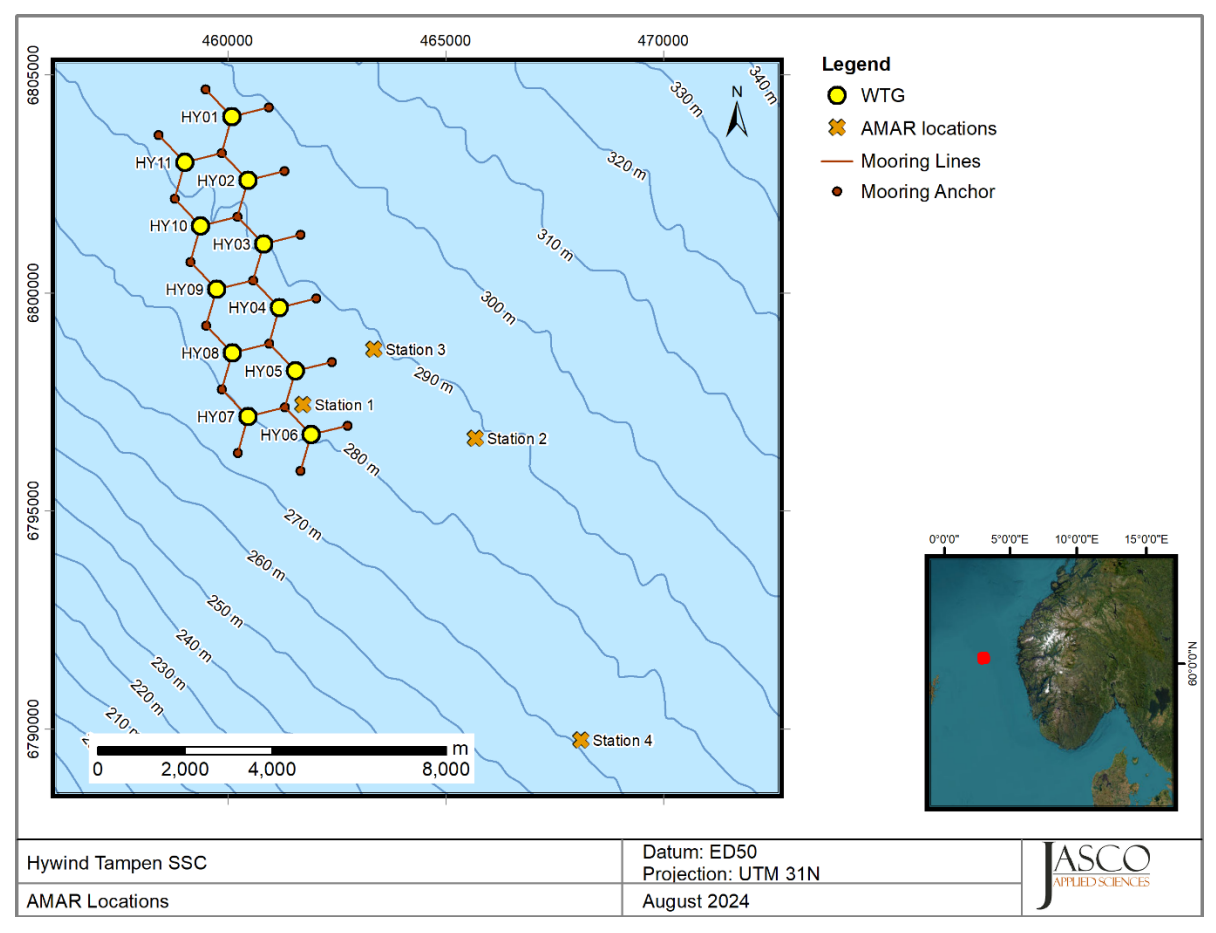


Figure 5. Map showing the AMAR deployment locations as numbered in Table 1.

Table 2. Distances of each of the wind turbine generators (WTGs) from the four Autonomous Multichannel Acoustic Recorders (AMARs) deployed.

Location	Distance (m)								
Location	Station 1	Station 2	Station 3	Station 4					
HY01	6803	9258	6255	16392					
HY02	5299	7897	4841	14947					
HY03	3795	6598	3503	13514					
HY04	2291	5407	2373	12099					
HY05	788	4412	1874	10708					
HY06	717	3770	2433	9351					
HY07	1281	5239	3275	10651					
HY08	2002	5912	3253	11954					
HY09	3302	6855	3868	13300					
HY10	4724	7972	4885	14677					
HY11	6185	9200	6107	16076					

# 2.1.2. Recording Parameters

All AMARs were fitted with M36-V35-900 omnidirectional hydrophones from GeoSpectrum Technologies Inc. (GTI). Each hydrophone was placed into a foam insert to mitigate against any flow noise from bottom currents and enclosed by a metal cage for protection. For the directional systems, the four hydrophones were fixed in a tetrahedral arrangement to allow determination of the time of arrivals from different directions (Figure 6). The relative distance of each hydrophone on the support structure was calculated to support post-processing directional calculations (Table 3).

Table 3. Relative distances between the four hydrophones (as labelled in Figure 6) mounted on the directional monitoring systems deployed at Stations 1 and 2.

Hydrophone	Length	ı (mm)
separation	Station 1	Station 2
A-B	770	775
A-D	775	770
B-D	667	670
B-C	480	497
C-A	595	595
C-D	470	482

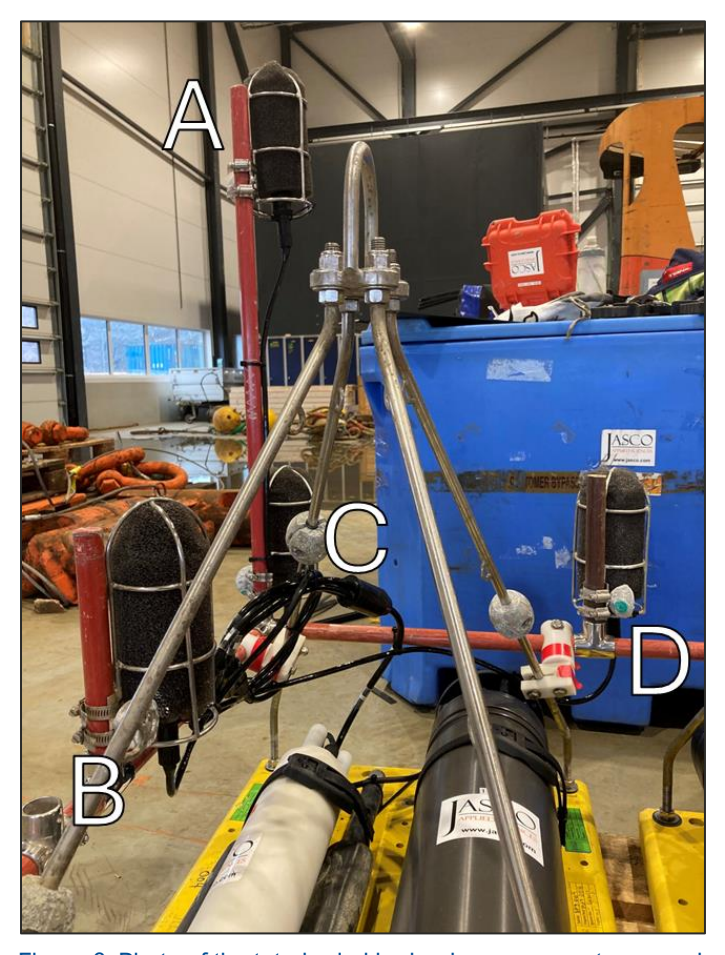


Figure 6. Photo of the tetrahedral hydrophone array set-up on a baseplate with fitted AMAR G4 (white tube) and battery pack (grey tube). Hydrophones are labelled as in Table 3.

The AMARs were configured to record at a sample rate of 64,000 Hz to return a recorded bandwidth of approximately 10 to 32,000 Hz. The recording channels had 24-bit resolution with a spectral noise floor of 20 dB re 1  $\mu$ Pa²/Hz and a nominal ceiling of 165 dB re 1  $\mu$ Pa. Acquired acoustic data from each channel were stored on internal solid-state flash memory. The omnidirectional systems and the directional system deployed for 3 months (Station 1) all recorded continuously with no duty cycle. The directional system deployed for 12 months (Station 2) was set to record with a duty cycle of 900 s on followed by 2700 s of sleep to preserve battery life and memory.

The directional recorder at Station 1 recorded for the targeted duration of 100 days until 29 May 2024, while the directional recorder at Station 2 and both omnidirectional recorders at Stations 3 and 4 recorded continuously for the full duration of their respective deployments: 384 days for Station 2 and 109 days for Stations 3 and 4. The total volume of data collected from all recording stations was approximately 13.3 TB.

Each AMAR was calibrated before deployment and after retrieval with a pistonphone type 42AC precision sound source (G.R.A.S. Sound & Vibration A/S; Figure 7). The pistonphone calibrator produces a constant tone at 250 Hz at a fixed distance from the hydrophone sensor in an airtight space with known volume. The recorded level of the reference tone on the AMAR yields the system gain for the AMAR and hydrophone. To determine absolute sound pressure levels, this gain is applied during data analysis. Typical calibration variance using this method is less than 0.7 dB absolute pressure.



Figure 7. GRAS 42 AC Pistonphone, sleeve coupler and hydrophone

#### 2.1.3. Retrieval

The retrieval process was carried out by ROV deployed from the DOF *Skandi Iceman*, professionally conducted by the vessel crew and ROV operators without the need for JASCO field staff presence. JASCO provided guidance on how to retrieve and handle the moorings safely, and once the equipment was ashore, a JASCO field engineer was sent to conduct the post-deployment calibration, download the data and disassemble the moorings. The three recorders at Stations 1, 3, and 4 were retrieved on 07 June 2024, while the recorder at Station 2 was retrieved on 08 March 2025.

# 2.2. Acoustic Data Management

The data acquisition process on each acoustic instrument continued uninterrupted throughout the three-month planned recording process and the anticipated volume and duration of data was captured. However, after retrieval of the instruments, an unrelated, external technical oversight matter arose which raised the requirement to redact a period of data from the total dataset. This period is therefore unavailable for analysis in this report. The redacted period was from 25 April to midnight on 22 May 2024, a duration of 28 full days. Within this redacted period, a short window from 08 May 2024 23:20 to 09 May 2024 02:20 was extracted for investigation based on meteorological conditions at the time but was ultimately rejected from further analysis due to contamination (see Section 3.2.6). The redacted window is evident in several of the following analysis results, typically as a blacked-out temporal period with the brief window of extracted data visible in the middle.

# 3. Results

The acoustic data analysis methods for basic metrics are contained in Appendix A. Acoustic terminology and analysis are in accordance with ISO standard 18405 (ISO 2017a).

#### 3.1. Total Sound Levels

This section presents the total omnidirectional sound levels from each of the stations to verify the quality of the recordings and as a summary of the received sound levels. Results are presented in four ways:

- 1. **Band-level plots**: These strip charts show the average hourly received sound levels as a function of time within a given frequency band. Sound levels are shown for the full recorded frequency range (10–32000 Hz) and the decade bands for 8.9–89.1, 89–891, 891–8913, and 8913–32000 Hz. The 8.9–89.1 Hz band is associated with fin, sei, and blue whales, large shipping vessels, seismic surveys, and flow and mooring noise. The 89–891 Hz band is generally associated with environmental noise from wind and wave action, but can also include sounds from minke, right, and humpback whales, nearby vessels, and seismic surveys. Sounds above 1000 Hz include humpback whale sounds, toothed whale and dolphin whistles and clicks, wind and wave noise, nearby vessels, seismic surveys, and sonars.
- 2. **Long-term Spectral Averages (LTSAs)**: These plots use colour to show power spectral density levels as a function of time (*x*-axis) and frequency (*y*-axis). The LTSAs are useful summaries of the temporal and frequency variability in the data.
- 3. **Decidecade band box-and-whisker plots**: These plots show the average and extreme sound levels in each decidecade band. The whiskers represent the maximum and minimum sound levels in each band, while the box represents the interquartile range between the 25th percentile ( $L_{25}$ ) and 75th percentile ( $L_{75}$ ). The 50th percentile (median,  $L_{50}$ ) and mean sound levels are also represented on the plots as horizontal lines.
- 4. Power Spectral Densities (PSDs): These plots show lines corresponding to various statistical sound levels in 1 Hz frequency bins. These levels can be directly compared to the Wenz curves. Shading on these plots represent the spectral probability density to assess whether the distribution is multi-modal. Spectral probability density presents the empirical probability density of levels in each 1 Hz frequency bin (Merchant et al. 2013) and is therefore an indication of the distribution of the spectra across the recorded duration.

Figures presented in this section for the directional recorder at Stations 1 and 2 are for a single hydrophone channel (i.e., omnidirectional) for ease of comparison with the other recorders. The data recorded on all four channels of the directional recorders produced very similar results. Individual results for all channels are presented in Appendix B.1.

Band levels and LTSAs are shown in Figures 8 to 11 for Stations 1 to 4. Stations 1 and 3 are closest to the Hywind Tampen array, and both show similar trends in their spectrograms and band level plots. Both feature prominent tones at around 25 and 75 Hz throughout, visible as horizontal lines on the spectrogram, with several harmonics also faintly visible at various points. These plots also feature transient broadband energy increases, typical of vessel passes. The tones at 25 and 75 Hz are also faintly visible in Figures 9 and 11 for the more distant directional recorder at Station 2 and the control recorder at Station 4, but the transient broadband features appear more prominently in the spectrograms than in Figures 8 and 10. A noticeable increase in broadband sound levels occurs at all stations from the start of the second period of recorded data on 23 May. This elevated noise level is associated with a relatively close seismic survey airgun source which is thought to have commenced at some point during the redacted period and was joined by a second survey source at a different location at a later date, creating elevated levels in the 8.9–89.1 Hz band. The 12 month spectrogram in Figure 9 shows this period of elevated noise lasted until late August, at which point a third seismic

survey, even closer than the previous two, caused a further increase in levels in the 8.9–89.1 and 89.1–891.3 Hz bands, lasting (excluding a brief drop in levels for a few days) until late September.

Analysis of the long-term recording at Station 2 gives an overview of how the overall levels in the wider Tampen area vary throughout the year. Table 4 shows the median hourly broadband sound pressure level (SPL) during each month of the study. The median hourly SPL noticeably increases during the months with significant seismic survey activity and is considerably lower and relatively similar in the months preceding and following. In months with seismic survey activity the median hourly broadband SPL was at least 10 dB higher than median hourly levels in months with none. Seismic survey activity was captured in at least 5 of the 12 complete months covered by the recording campaign, though it is not clear whether this is representative of typical activity in the area over a longer period.

Table 4. Median hourly broadband SPL in each month of deployment at Station 2.

				Medi	an hourly	broadba	nd SPL (	dB re 1 μ	Pa)				
Feb 2024 ¹		Apr 2024 ²	May 2024 ²	Jun 2024	Jul 2024	Aug 2024	Sep 2024	Oct 2024	Nov 2024	Dec 2024	Jan 2025	Feb 2025	Mar 2025 ¹
115.3	115.0	115.5	129.1	128.4	127.2	125.9	127.5	115.5	114.8	115.6	115.1	115.4	115.2

¹ Partial month

² Some data redacted

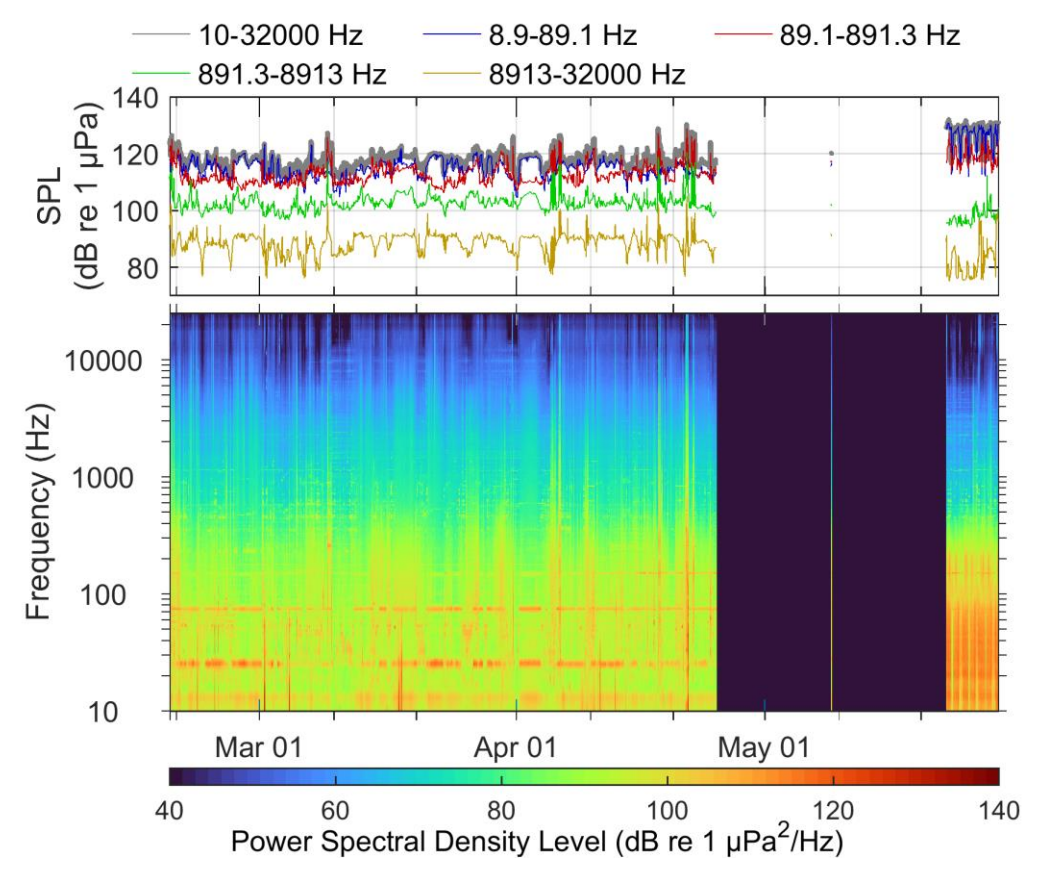


Figure 8. Long term acoustic summary for the AMAR at Station 1 (channel D).

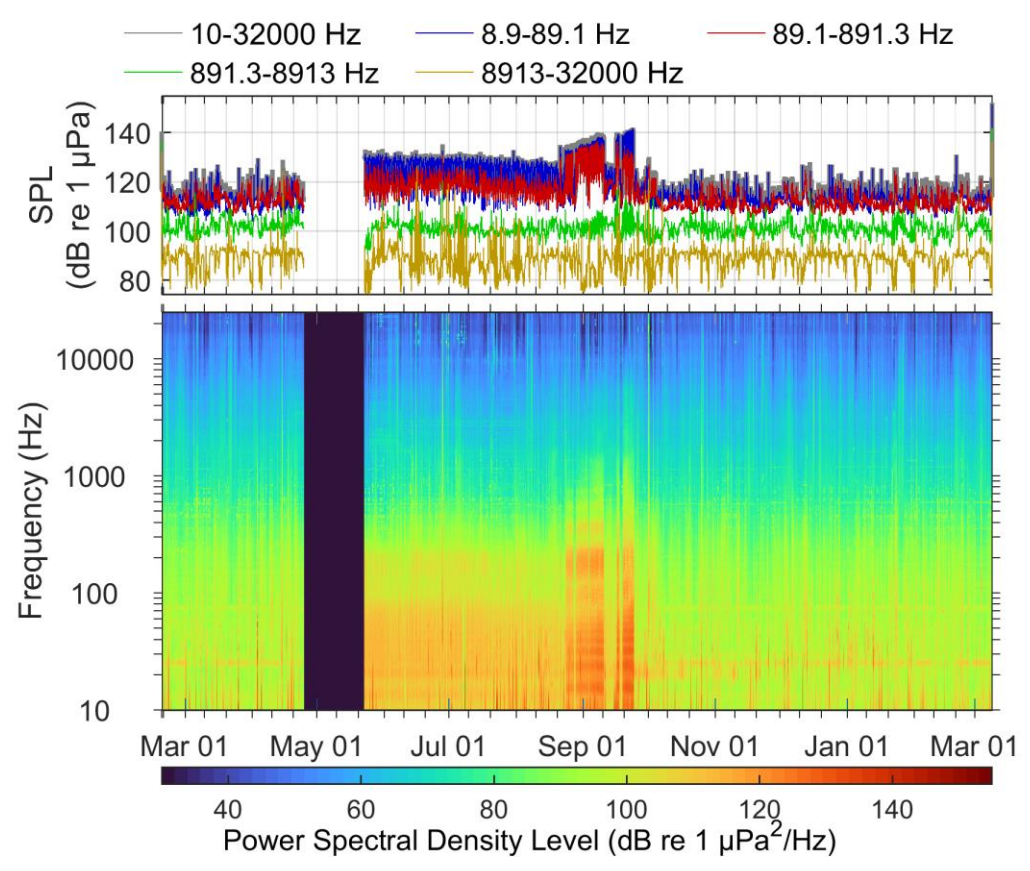


Figure 9. Long term acoustic summary for the AMAR at Station 2 (channel D).

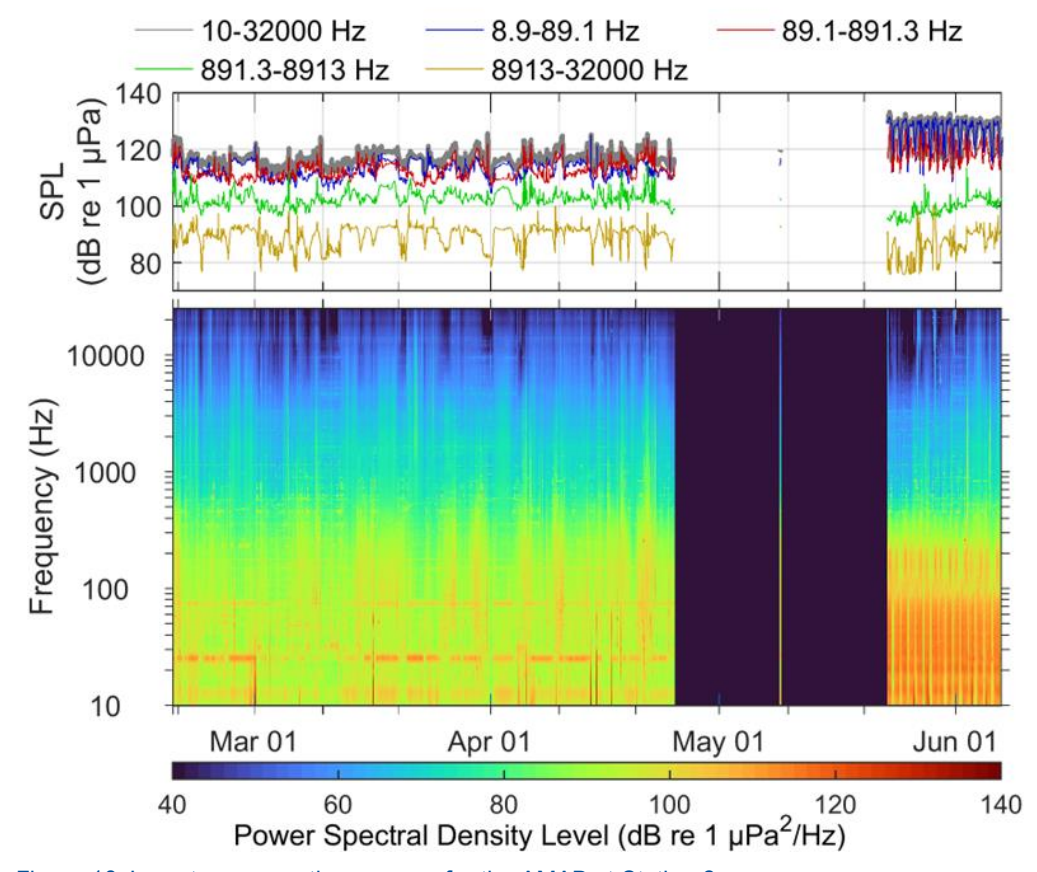


Figure 10. Long term acoustic summary for the AMAR at Station 3.

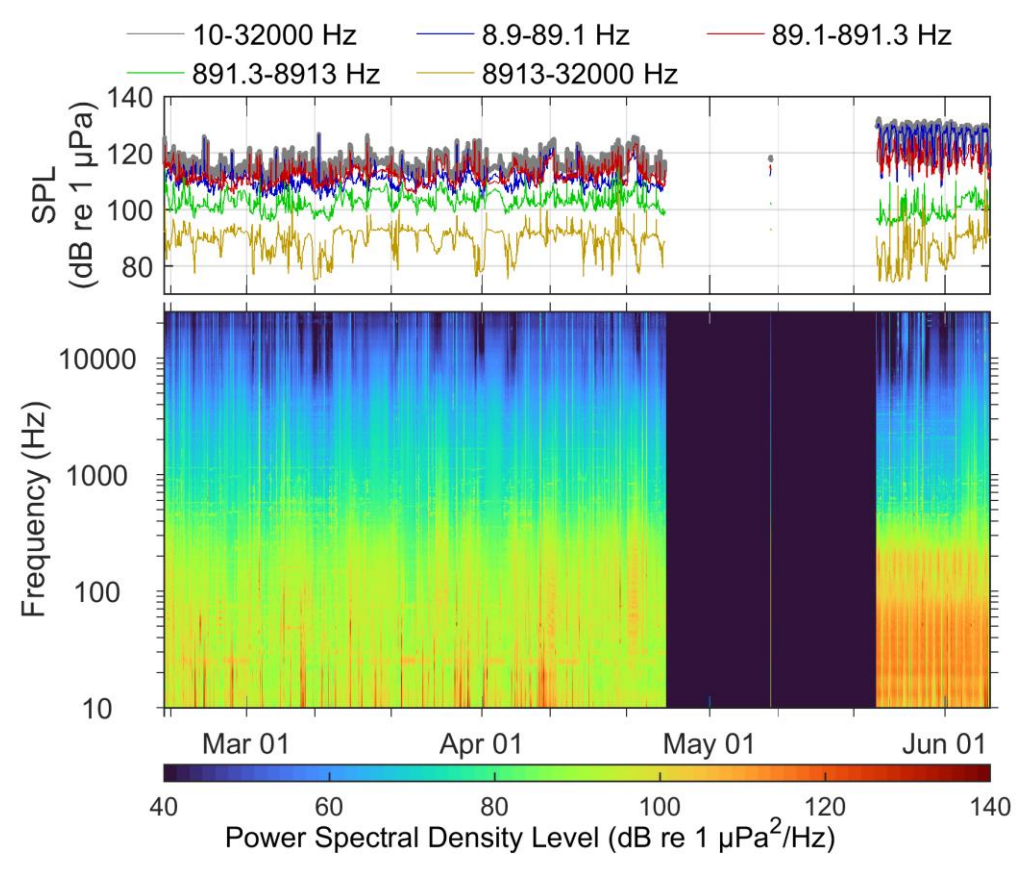


Figure 11. Long term acoustic summary for the AMAR at Station 4.

PSD and decidecade box-and-whisker plots are shown in Figures 12 to 15 for Stations 1 to 4. The shapes of the spectra are broadly similar for all four stations, and the most noticeable features in the PSDs are the peaks in the spectra at 25 and 75 Hz (see also Figure 16). These peaks are present at all four stations, most prominently the peak at 25 Hz, though they are far more pronounced compared to the adjacent frequencies at the two AMARs closest to the Tampen site (Stations 1 and 3). These are the same frequencies which were present in the analysis for the Hywind Scotland systems (Burns et al. 2022), although in that report these tones were not evident in the control recordings. It is noted however that there are more than twice the number of WTGs at the Hywind Tampen site (11) compared to the Hywind Scotland site (5), and the control recorder was located closer to the Hywind Tampen site (approximately 9 km) than at Hywind Scotland (approximately 13 km).

All four stations show elevated levels at frequencies below 100 Hz, which can be seen in the spectral probability density shading and the  $95^{th}$  percentile levels ( $L_{95}$ ). This is a result of the presence of relatively high levels of seismic survey noise starting from the second period of recorded data on 23 May which abruptly elevated the sound levels in this frequency range, leading to the distinct separate shaded line in the spectral probability density rather than an even distribution. This effect is most noticeable in the spectrum of the long-term recorder at Station 2 in Figure 13. The  $75^{th}$  percentile levels ( $L_{75}$ ) in the Station 2 spectrum are distinctly flatter in shape and elevated above the median spectrum, which reflects the fact that noise from seismic surveys was present in the data for a considerable proportion of the overall recording period, i.e. 4 out of 12 months. Additionally, a second, fainter line is visible in the spectral probability density shading above the one present in Figures 12, 14 and 15 as a result of the additional closer seismic survey operating from late August to late September.

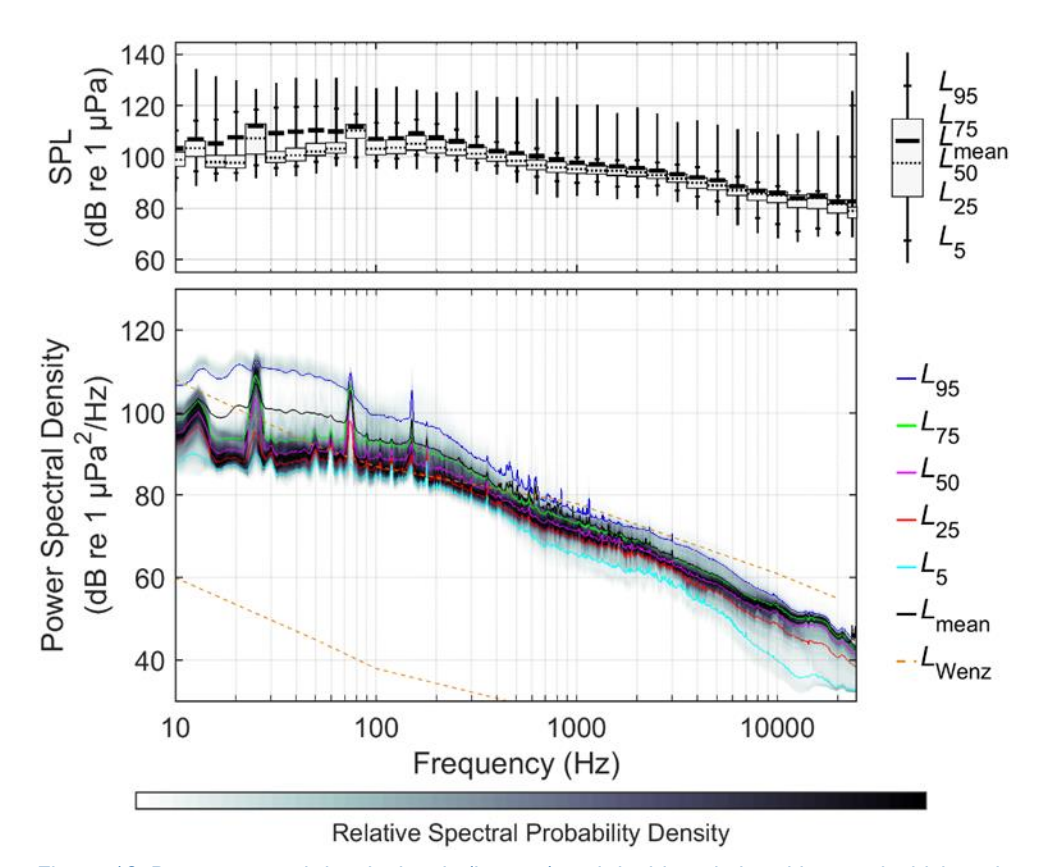


Figure 12. Power spectral density levels (bottom) and decidecade band box-and-whisker plots (top) for the AMAR at Station 1 (channel D).

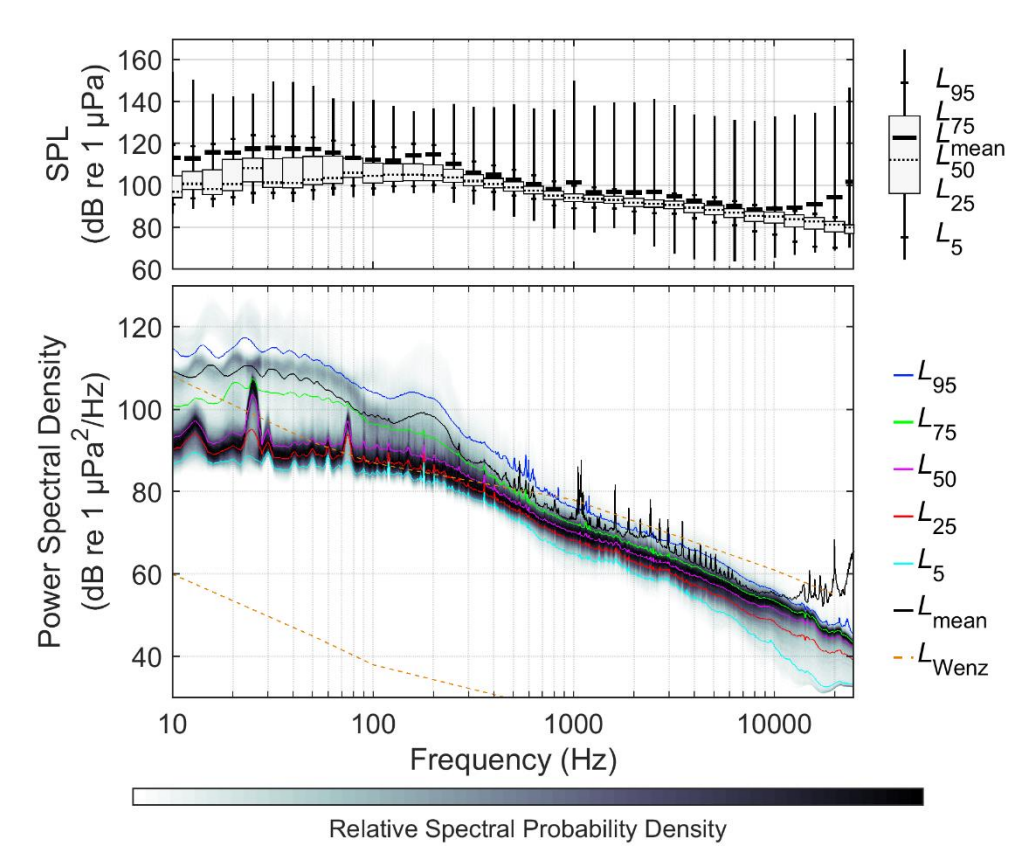


Figure 13. Power spectral density levels (bottom) and decidecade band box-and-whisker plots (top) for the AMAR at Station 2 (channel D).

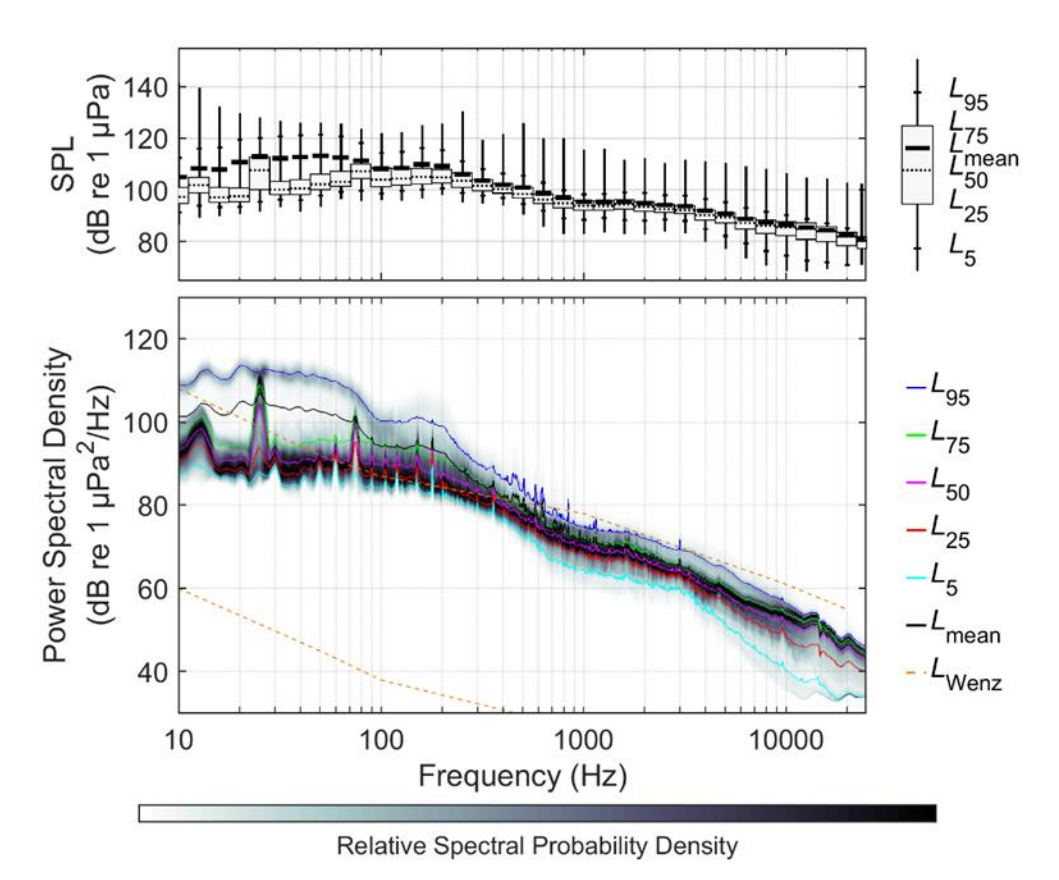


Figure 14. Power spectral density levels (bottom) and decidecade band box-and-whisker plots (top) for the AMAR at Station 3.

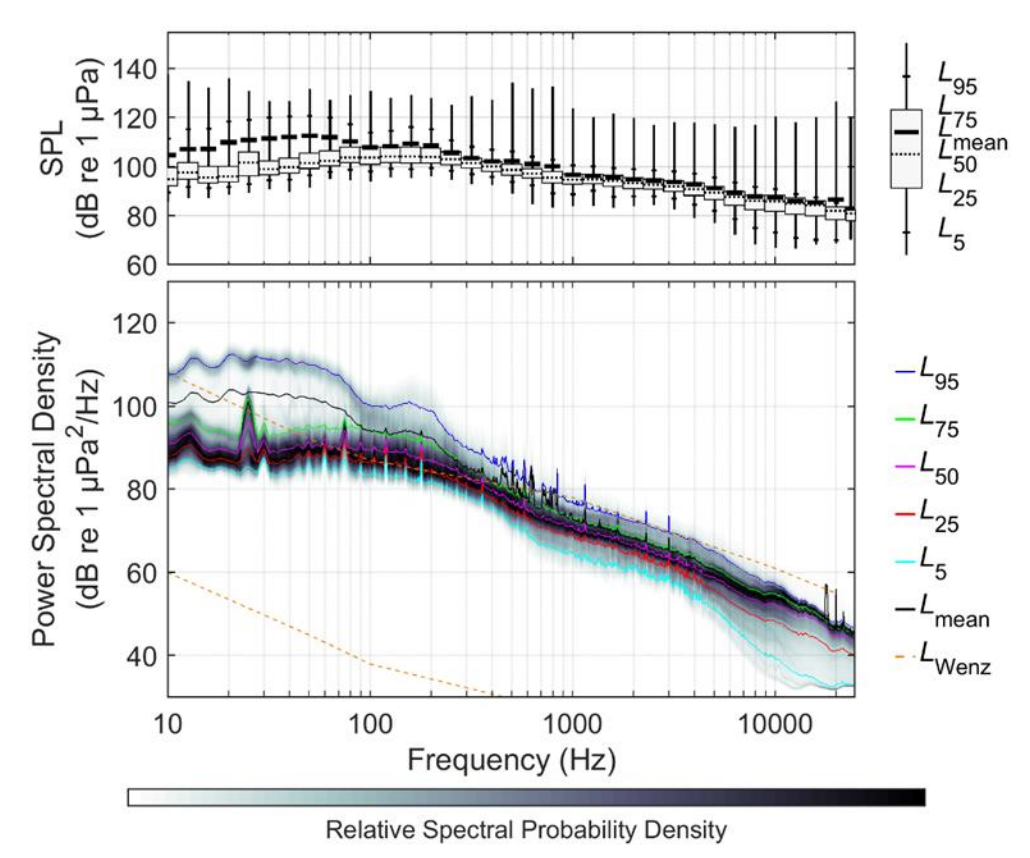


Figure 15. Power spectral density levels (bottom) and decidecade band box-and-whisker plots (top) for the AMAR at Station 4.

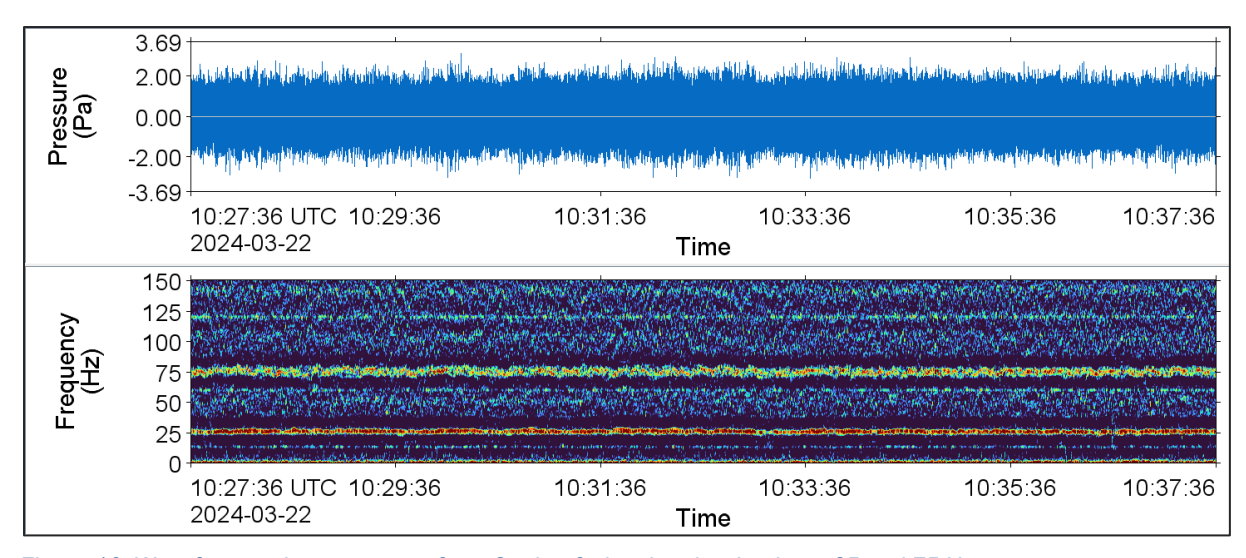


Figure 16. Waveform and spectrogram from Station 3 showing the dominant 25 and 75 Hz tones.

# 3.2. Acoustic Analysis of Omnidirectional Noise

Acoustic analysis of the WAV files was carried out using a combination of high-speed auto-processing and event detection, manual spectral analysis of individual time periods, and Passive Aural Listening. Operational logs were provided by Equinor which provided information about WTG operational state and other useful performance rates such as rotor speed in revolutions per minute (RPM). In addition to turbine related parameters, Equinor also provided 10-minute averaged wind speed recorded at each turbine nacelle, and wave and swell data in hourly intervals from the ERA5 dataset (Hersbach et al. 2023).

In Burns et al. (2022), the types of noise found in the recorded data were broadly divided into three separate categories based on likely origin. These categories were:

- Turbine related mechanical and electrical noise,
- Noise originating from the mooring system, and
- Other noises of indeterminate origin.

This report aims to similarly assess noise within these categories. Analysis in this section is focused on an analysis of the characteristics, frequency distribution and intensity of turbine-related noise and the likely source of each tone or family of related tones, based on omnidirectional recordings. A detailed analysis and comparison of turbine related noise from the more specific directional processing is presented in Section 3.4.

Windows for analysis were selected based on the reported wind speed at the turbine nacelles. The World Meteorological Organization (WMO) recommends reporting wind speed in m/s, but acknowledges other units are in common use (WMO 2023). The unit of knots (kn) for wind speed has been used throughout this report for comparability with the analysis of the sound levels generated at Hywind Scotland (Burns et al. 2022). The chosen wind speeds were from 5 to 40 kn in 5 kn intervals, and the window selected for analysis was chosen as the longest consecutive period where the reported wind speed remained within ±1 kn of the target wind speed. The equivalent wind speed intervals in units of m/s are presented in Table 5.

Knots	(kn)	Metres per s	second (m/s)
Bin centre	Bin interval	Bin centre	Bin interval
5	4-6	2.6	2.1-3.1
10	9-11	5.1	4.6-5.7
15	14-16	7.7	7.2-8.2
20	19-21	10.3	9.8-10.8
25	24-26	12.9	12.3-13.4
30	29-31	15.4	14.9-15.9
35	34-36	18.0	17.5-18.5
40	39-41	20.6	20.1-21.1

The dominant operational noise from the Hywind Tampen turbine system appears to consist primarily of multiple, distinct, low frequency tonal sounds (i.e., narrowband, continuous sounds), some of which are very stable, regardless of changes in WTG performance, and others that are very unstable and have a significant frequency range over which they vary. The most dominant tones, in terms of intensity, are evident below 100 Hz and are directly related to rotor speed (see Section 3.2.1) but there are several related and unrelated tones at higher frequencies.

Very stable tonal sounds are common for electrical generators with a steady source of energy input such as an engine or steam turbine, and it is typically the case that the more dominant tones directly related to the generator, its pole configuration and the rotor RPM. Other tonal sets unrelated to the generator or rotating energy source can be present and are often associated with separate motors, pumps or transformer components of the system. Wind turbine generator and drive shaft related rotational tones are, however, typically less stable as the WTG rotor speed usually fluctuates over short periods of time due to changes in wind speed or gusts. In many systems, there is an upper limit to the frequency of these tones as the rotor RPM is limited to a maximum speed to prevent over speeding of rotor tips or other potentially damaging effects of high shaft speeds.

The Hywind Tampen system is understood to be a Permanent Magnet Direct Drive (PMDD), Horizontal Axis Wind Turbine (HAWT) design with the hub and attached blades directly linked by a drive shaft to the generator rotor. As expected for a direct driven system, there is no intermediate gearbox in the design and the acoustic signature found in the recorded data accordingly reflects the lack of additional gearing tones that usually contribute significantly to the noise signature of geared WTGs. Reported 10-minute average operational rotation speeds are found up to but never exceeding 10.5 RPM, which is the governed maximum rotation speed for this turbine, though lower rotational speeds were routinely recorded at lower wind speeds. Each generator has 144 pole pairs, which at the systems maximum operating rotational rate of 10.5 RPM corresponds to a theoretical fundamental generator frequency of 25.2 Hz.

There are two principal families of tones evident in the data. The first set are variable in frequency, which are typically visible from below 10 Hz to a maximum of around 75 Hz and have a direct relationship with rotor speed. The second set of tones are much more stable in nature, less intense than the rotor-related tonal noise, and do not fluctuate with rotor speed.

# 3.2.1. Rotor Speed Related Aerodynamic and Mechanical Tones

The range of rotor RPM for the Tampen WTG is an important consideration when assessing the noise sources related to it. From analysis of the operational data provided for the recording period, below 3 kn of wind, the rotors do not appear to turn, and onset of rotation occurs at approximately 3.5 kn. At 10 kn rotor RPM reaches approximately 5.5 RPM and at 15 kn it is 8 RPM. Critically, at 20 kn of wind the rotor RPM reaches a governed upper limit of 10.5 RPM which is not seen to be exceeded at any

time in the supporting Tampen operational data. Figure 33 shows a statistical correlation of wind speed and rotor RPM in a further analysis of wind related noise levels.

The source and conditions required for the generation of extremely low frequency (ELF) 'infrasonic' modulated noise below 20 Hz, referred to as blade 'thump' or 'swish' in some papers, is believed to be caused by interaction between the blades and the supporting tower (van den Berg 2005). Other forms of aerodynamic noise from the blades are known to generate higher frequency broadband noise, often audible to humans in air, but against the levels of background noise in the water at the Tampen site, it was difficult to discern as a significant contributor to the overall noise. Some effort was expended in reviewing the recorded data for the ELF blade swish noise based on the rotor speed of the Tampen WTG which, at its highest regulated limit of 10.5 RPM, is relatively slow. Given that the system employs a three-bladed rotor, the maximum blade rate frequency is therefore 0.525 Hz. This frequency of noise is considerably below the roll off frequency for a standard hydrophone and so quantifying the intensity of this noise is problematic for a wide band recording system and would require a more dedicated recording approach. There is apparent ELF energy in some of the time periods assessed, but it is not present throughout and the frequencies are so low that it is not possible to compare any variation in tone with rotor speed. Whilst inconclusive, the evidence suggests, therefore, that there is occasional ELF noise below 1 Hz, that it is loud enough to exceed the background noise at the recording distance from the WTG, but that it is not a constant feature of the noise signature. This noise can be seen in Figure 17 at the very bottom of the spectrogram but it is absent in many of the other spectrograms presented.

The most dominant, rotor speed related tone appears to be the main generator fundamental tone. The frequency of this tone appears directly related to the rotor RPM and the number of generator pole pairs (144) by the following relationship:

$$f = \text{RPM}\left(\frac{pp}{60}\right) \tag{1}$$

where *f* is the tone frequency in Hz, RPM is the rotational rate of the turbine in revolutions per minute, and *pp* is the number of pole pairs present in the generator. At the maximum rotor RPM, it displays a relatively stable tone at the expected 25.2 Hz, and this is the dominant noise source within the overall system signature (Figure 17).

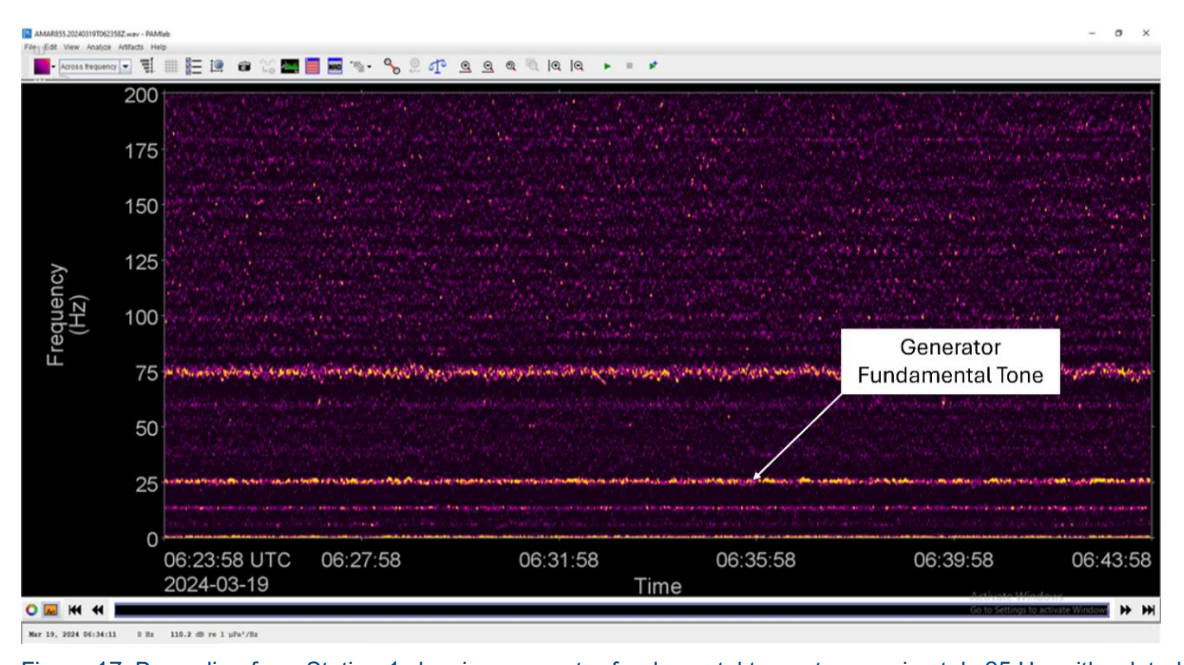


Figure 17. Recording from Station 1 showing generator fundamental tone at approximately 25 Hz, with related rotational tone at approximately 75 Hz and evidence of extremely low frequency energy.

This fundamental tone is never seen to be perfectly stable, but given the nature of the driving force, this is not unexpected. This tone can be seen intermittently or not at all at lower wind speeds when some of the audible turbines are showing slower rotation rates, but the omnidirectional noise data does not provide the fidelity to determine which turbine and which rotation rate is related. What is clear is that this fundamental generator tone is much less apparent and does not dominate the overall noise signature in lighter wind speeds which may reflect periods when generators revert to an idle mode.

In addition to the generator fundamental, there is a second important mechanical tone (also seen in Figure 17) which appears to have a slightly more complex relationship with the generator parameters. This tone also appears directly related in frequency to the rotor RPM and the number of generator pole pairs, this time by a multiple of three. The frequency association is unwavering and the tone, seen in the same spectrogram from a number of different WTGs, rises and falls directly with the rotor RPM of each one and conforms precisely with the following relationship:

$$f = 3 \times \text{RPM} \left(\frac{pp}{60}\right) \tag{2}$$

It is unclear, whether this factor of three is associated with the number of blades (unlikely), a three-phase power output or some other feature of the design such as the direct drive bearings. Hence from acoustic analysis alone, it remains uncertain exactly how this tone is being created but the relationship to the number of pole pairs is evident. Since this tone is directly related to the rotor RPM, at RPM rates below the system maximum in lower wind speeds the tone can be somewhat unstable as the rotor rate responds to the changing wind speed. A set of these highly unstable tones from multiple WTGs is presented in Figure 18, at relatively light wind speed and rotor rates below the maximum 10.5 RPM. A generator fundamental tone from one of the WTGs, at 25.2 Hz, is evident at the beginning of the period but it is weak and fades in intensity, which is typical of its nature.

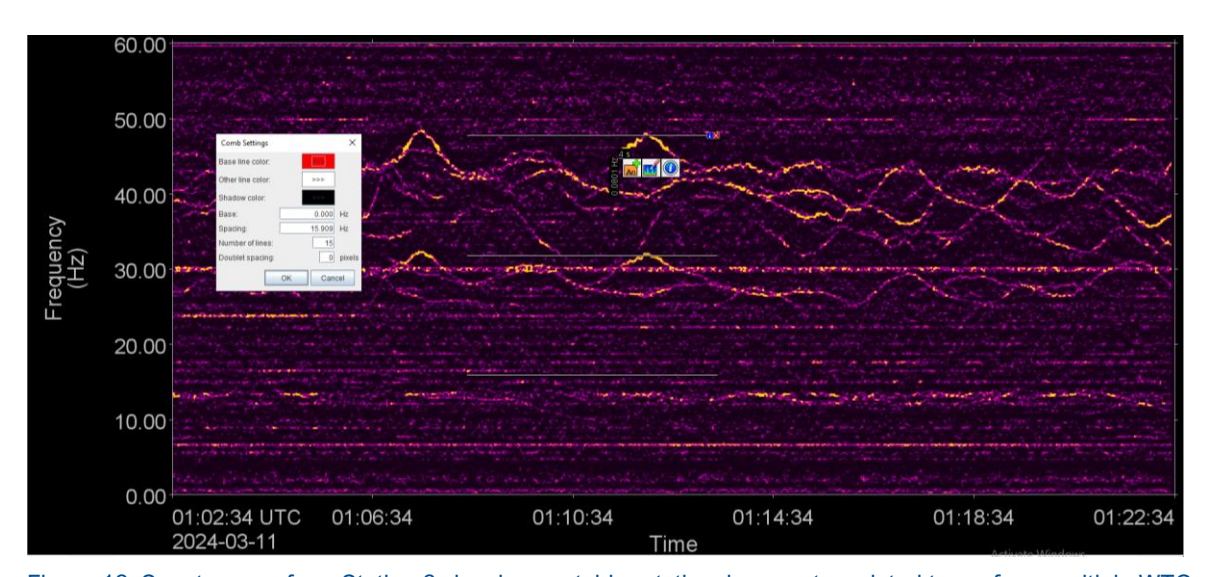


Figure 18. Spectrogram from Station 3 showing unstable rotational generator related tones from multiple WTGs at low rotation rates with weak, intermittent generator fundamental at 25 Hz.

At wind speeds above 20 kn, when the rotor RPM is consistent at its limit of 10.5, the instability in the tones diminishes, and they remain at their maximum of 75 Hz as defined by Equation 2 (Figure 19). Additionally, this tone regularly exhibits a second harmonic, particularly when the generator is operating at higher wind speeds and occasionally a third at the highest power outputs. In addition, the generator fundamental at 25.2 Hz also increases in intensity to become the dominant noise source.

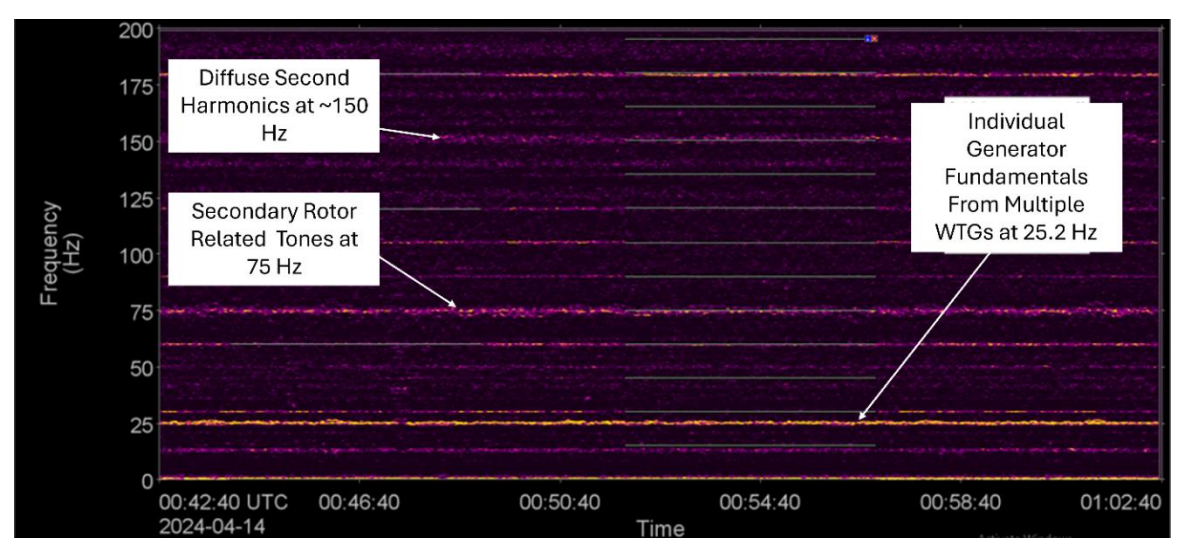


Figure 19. Spectrogram from Station 3 in 20 kn wind speed, 10.5 RPM, stability in the secondary generator tones at 75 Hz and elevated levels of the generator fundamental tone at 25.2 Hz. A diffuse second harmonic of the 75 Hz tone is seen at around 150 Hz.

#### 3.2.2. Tones Not Related to Rotor RPM

There is a further family of tones, which display a classic harmonic structure often seen in many types of motor and has no apparent association with the main WTG rotor RPM. These tones are much more stable regardless of variability in the wind, with a fundamental fractionally above 15 Hz. This source is significantly quieter than the main generator related tones but does manifest a series of harmonics which at times reach as high as the eleventh harmonic (Figure 20). This noise is thought to be related to either a smaller multi-pole motor or other electrical system in the WTG which operates at a more constant rotational rate than the main generator itself. The consistent stability of these tones suggests that the source is powered by a stable electrical input rather than being a feature of variable power generation itself. There is occasional evidence of abrupt, but small frequency shift which may point to the system being under a switchable load. Passive acoustic listening does not reveal any audible emissions even at 1/10th playback rate which indicates that, whilst being an important contributor to the spectrum, this is not a major source of noise from the WTG. Speculation, based on the acoustic evidence, suggests that this noise may be related to an auxiliary system such as a blade pitch or yaw control server, pump or cooling fan, or similar, that operates from a conditioned power supply.

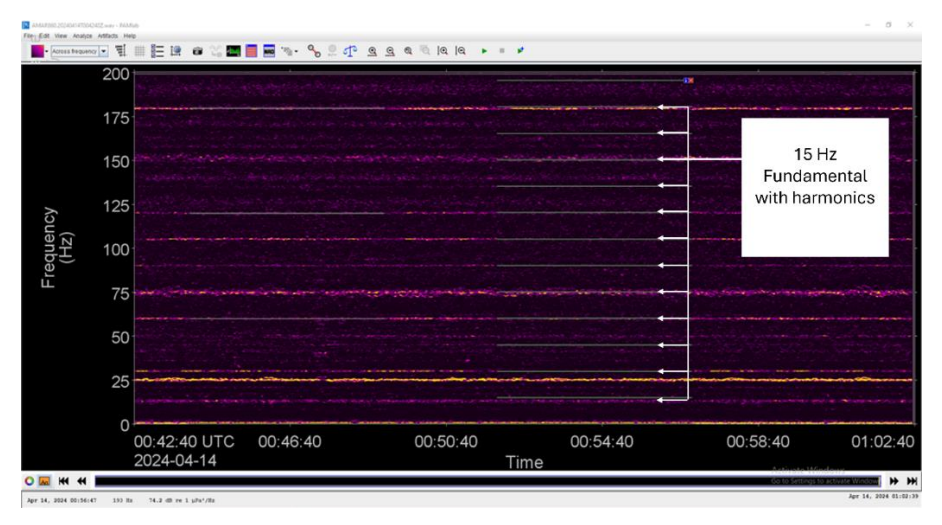


Figure 20. Spectrogram from Station 3 showing 15 Hz fundamental tone with ascending related harmonics and coincident overlap at 75 Hz with the generator secondary tone.

At the upper limit of rotor RPM, the fifth harmonic of this 15 Hz fundamental coincides with the dominant ~75 Hz rotational tone described above, and this leads to a minor enhancement of the intensity in this part of the spectrum. In most cases, however, the motor stable tone is usually lost beneath the slightly unstable but more dominant rotor-related tones. As wind speed increases, the number of harmonics visible in the spectrogram also increases.

Additional tonal elements are seen further up the frequency scale but, without exception, they display a lower intensity than the dominant generator tones; these tones are evident as lower intensity and less pronounced peaks in the spectra in Figures 12 to 15. There are several higher frequency tones that show no direct association with the 15 Hz motor fundamental or the primary generator tones described above. Some display intermittent operation, with abrupt stop and start events which would be expected of a hydraulic accumulator pump or nacelle yaw control event, whereas others show continuous, unstable behaviour suggestive of an input device such as blade pitch actuator. Figure 21 shows an example of these tones at 25 kn of wind, when pitch actuation is likely to be active. It is notable that these tones are less evident at lower wind speeds when blade adjustment may be less dynamic or frequent. The first tone centred at approximately 900 Hz, is continuous and highly unstable with no observable pattern to the instability and this tone is thought to be related to pitch actuation. The second tone at 1,118 Hz is remarkably stable and displays both an abrupt stop and abrupt start event; the grey line between these events in Figure 21 is that of an analysis comb and not a continuation of the noise. These are characteristics expected of a hydraulic pump system maintaining pressure in an accumulator, such as one potentially used by the pitch control system.

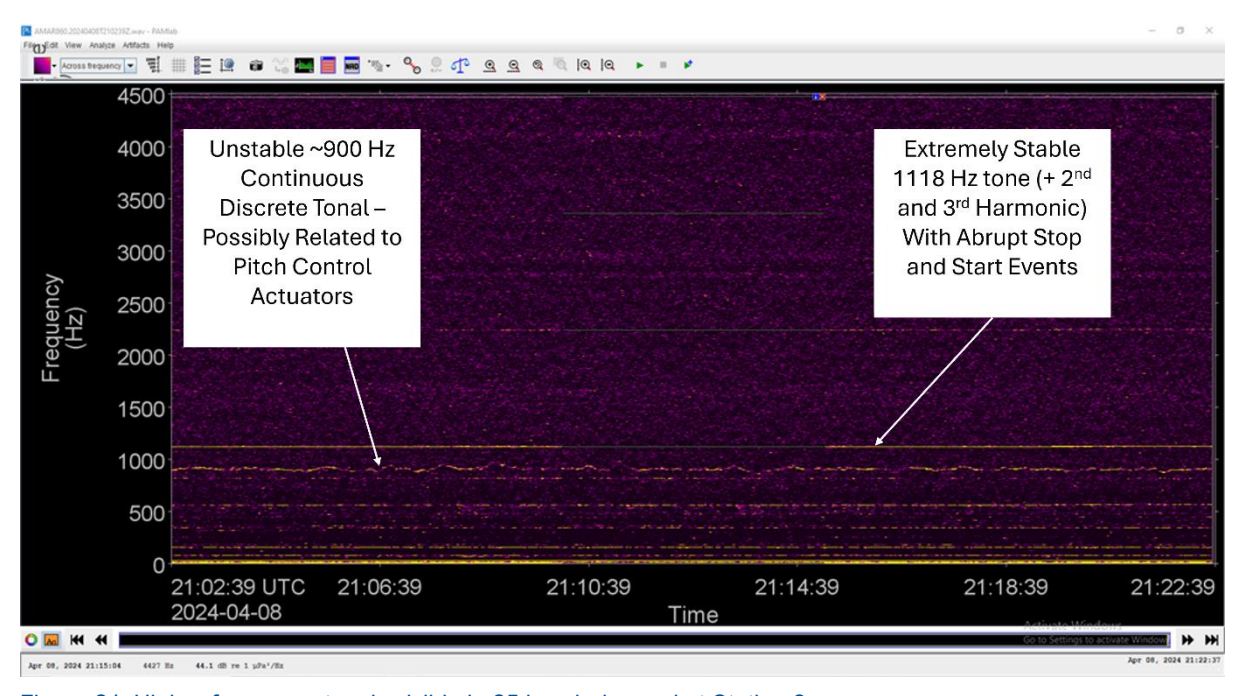


Figure 21. Higher frequency tonals visible in 25 kn wind speed at Station 3.

## 3.2.3. Combined Overall Omnidirectional Tonal Noise

Considering the omnidirectional noise from multiple Tampen WTGs, the aggregate spectrum is characterised by elevated levels of discrete narrowband frequencies related to rotor speed or installed machinery, but there are no noticeable broadband noise sources; this is confirmed by the long-term power spectral density levels at all four stations (Figures 8 to 11). The dominant noise is at the very bottom of the spectrum, mainly below 100 Hz, with less dominant tones occurring intermittently up into the low KHz. Figure 22 shows an omnidirectional spectrogram of the total Tampen noise field from

Station 1, from 10 Hz to 4,500 Hz at 35 kn. As described, the most intense noise is clearly below 100 Hz with only a limited number of weaker control system tonals evident above 500 Hz.

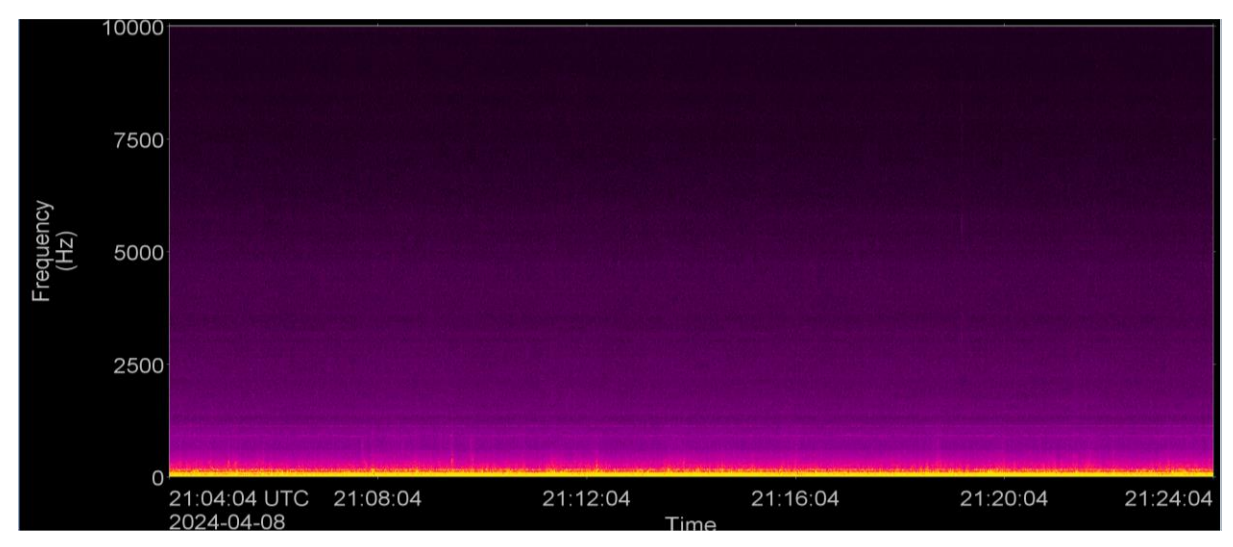


Figure 22. Relative intensity and spectral contribution of the Tampen wind farm to the soundscape (Station 1).

## 3.2.4. Mooring System Noise

Previous analysis of the Hywind Demo (Martin et al. 2011) and Hywind Scotland recordings (Burns et al. 2022) revealed multiple transient sounds attributed to tension release caused by vertical heave motion on the floating structure itself. In those recordings, mooring transient sounds were identified as typically broadband with varying degrees of impulsiveness. The sounds were then categorised qualitatively by their audible characteristics as 'snaps', 'creaks', 'bangs', and 'rattles'. The Hywind Tampen dataset was, similarly, manually analysed for such transients in wind speed bins of 5 kn. However, where in the previous Hywind datasets mooring transients were apparent as high intensity peaks in both the pressure signal and spectrograms, barely any such signals were found in the Hywind Tampen recordings.

Audible events that were identified in the Tampen data as potential mooring transients had little resemblance to the 'snaps', 'creaks', 'bangs', and 'rattles' of the Scotland recordings. The only candidate noises that emerged from early analysis were temporally impulsive, with frequency content predominantly below 1 kHz, but qualitatively sounded like a faint 'knock'. An example of some of these suspected mooring transients is shown in Figure 23. Very few such events were discovered in the data, and those that were identified were only found in periods where wind speed was greater than 30 kn. Due to the relative paucity of transients identified through impulse auto-detection, there were not enough events to adequately tune JASCO's automated impulse detector to quantify the number of mooring transients present within the entire dataset.

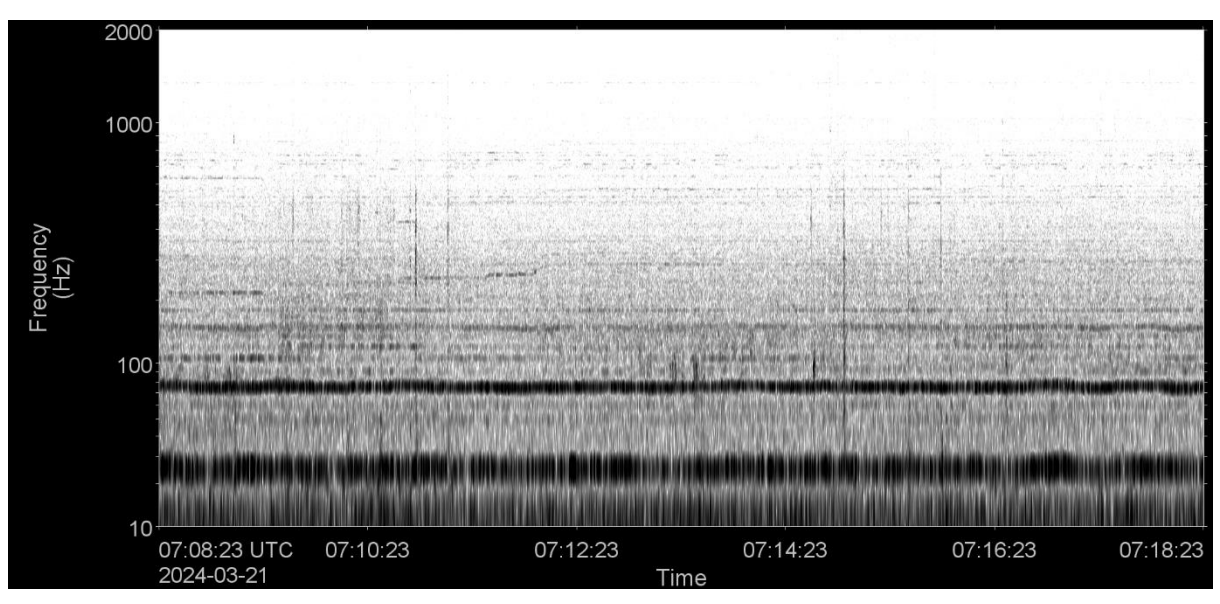


Figure 23. Spectrogram showing suspected mooring transients (vertical lines) from Station 1 among tonal turbine related noise (horizontal lines).

The water depth and swell fetch at the Tampen site are conducive to the propagation of even greater swell heights than at the Hywind Scotland site and yet, despite this, transients at Hywind Scotland were frequent and evident at much lower wind speeds than in this study. This suggests that the relative lack of mooring noise at Tampen is related to differences in either the floating structure, the mooring system, or both, rather than any difference in exposure to swell or other environmental factors. It is possible that the buoyancy performance of the Tampen spar is such that it reduces the structure's response to swell and elicits less vertical heave, placing less tension on the mooring system. It may also be the case that the small-scale components of the Tampen mooring system simply generate less noise, despite managing equal or greater magnitudes of spar heave. In one period where a small number of possible mooring transients was highlighted, two sperm whales were also audible at relatively close range, identified by two extensive click trains (Figure 24)

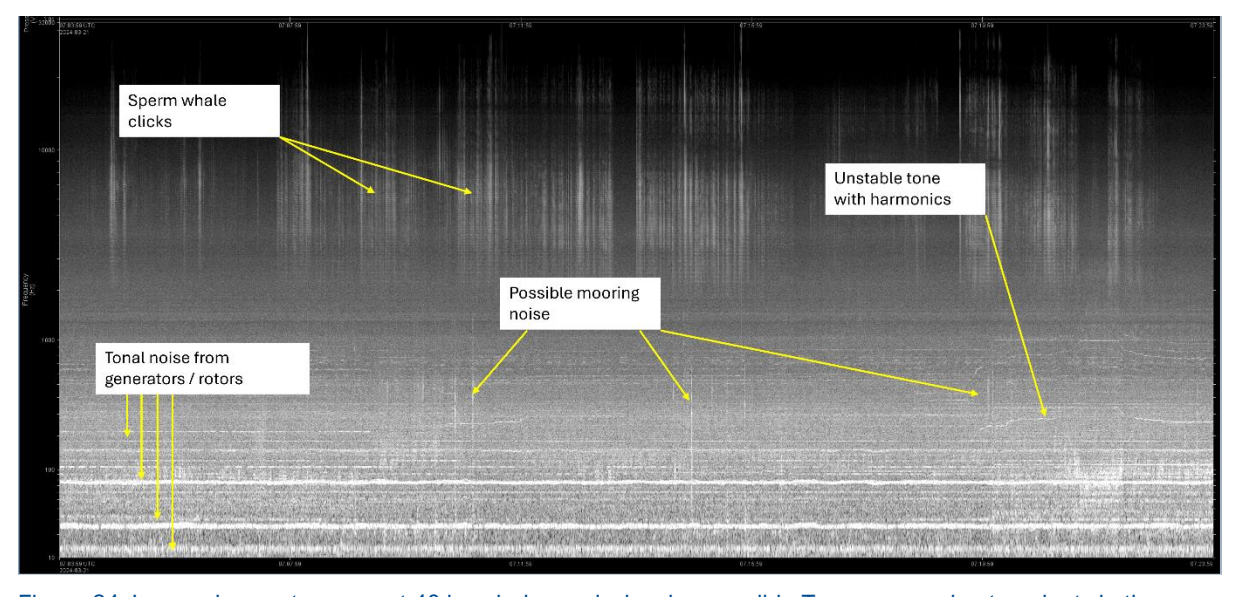


Figure 24. Log scale spectrogram, at 40 kn wind speed, showing possible Tampen mooring transients in the presence of two echolocating sperm whales.

To further explore the mooring noise issue, directional analysis was then conducted on the potential mooring noises shown in Figure 23 and Figure 24 to try to establish whether this noise could be directly attributed to a particular Tampen structure or location in the honeycomb mooring layout. On processing, the transients were clearly visible in the directogram (Figure 25) but it was immediately apparent that the source of the noise was from an Easterly direction from Station 1 and therefore most unlikely to be attributable to the Tampen mooring system.

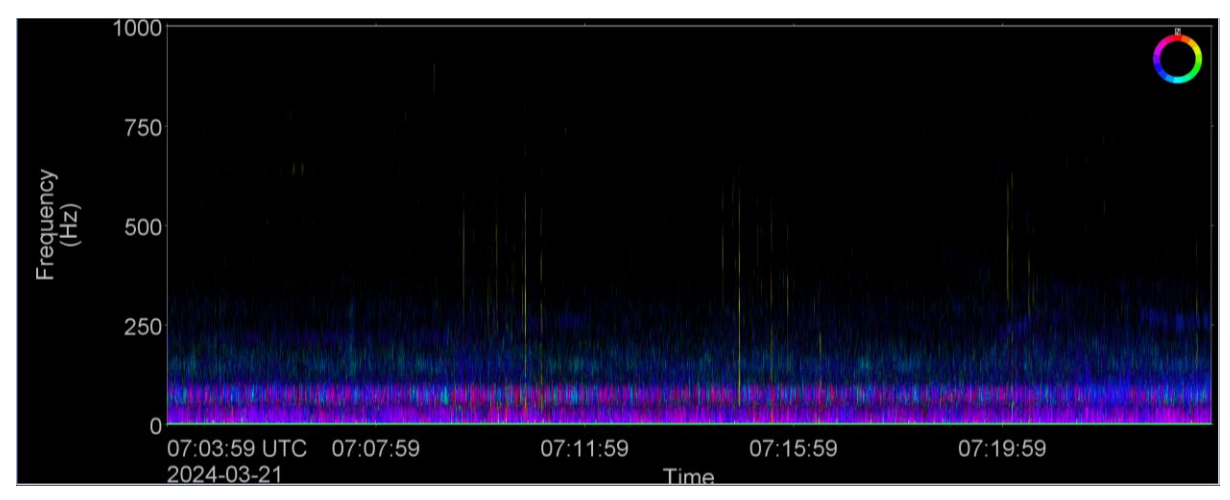


Figure 25. Directogram of suspected mooring noise – showing the origin of the impulses from outside the wind farm. Colours indicate the likely direction of origin of sounds according to the displayed colour wheel, orientated conventionally with north at the top.

To provide an alternative investigative approach to the number of transients in the recorded data, the overall impulsiveness of the data was interrogated. This method has a wider utility as it is also important to characterise the impulsiveness of the overall noise field from the Tampen site to determine which hearing threshold shift regulatory criteria are most appropriate to apply for impact assessment. Impulses are, by definition, acoustic events that are both broadband and of short duration (<1 s) with high peak sound pressures and short rise times (NIOSH 1998, NMFS 2018).

Kurtosis is one approach which has been suggested to quantify the impulsiveness of an acoustic signal (Martin et al. 2020). Kurtosis ( $\beta$ ) is defined as the ratio of the fourth moment to the squared second moment of the instantaneous sound pressure:

$$\beta = \frac{\frac{1}{N} \sum_{N} (p_i - \overline{p})^4}{\left[\frac{1}{N} \sum_{N} (p_i - \overline{p})^2\right]^2}$$
(3)

where  $p_i$  is the *i*th sample of instantaneous sound pressure,  $\overline{p}$  is the arithmetic mean of sound pressure, and N is the number of data samples in the analysis window that affects resulting value for  $\beta$ . As suggested in Martin et al. (2020), a one-minute analysis window was used for this project. Kurtosis of 3 represents random Gaussian noise, while kurtosis of 40 is used as a threshold for determining if a soundscape is impulsive for purposes of determining if an impulsive or non-impulsive hearing threshold shift threshold is exceeded (Southall et al. 2019). Kurtosis for wind driven underwater ambient noise is also  $\sim$ 3.

A comparison of the distribution of one-minute kurtosis of the unweighted acoustic data from each recorder up to 25 April is presented in Figure 26. The empirical cumulative distribution functions for one-minute kurtosis are very similar for all recorders, with the shape of the curves indicating the data at the two recorders farther from the array (Stations 2 and 4) may be fractionally more impulsive than either of the recorders closer to the turbines. The kurtosis at all four recorders is extremely low, however; at all recorders a minimum of 97% of observations had a kurtosis of 4 or below, which is well

below the threshold of 40 for fully impulsive data. Additionally, the occurrence of highly impulsive minutes ( $\beta$  > 40) is exceptionally rare at all recorders. Use of the non-impulsive thresholds from Southall et al. (2019) is therefore recommended.

Based on this and the manual analysis of the windows selected based on consistent wind speed, it appears there are far fewer transients originating from the Hywind Tampen mooring system than the Hywind DEMO or Hywind Scotland systems.

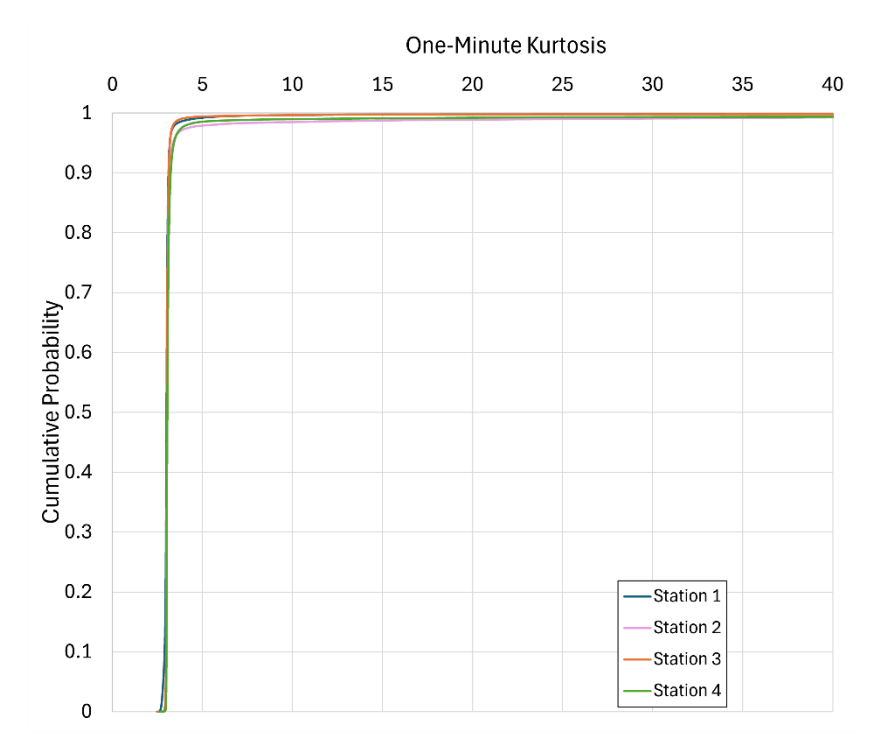


Figure 26. Empirical cumulative distribution functions for the one-minute kurtosis of unweighted signals at Stations 1 to 4.

Consequently, manual and kurtosis analysis failed to reveal the presence of any significant transient mooring noise that was being generated at levels exceeding the background noise, even at wind speeds exceeding 30 kn. This marks a significant departure from previous Hywind floating WTG designs and is a significant factor in reducing the overall system underwater noise.

#### 3.2.5. Cod Vocalisation Detection

One secondary aim of this study was to assess the presence of spawning North Atlantic Cod (*Gadus morhua*) vocalisation noise in the data. A combination of automated detector-classifiers (referred to as automated detectors) and manual review was used to identify cod sounds in the acoustic data. In addition to automated detectors for cod, automated detectors were also run to detect the presence of marine mammals; results for the marine mammal detectors are presented in Appendix D.

Cod grunt detectors were applied to the full data set in the first instance. The automated tonal signal detector identified continuous contours of elevated energy and classified them against a library of cod grunt frequency and time characteristics. In addition to JASCO's contour detectors, a recently published fish detector (Mouy et al. 2024) was run against the data. This detector is comprised of a convolutional neural network that was trained to recognize a variety of fish sounds occurring in the 0-1200Hz band. Automated detectors are developed, trained, and tested to be as reliable and broadly applicable as possible. However, the performance of automated detectors varies across acoustic environments (e.g., Hodge et al. 2015, Širović et al. 2015, Erbs et al. 2017, Delarue et al. 2018).

Therefore, automated detector results must always be supplemented by some level of manual review to evaluate automated detector performance. Here, a subset of acoustic files was manually reviewed for the presence/absence of cod acoustic signals via spectrogram review in JASCO's PAMlab software. The subset, representing 100 sound files per station (~33 h worth of 20 min 64 kHz sound files), was selected based on automated detector results via JASCO's Automatic Data Selection for Validation (ADSV) algorithm (Kowarski et al. 2021).

No cod grunts were confirmed during the manual review of acoustic data. Although acoustic detection does indicate presence, an absence of detections does not necessarily indicate absence of cod. An animal may be present but not detected if no individuals were vocalizing near the recorder, their signals were masked by environmental and/or anthropogenic noise sources, or a combination of these factors. Different sound propagation environments and different seasonal effects will impact the detection range of a given signal over time and, therefore, influence the number of detectable signals. Seasonal variations in vocalizing behaviour can also influence the detectability of a species.

Since detection of cod vocalisation was only a secondary aim of this analysis, the placement of acoustic recorders and other decisions related to study design were not considered with this purpose in mind. A more comprehensive study designed explicitly for this purpose would be required to infer the presence of cod. For this and the reasons outlined above, the lack of cod grunt detections in this study should not be used to conclude the absence of in the Hywind Tampen area.

## 3.2.6. Other Anthropogenic Noise

In addition to the Tampen WTG and mooring system noise, several other sources of noise contributed to the overall soundscape. One significant and contaminating source unrelated to the Tampen wind farm was seismic survey airgun signatures, particularly towards the end of the first recording period, continuing into late September in the long-term recorded data. It is unknown exactly when the seismic survey began as that start event occurred during the data outage period, but regular seismic airgun pulses were observed in a small window of data on 8 May 2024 so the onset must have been before that date. It is not known whether the seismic survey started before then or if it was in constant operation throughout the data redaction period.

Evidence of this noise, characterised as a continuous series of low frequency, repetitive, impulses, can be seen in the elevated levels present at the corresponding times for all stations in Figures 8 to 11. A second, louder period of seismic activity can be seen in the Station 2 LTSA (Figure 9) beginning in late August. The seismic surveys increased noise levels below 100 Hz at all Stations masking all tonal noise from the turbines during this time. A waveform and spectrogram showing a short period of seismic activity is shown in Figure 27. The seismic airgun signal can be seen to totally dominate the waveform and the low frequency energy in the spectrogram in Figure 27. Closer inspection reveals multiple seismic sources: one with a shorter gap between pulses with energy predominantly below 50 Hz, and a second with a longer inter-pulse interval with more energy above approximately 250 Hz.

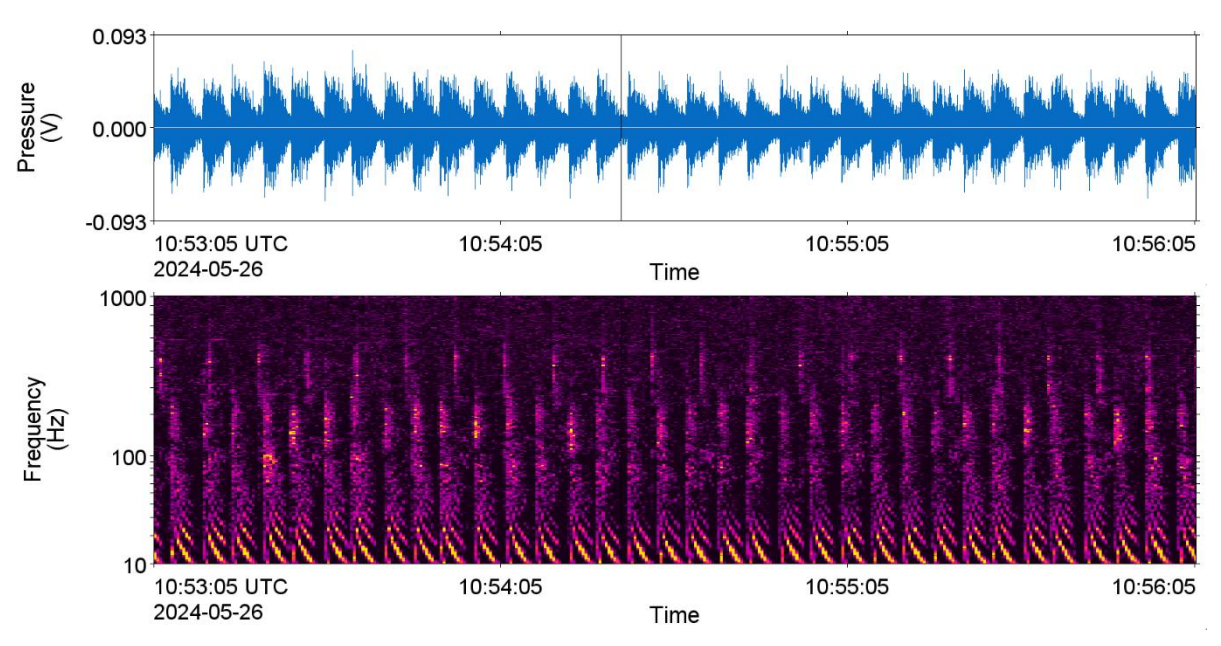


Figure 27. Spectrogram and waveform showing assumed seismic survey noise at Station 1.

Directional analysis (see Section 3.4.1 for details) of the seismic survey activity at Station 1 clearly identifies the two separate events. One survey is located to the south of the Tampen area and the second survey to the northeast, the survey to the south being somewhat closer to the Tampen site (Figure 28). Similar directional analysis of the louder period of seismic activity at Station 2 identified at least five distinct seismic sources operating concurrently from different directions with individual temporal and frequency characteristics (Figure 29), including one source apparently much closer than the others which further dominated the total sound levels. The closest, and hence loudest source, appears to be north of the station, with the corresponding peaks in the waveform much higher than the other sources. Other apparent sources include one to the west with a comparatively rapid interpulse interval (shown in purple), one to the south east with a narrow pulse and energy above 100 Hz (dark blue), one to the south only faintly visible in the directogram with energy predominantly between 100 and 300 Hz (light blue), and one to the northeast with only faint, indistinct pulses and energy primarily below 100 Hz (yellow).

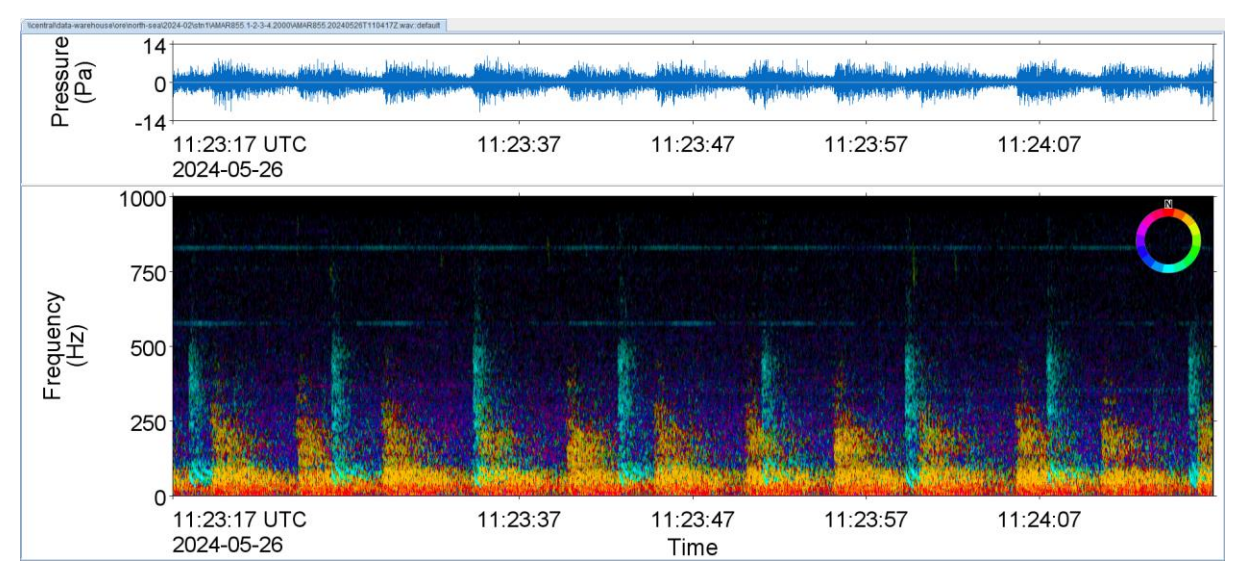


Figure 28. Directional processing at Station 1 reveals two separate seismic surveys to the North and to the South.

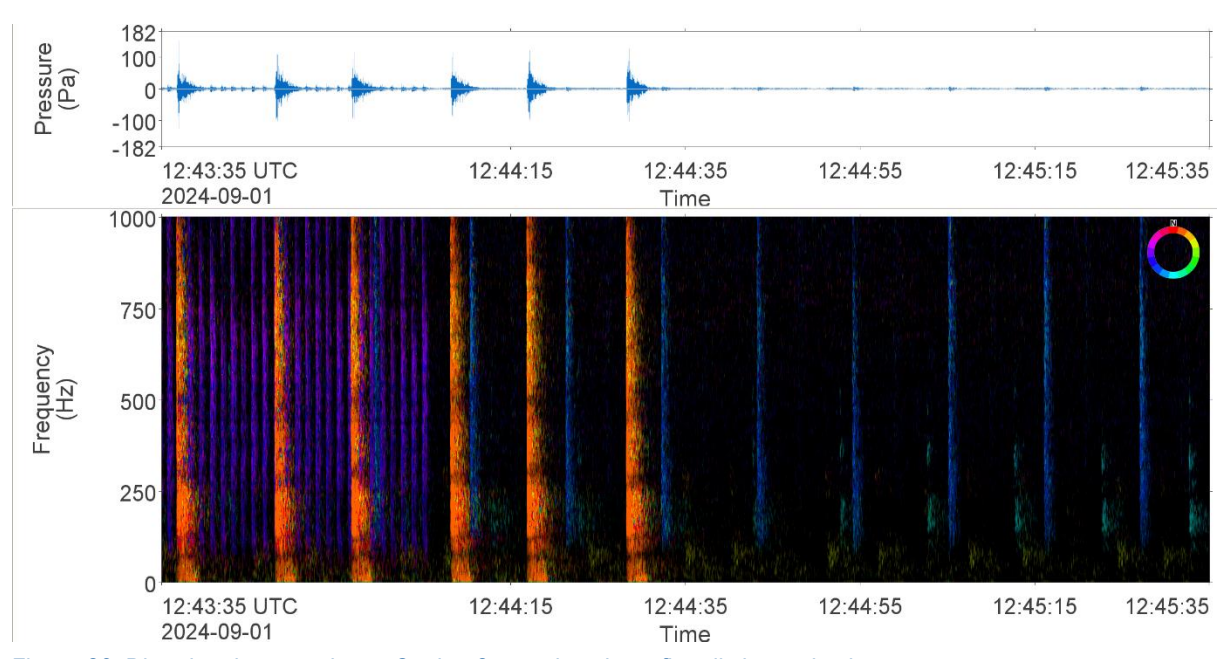


Figure 29. Directional processing at Station 2 reveals at least five distinct seismic sources.

Occasional evidence of vessel activity was also present in the sound files, with one example shown in Figure 30. The vessel engine signature is apparent before it starts its drive train, which is seen as a sudden onset of cavitation noise which lasts for approximately 20 minutes before the drive train is stopped. Noise levels are instantaneously and visibly increased at frequencies below 15 kHz, and tones that are associated with the Tampen WTGs appear masked during this period. The vessel is either stationary, or station keeping and does not appear to be transiting through the area as there is no clear doppler change to any of the engine tones, nor a characteristic passing vessel broadband pattern to the cavitation. This may be a maintenance or guard vessel operating within or close to the wind farm and the broadband cavitation could be associated with thrusters in a dynamic positioning system. A more detailed and annotated spectrogram of this event, highlighting the components of the signal is presented in Figure 31.

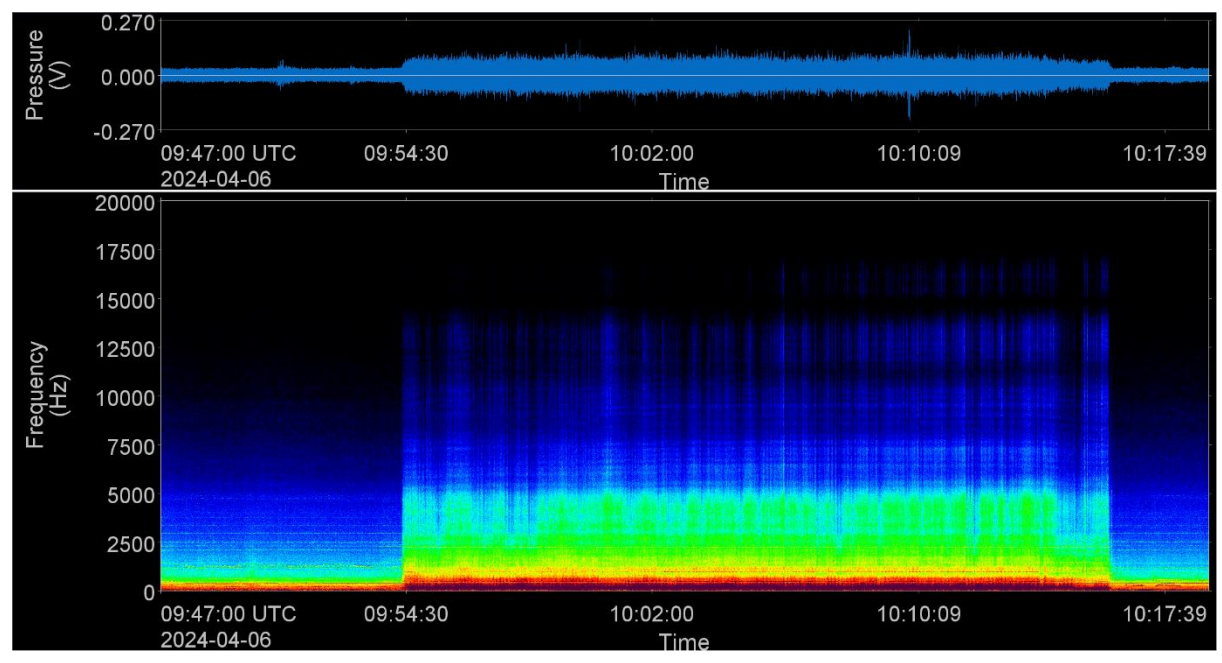


Figure 30. Spectrogram and waveform of suspected vessel on dynamic positioning. The period of high intensity sound starts and stops abruptly and lasts for approximately 20 minutes.

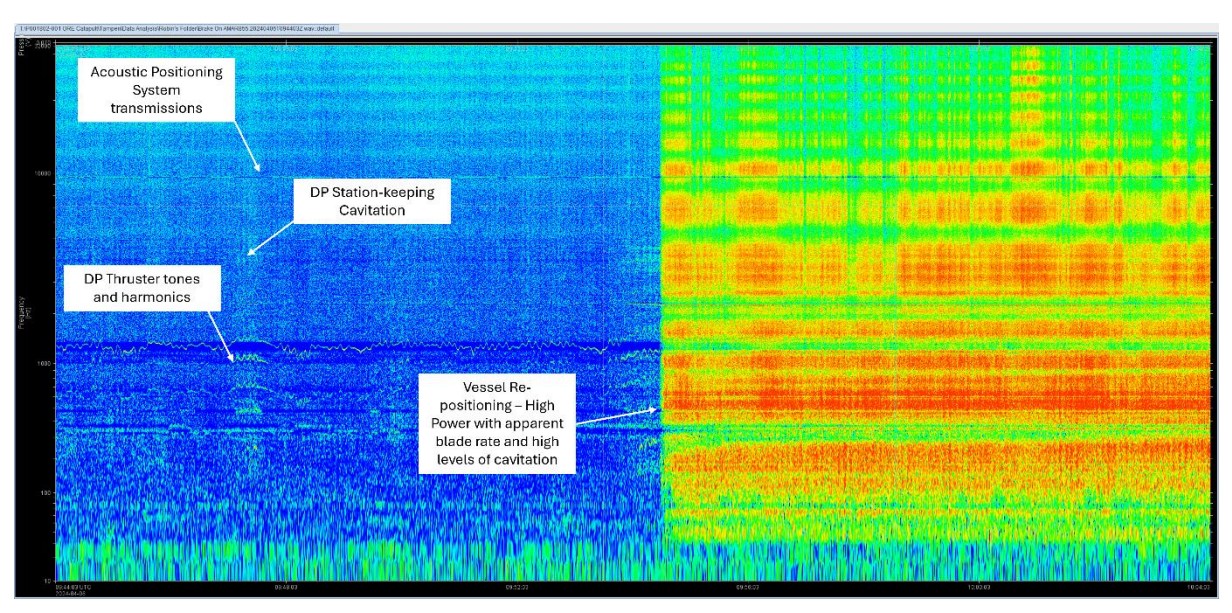


Figure 31. Annotated spectrogram showing onset of high-power dynamic positioning (DP).

Other, more distant vessel activity was observed in certain sound files with one example shown in Figure 32. The vessel's cavitation noise is visible as regular broadband sounds, lasting approximately 2-3 seconds each, fading in and out of audibility. The signal shows characteristics of propeller cavitation for a vessel underway in higher sea states, where the propeller(s) depth increases and decreases as the stern of the vessel rises and falls on the waves. As the propeller comes up towards the surface, cavitation occurs but as it moves deeper into the water, the ambient water pressure rises and suppresses cavitation. Engine and drive train tones are also evident.

When selecting periods to highlight the tonal elements of the Tampen noise signature, there was a minor degree of contamination from vessel noise which introduced unrelated engine tones to the noise field and occasionally cavitation noise. Every effort was made to reject these periods, but it is evident in one or two spectrograms that there are faint engine tones from distant vessels.

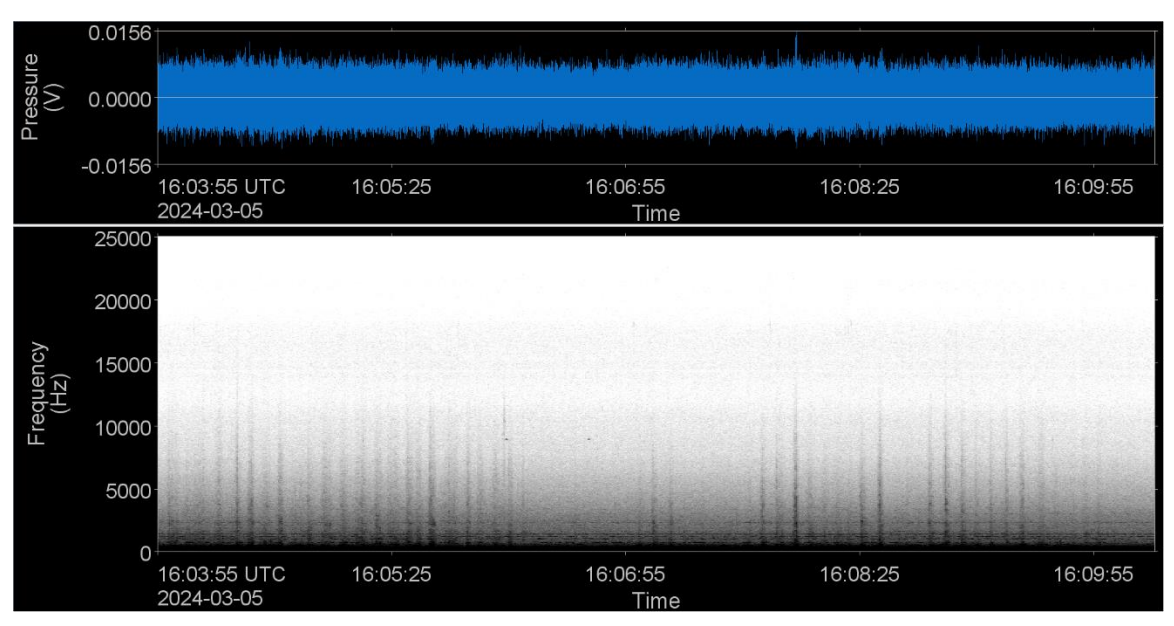


Figure 32. Spectrogram and waveform showing vessel noise at Station 1.

### 3.3. Comparison of Sound Levels with Ambient Conditions

This section presents correlation analyses between sound levels in representative decidecade bands (also called third-octave bands, see Appendix A.2) at all recording stations, wind speed reported at the turbine nacelles, and WTG rotor RPM. Wind speed and rotor RPM values presented in this section were averaged over all turbines in the array. The decidecade bands chosen were the same as those used to compare noise levels to environmental conditions in the analysis of sound levels at Hywind Scotland (Burns et al. 2022), with the addition of the 25 Hz decidecade band which contains the prominent tone identified in Sections 3.1 and 3.2. Data from the beginning of the recording campaign up to 25 April 2024 was considered to avoid contamination from the seismic survey noise.

The correlation coefficient,  $\rho$ , presented above each figure in this section indicates the strength and direction of any monotonic correlation, i.e. a check if the data series is entirely non-decreasing or non-increasing. The magnitude of correlation coefficient indicates the strength of correlation, while the sign indicates direction of correlation, i.e. a value of 1 indicates perfect positive correlation, -1 indicates perfect negative correlation, and 0 indicates no correlation.

A comparison of wind speed with the rotor RPM averaged across all turbines is shown in Figure 33, with an evident strong positive correlation between the two parameters. A prominent upper governed limit of the rotor, at 10.5 RPM, is evident as the wind approaches 20 kn, with this limit never exceeded regardless of the increase in wind speed above this. There is also an apparent lower limit of the rotor at approximately 3.5 RPM, though it is not clear whether this is a true minimum RPM of the system or if wind and rotor speeds below this are not reported in the software. The rotor RPM appears to increase approximately linearly from the minimum to the maximum RPM between approximately 8 kn and 20 kn.

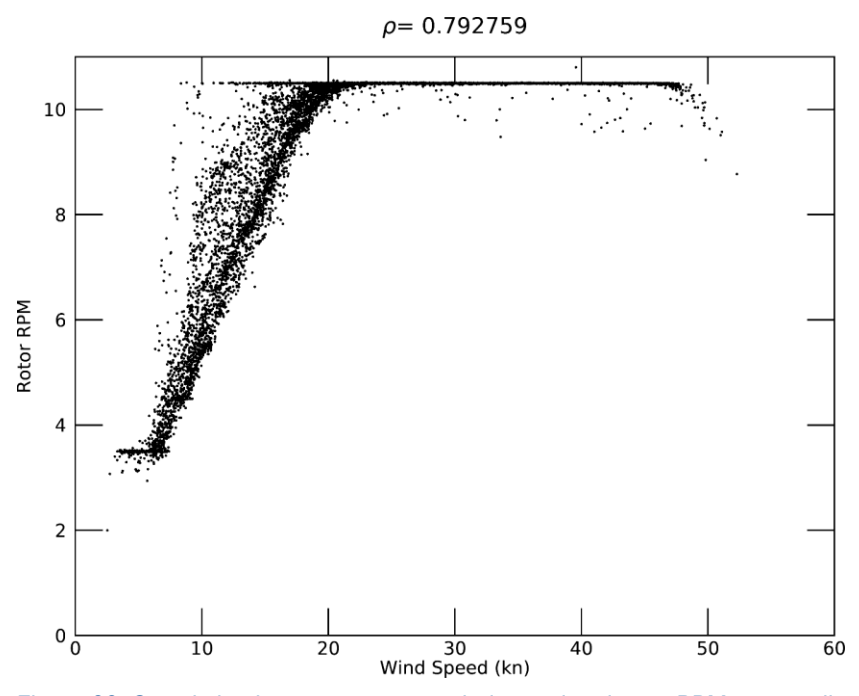


Figure 33. Correlation between average wind speed and rotor RPM across all turbines.

## 3.3.1. Correlation With Wind Speed

Results of correlation analysis between wind speed and the sound levels in the selected decidecade bands are shown in Figures 34 to 37. The plots indicate a strong positive correlation between wind speed and levels in the 25 Hz band (associated with the strong tone seen throughout many

recordings), and weak to moderate positive correlation in the 20 Hz band, as evidenced in Figures 34 to 37. The test for correlation only considers a monotonic relationship, while the relationship between wind speed and levels in these bands appears to be somewhat more nuanced, particularly at Stations 1 and 3 closer to the turbines. In these plots, there appears to be an increase then decrease in levels in the 20 Hz band centred on a wind speed of approximately 15 kn, before a more gradual increase in levels with wind speed. Similarly, in the 25 Hz band there appears to be reduction in levels centred on this same wind speed, before a rapid increase in levels with wind speed and an apparent plateau. Given the relationship between wind speed and rotor RPM observed in Figure 33, this supports the observation that the fundamental tone described by Equation 1 is related to the generator rotation rate rather than wind speed directly; the relationship with RPM is explored in more detail in Section 3.3.2. Correlation between levels in the 80 Hz decidecade band (which contains the tone at approximately 75 Hz; Figures 34 to 37) varies from strong to weak with increasing distance from the wind turbines. This 75 Hz tone is also rotationally related to the turbines by a factor of three as described in Equation 2, but does not appear to be as strongly discernible as the fundamental tone at distance.

All four stations show moderate to strong positive correlation between average wind speed and levels in the 3,150 and 12,500 Hz decidecade bands (Figures 34 to 37). Levels in this frequency range are known to increase with increasing surface agitation as caused by increasing wind speed (Wenz 1962). Conversely, all four stations show only very weak correlation between wind speed and sound levels in the 630 Hz band (Figures 34 to 37), indicating there is little turbine related noise or wind agitation related noise in this band.

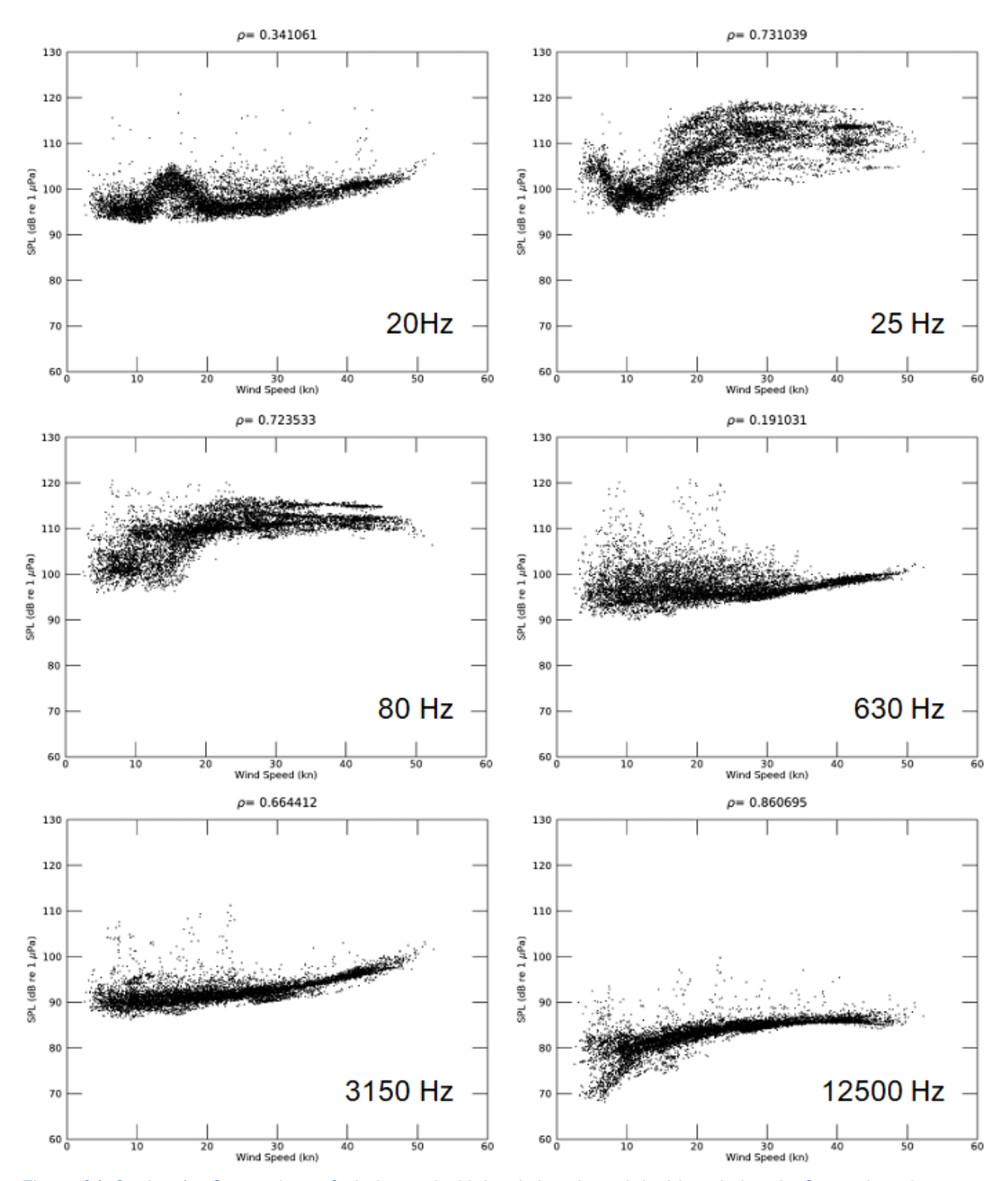


Figure 34. Station 1 – Comparison of wind speed with levels in selected decidecade bands. Strength and direction of correlation between average wind speed in knots across all turbine nacelles compared to levels in the stated decidecade bands.

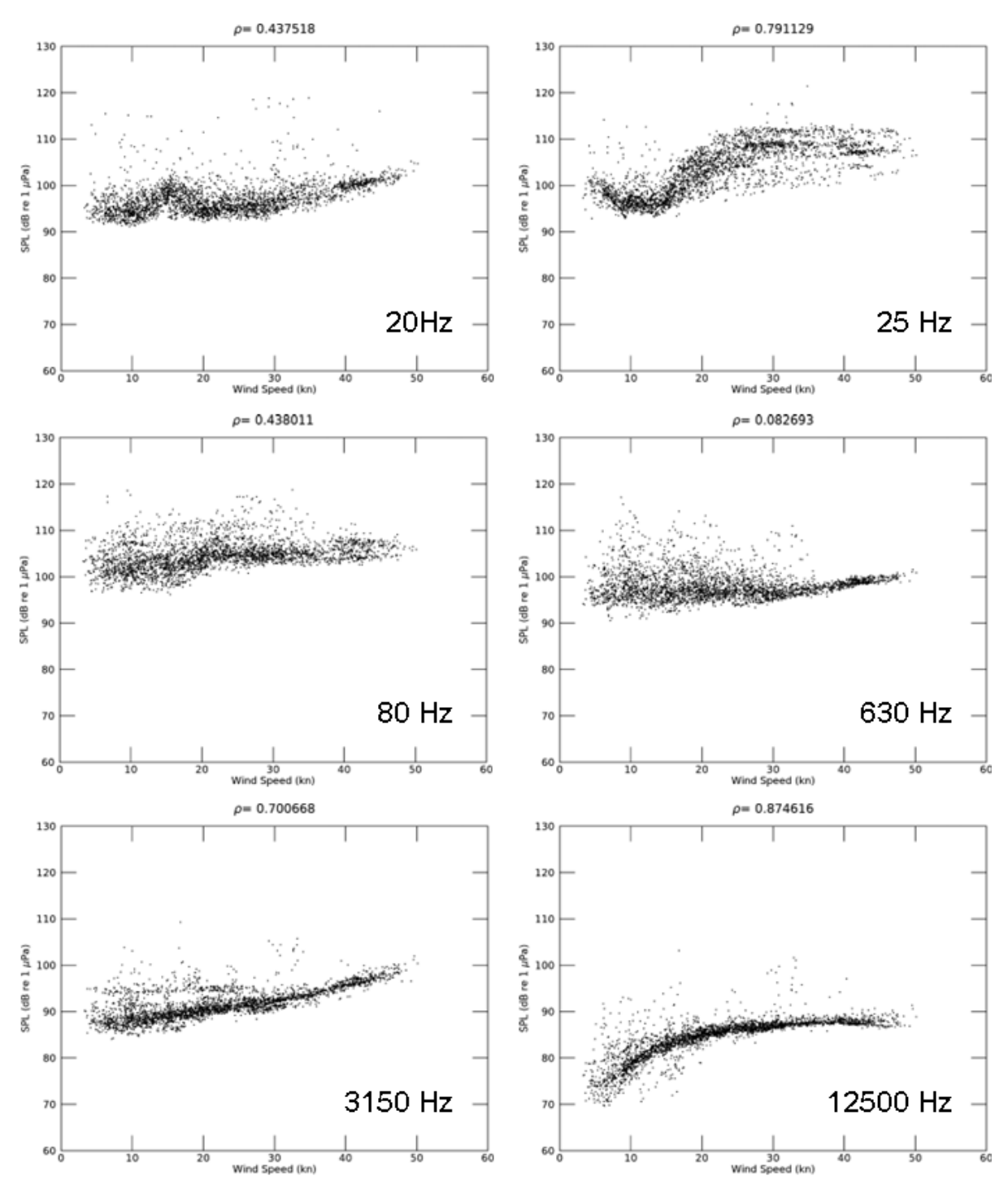


Figure 35. Station 2 – Comparison of wind speed with levels in selected decidecade bands. Strength and direction of correlation between average wind speed in knots across all turbine nacelles compared to levels in the stated decidecade bands.

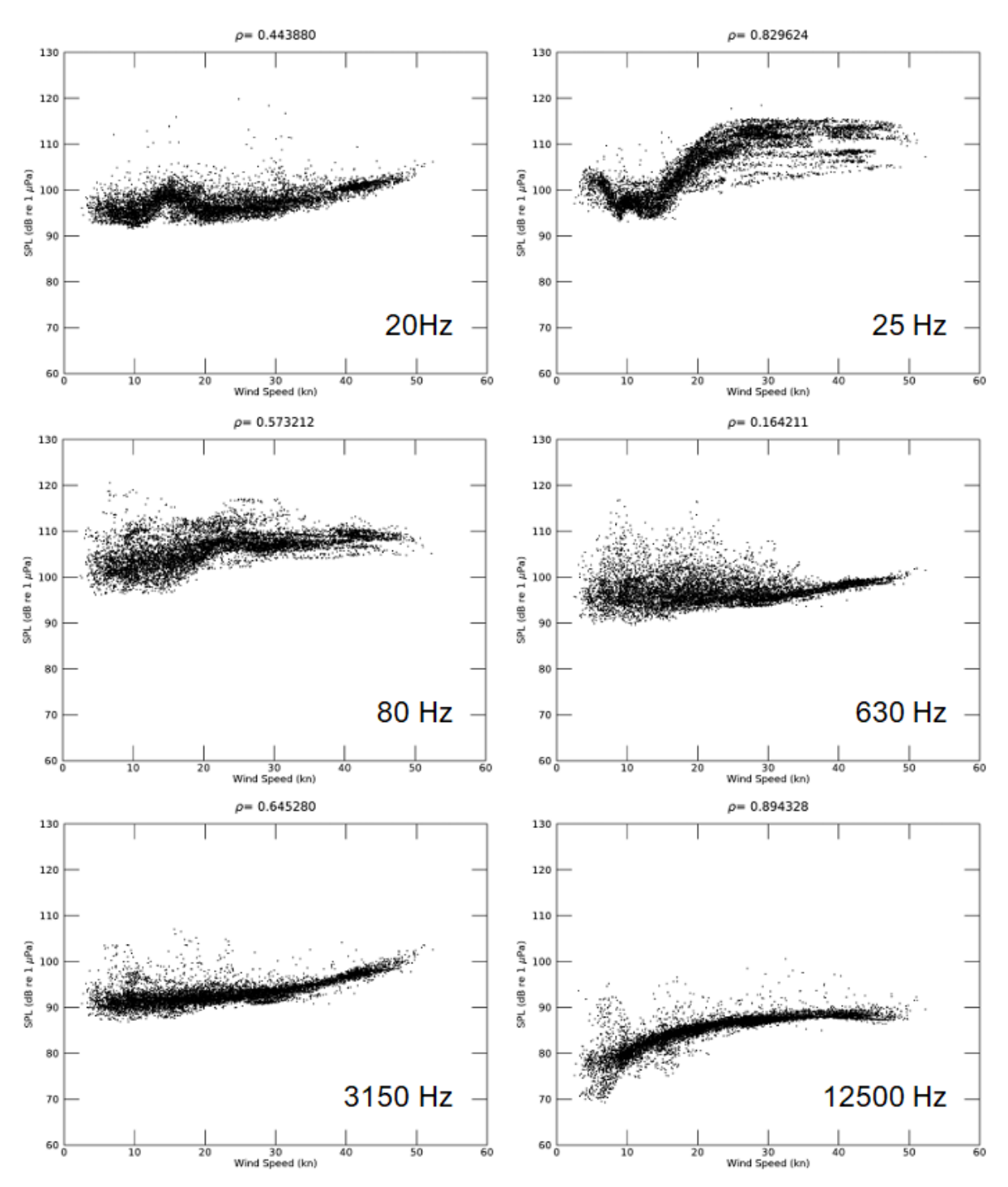


Figure 36. Station 3 – Comparison of wind speed with levels in selected decidecade bands. Strength and direction of correlation between average wind speed in knots across all turbine nacelles compared to levels in the stated decidecade bands.

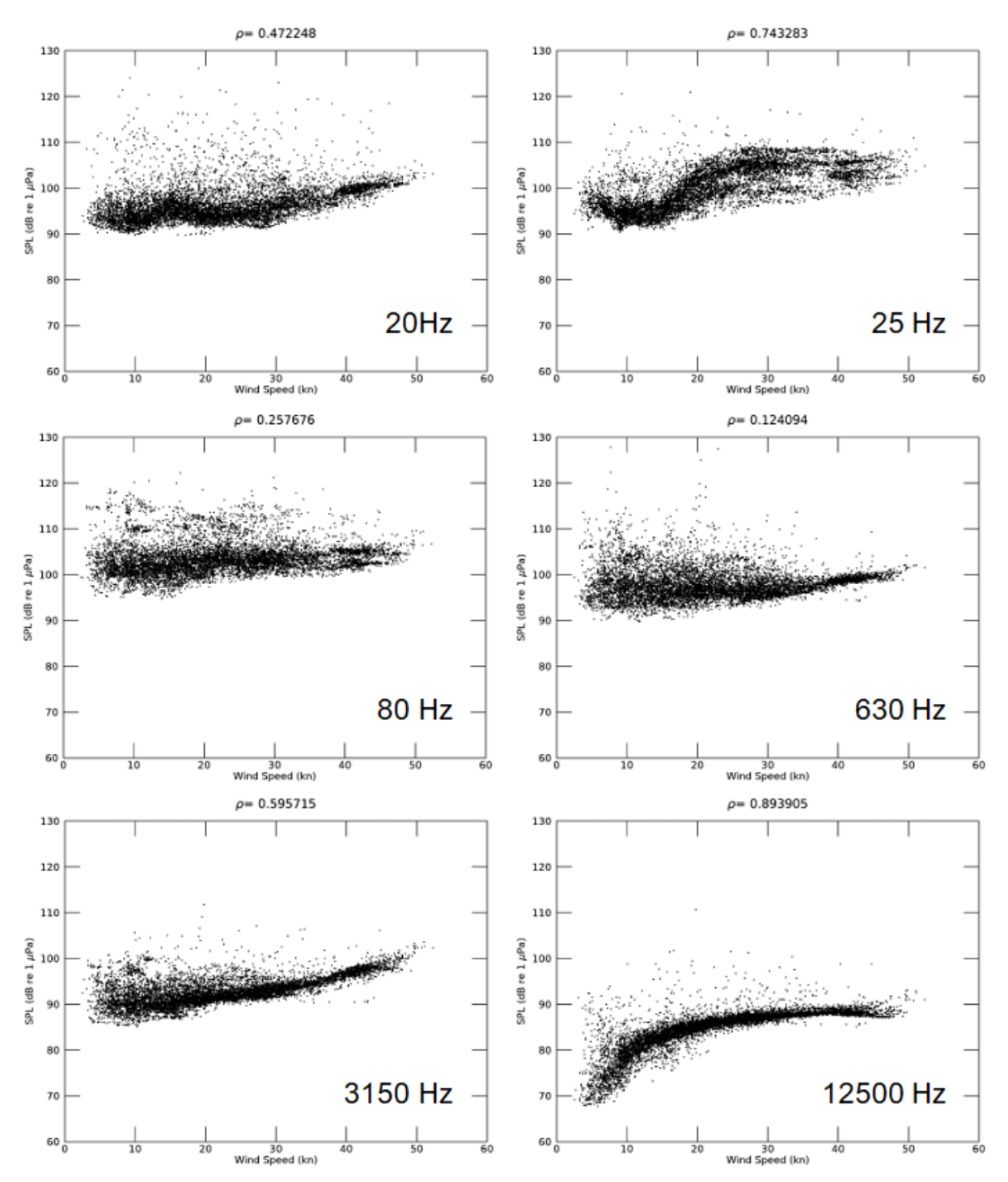


Figure 37. Station 4 – Comparison of wind speed with levels in selected decidecade bands. Strength and direction of correlation between average wind speed in knots across all turbine nacelles compared to levels in the stated decidecade bands.

#### 3.3.2. Correlation With Rotor RPM

Results of correlation analysis between rotor RPM and the sound levels in the selected decidecade bands are shown in Figures 39 to 42. Similar trends can be observed in these figures as in Section 3.3.1, however, given the apparent upper and lower limit of rotor RPM (Figure 33) this results in large clusters of data points at these limits.

There remains very weak to no correlation in the 630 Hz band, and moderate correlation in the 3,150 and 12,500 Hz decidecade bands. As explained in Section 3.3.1 however the correlation in the latter two bands is more likely a result in an increase in surface agitation due to wind speed.

There again appears to be a somewhat nuanced, nonmonotonic relationship between rotor RPM and levels in the 20, 25, and 80 Hz bands. In the 20 Hz band, there appears limited change in level with increasing rotor RPM except for a small increase and decrease in levels centred around approximately 8.5 RPM. In the 25 Hz band, levels appear to decrease between 3.5 and 7 RPM, before increasing again between 7 and 10.5 RPM. Finally in the 80 Hz band, there appears a gradual increase in levels with increasing rotor RPM, with a slightly sharper increase as RPM reaches the maximum. These trends can be explained by examining the change in the fundamental and triplet tones described by Equations 1 and 2 with increasing rotor speed compared to these bands, illustrated in Figure 38. The fundamental tone reaches the 20 Hz band at a speed of approximately 7.5 RPM, and this tone exceeds the upper edge of the 20 Hz band at approximately 9.5 RPM, explaining the slight crest in levels centred around 8.5 RPM seen in Figures 39 to 42. In the 25 Hz band, the triplet of the fundamental tone is 25.2 Hz at 3.5 RPM, but as RPM increases the triplet tone exceeds the upper edge of the 25 Hz band above approximately 4 RPM, corresponding to the initial decline in levels. As RPM further increases towards maximum, the fundamental tone eventually reaches a maximum of 25.2 Hz at 10.5 RPM, corresponding to the subsequent increase in levels in this band. In the 80 Hz band the triplet tone approaches the maximum of 75.6 Hz with increasing RPM, with this tone reaching the 80 Hz band above 10 RPM, explaining the steeper increase in levels above this rate in Figures 39 to 42.

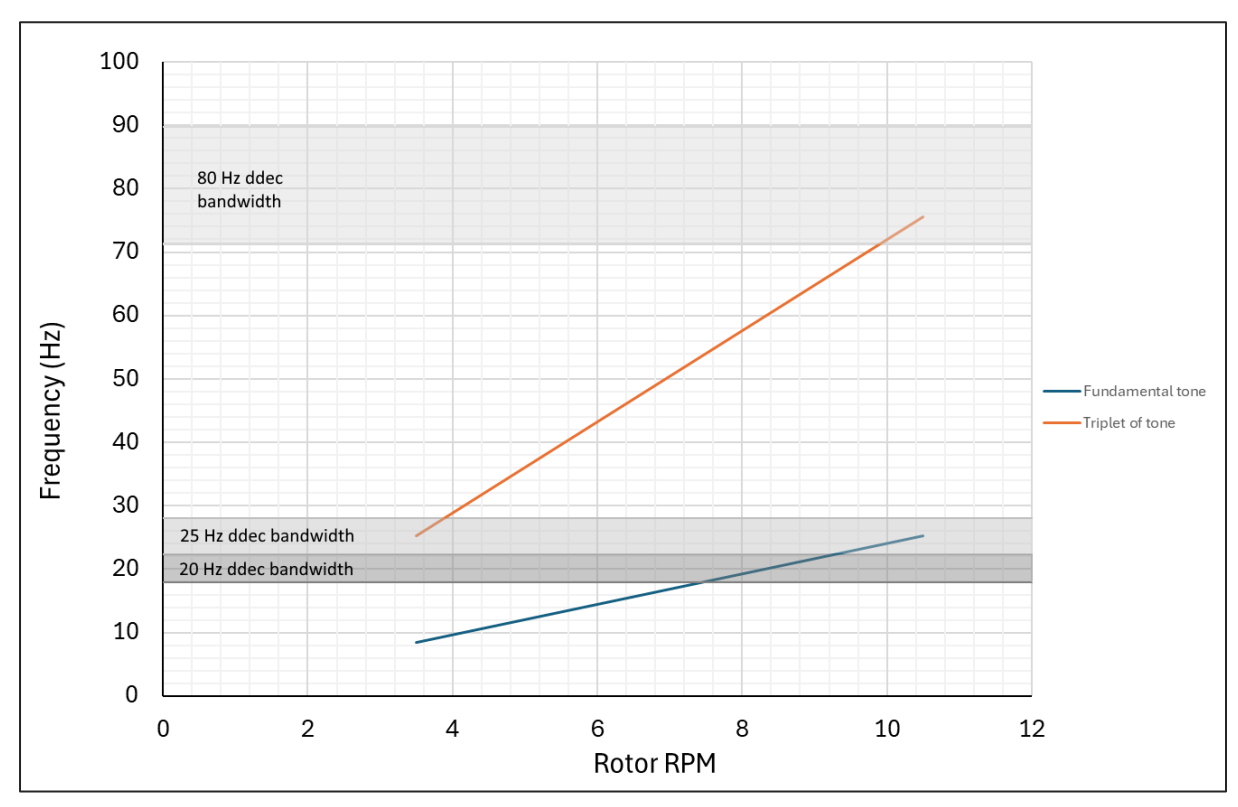


Figure 38. Relationship between identified rotor related tones and rotor speed, with decidecade (ddec) bandwidths of interest highlighted. The blue line (fundamental tone) is described by Equation 1 and the orange line (triplet of tone) is described by Equation 2.

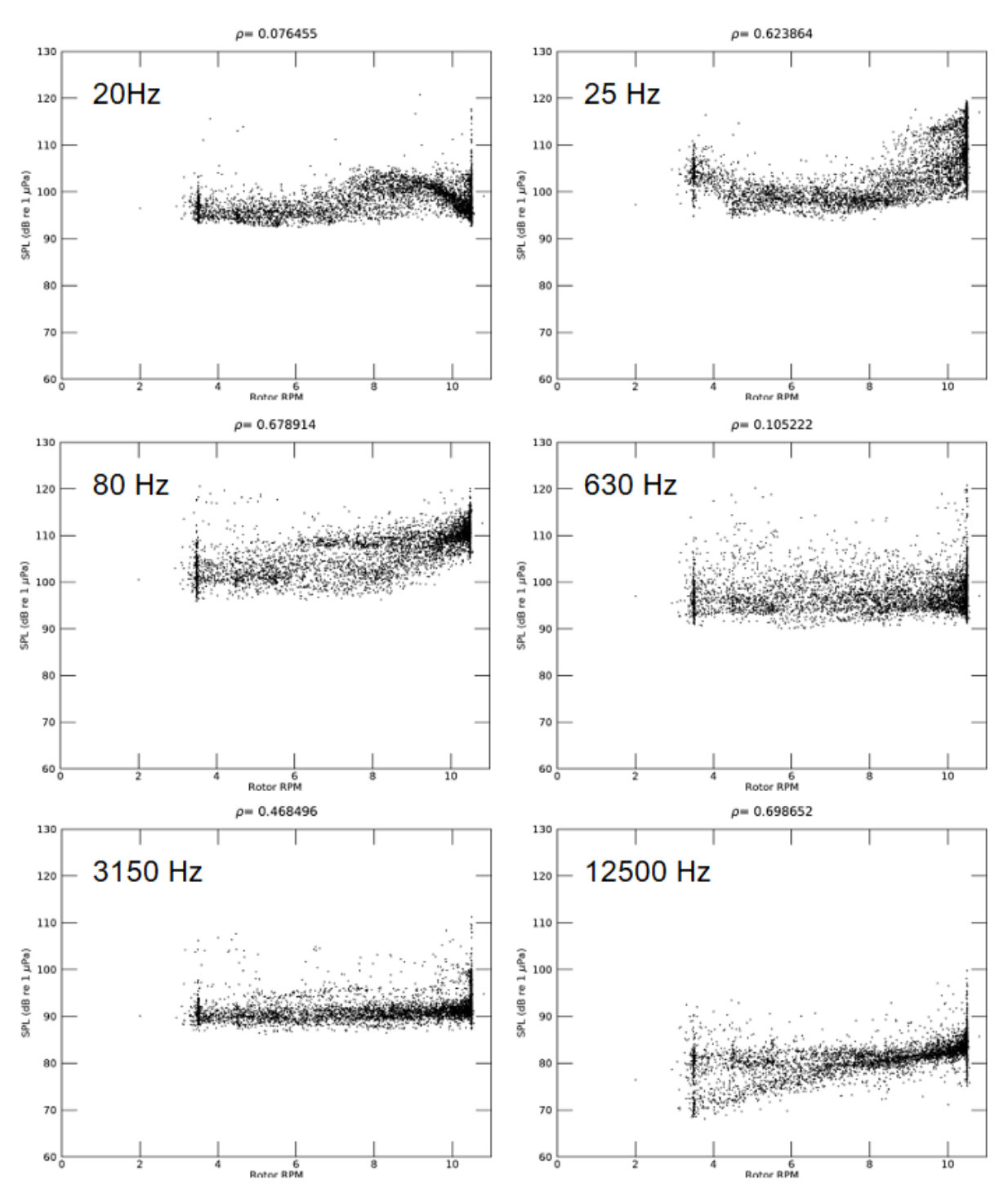


Figure 39. Station 1 – Comparison of rotor RPM with levels in selected decidecade bands. Strength and direction of correlation between average wind speed in knots across all turbine nacelles compared to levels in the stated decidecade bands.

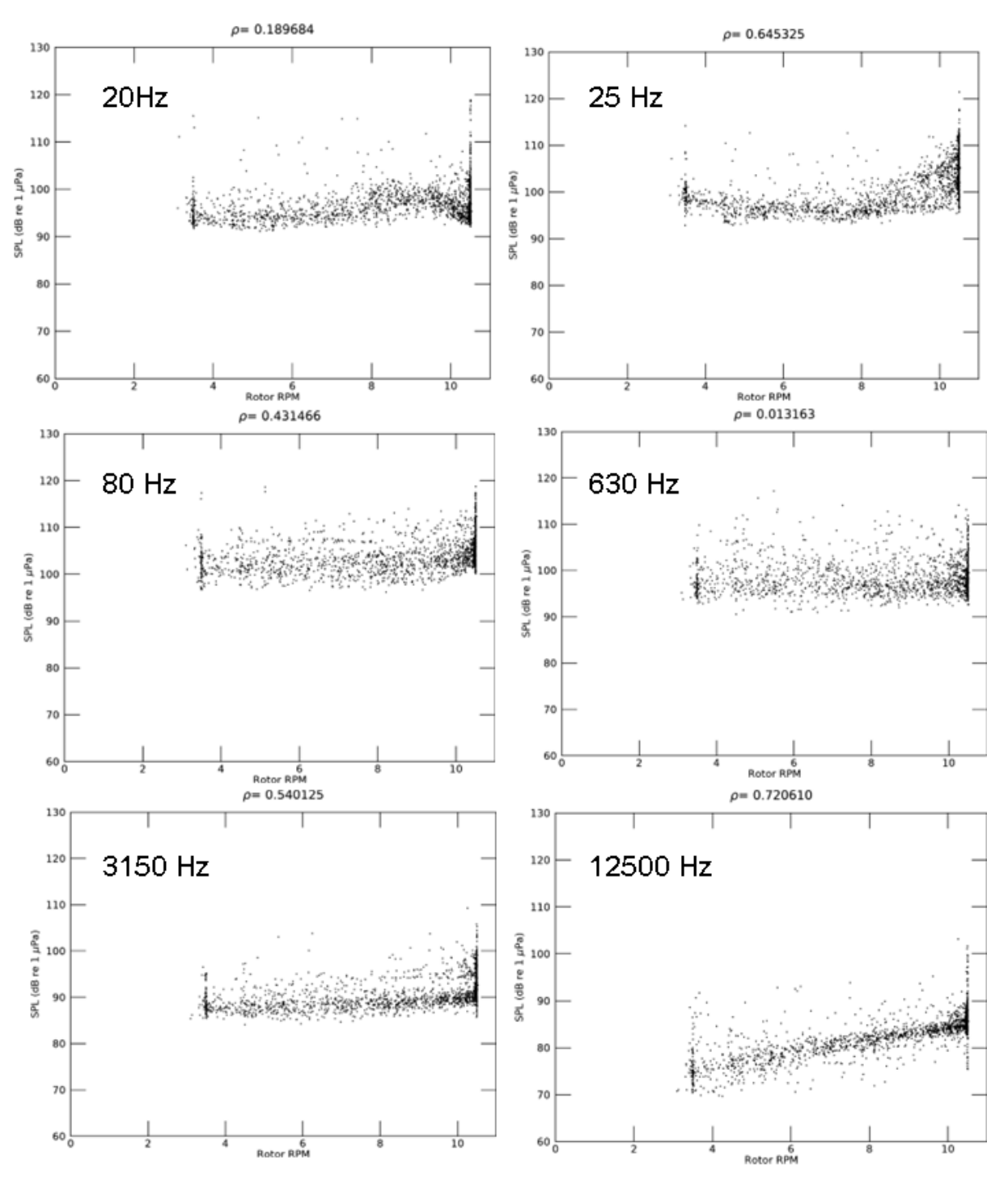
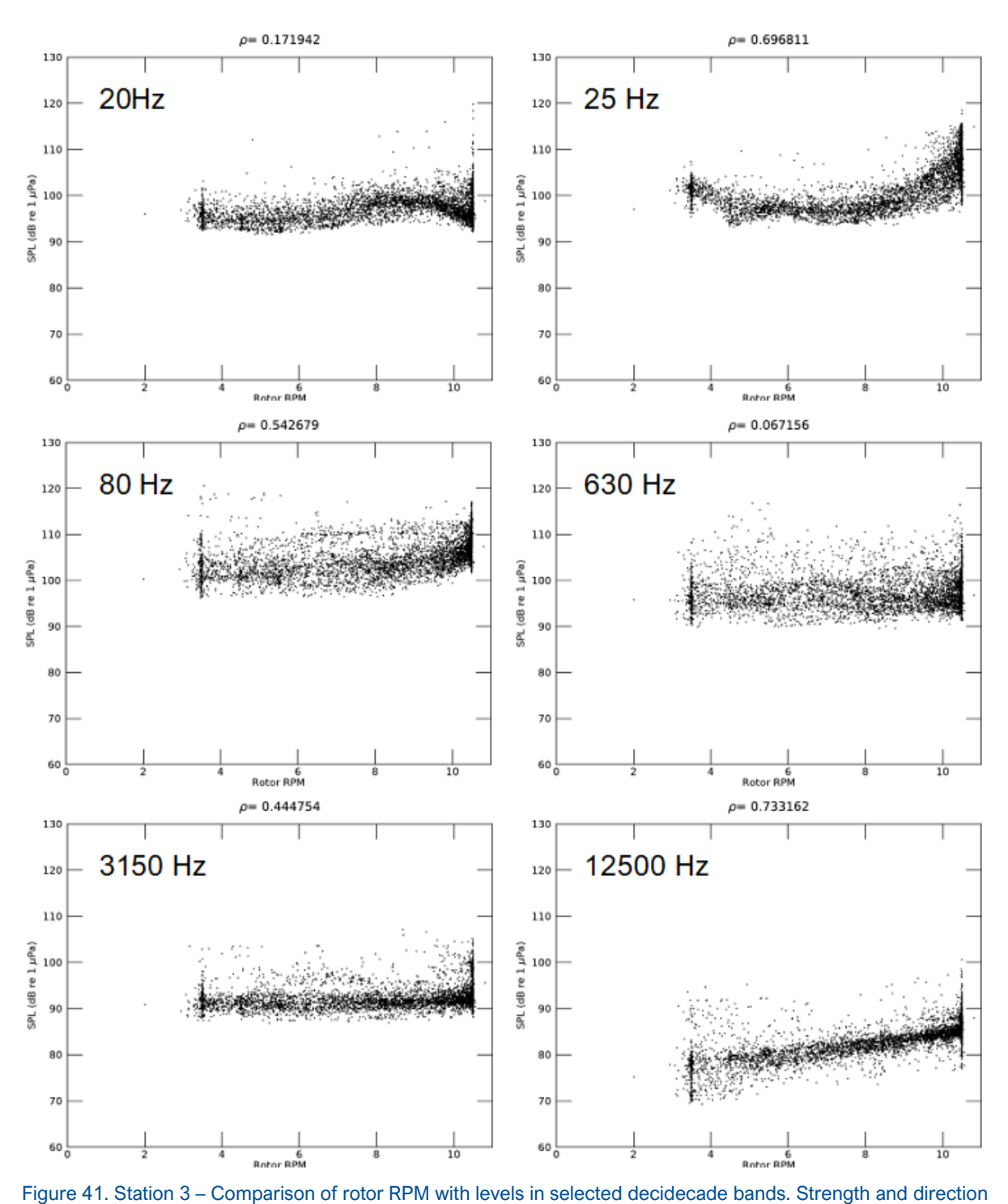


Figure 40. Station 2 – Comparison of rotor RPM with levels in selected decidecade bands. Strength and direction of correlation between average wind speed in knots across all turbine nacelles compared to levels in the stated decidecade bands.



of correlation between average wind speed in knots across all turbine nacelles compared to levels in the stated decidecade bands.

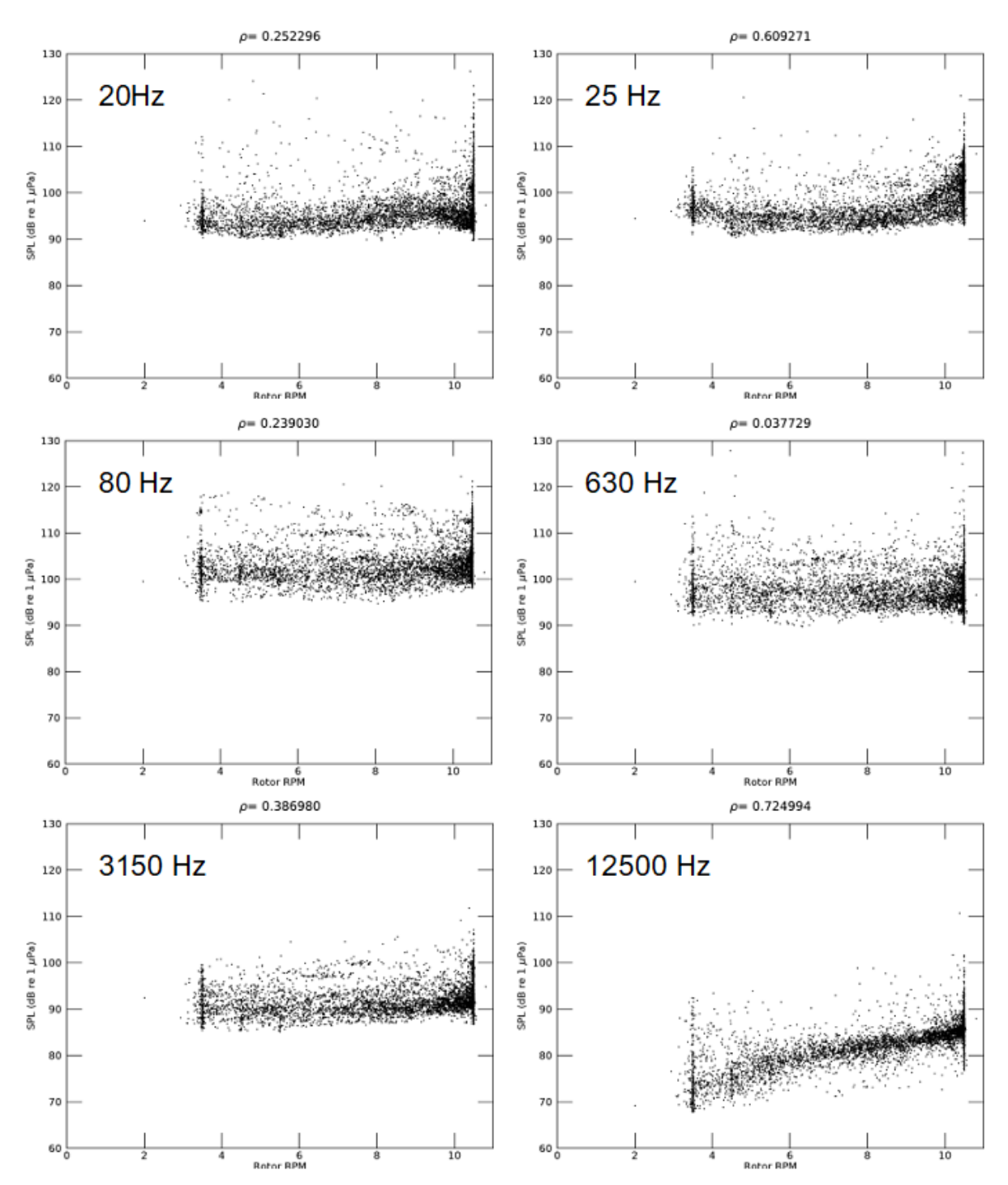


Figure 42. Station 4 – Comparison of rotor RPM with levels in selected decidecade bands. Strength and direction of correlation between average wind speed in knots across all turbine nacelles compared to levels in the stated decidecade bands.

## 3.3.3. Comparison With Distance to Closest Turbine

A comparison between the omnidirectional broadband received levels and distance from the nearest turbine is shown in Figure 43 for wind speed bins from 5 to 40 kn; underlying data for this plot is presented in Appendix F. Given the spatial distribution of the turbines, the relative proximity between the recording stations and the turbines, and the lack of a single connecting transect between all recording stations, there is no appropriate single reference point from which to measure distance.

Consequently, the distances for each station are referenced to the nearest turbine to give a rough approximation of the decay of broadband sound levels over distance.

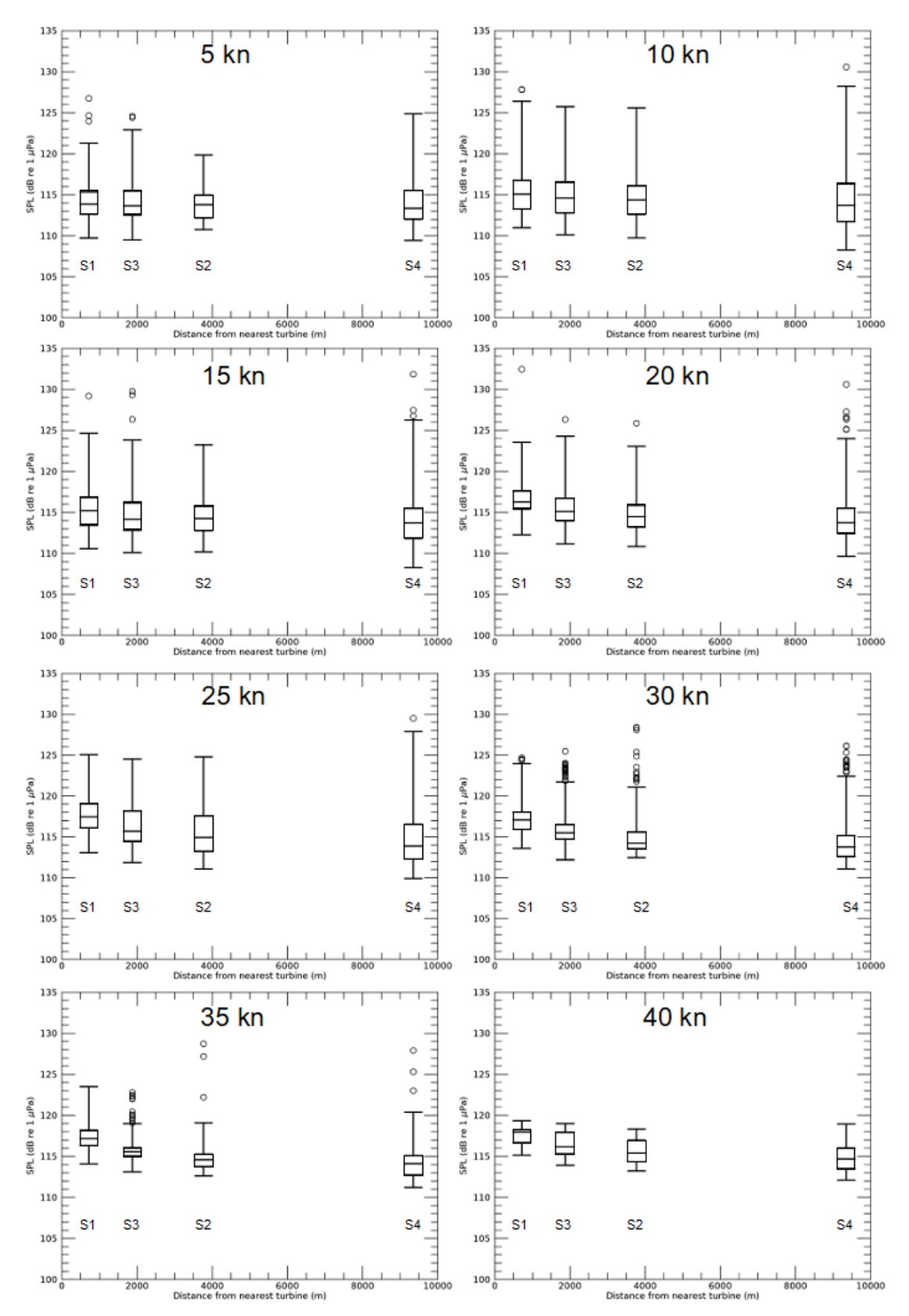


Figure 43. Comparison of broadband received levels at each Station with distance from the nearest wind turbine for wind speed bins from 5 for 40 kn. Station numbers indicated below each box plot. Data for these plots are presented in Appendix F.

The plots indicate there is a slight reduction in median broadband sound levels with increasing distance from the turbines, indicating that the sound from the turbines is above ambient sound levels close to the wind farm. The spectra presented in Section 3.1 indicate that some turbine noise is still audible at Station 4, almost 10 km from the nearest turbine, and it is unclear how much of the broadband signal at this distance is part of the ambient soundscape.

## 3.4. Directional Analysis of Recorded Noise

### 3.4.1. Methodology and Presentation of Directional Data

The four hydrophone channels on the AMARs at Stations 1 and 2 allow the spatial discrimination of bearing and elevation of detected sound, as outlined in Appendix C. The analysis was performed using a maximum likelihood estimation (MLE) beamformer (Urazghildiiev and Hannay 2017). This beamformer estimates the sound level assuming the sounds are arriving from azimuthal bins that are 15 degrees wide (total of 360/15=24 bins), and for each azimuth it evaluates 3 elevation angles 30 degrees wide (from horizontal to vertical for a bottom-mounted recorder; 90/30=3), for a total of 24x3=72 'look directions' or beams. The beam with the greatest received sound level is selected as the most likely direction of arrival for each time-frequency bin. Broadband impulsive events are relatively easy to process for directionality as they offer a wide range of frequencies to contribute to the processing compared to tonal noise which, while continuous in nature, offers a typically narrow band of frequencies to the process due to their narrow bands.

The orientation of each directional array on the seafloor was determined using the ROV onboard compass and camera during both deployment and retrieval. Additionally, the acoustic signature of the *Skandi Iceman* immediately after deployment was correlated with known positions obtained from the vessel's GPS track log to confirm the orientation of the directional arrays. Bearings and distances between the directional recording instruments and each of the turbines were calculated using GIS software and are presented in Table 6. A description of the directional analysis is contained in Appendix B.

Table 6. Distances and bearings of each of the wind turbine generators (WTGs) from the two directional Autonomous Multichannel Acoustic Recorders (AMARs) deployed.

Location	Statio	on 1	Station 2		
	Distance (m)	Bearing (°)	Distance (m)	Bearing (°)	
HY01	6803	345.6	9258	322.3	
HY02	5299	345.6	7897	318.0	
HY03	3795	345.7	6598	312.0	
HY04	2291	345.9	5407	303.2	
HY05	788	347.0	4412	290.0	
HY06	717	163.7	3770	270.8	
HY07	1281	257.0	5239	274.9	
HY08	2002	305.6	5912	288.8	
HY09	3302	322.6	6855	299.4	
HY10	4724	329.7	7972	307.2	
HY11	6185	333.5	9200	313.0	

The 'directograms' presented below apply a colour to audible noise processed for each beam according to the colour wheel shown in the top right corner of the gram. Beamforming allows for discrimination between noise sources in different directions and allows for the association of tones and other noises with a single unit. This is significantly more useful than omnidirectional recordings which can only present the aggregate noise field, captured in all directions.

Figure 44 shows a plot of the Tampen system positions and the recording geometry for directional array AMAR at Station 1 and the omnidirectional AMAR at Station 3. The position of Station 1 was selected to enable the directional isolation of HY06, to the South and HY07 to the West with no other Tampen WTG within, or close to those beamformed sectors. HY05 is partially isolated but other Tampen systems are relatively close to this direction and so the process of extracting measured levels of noise to describe a single Tampen systems was focussed only on HY06. The directional processing colour wheel is shown in the figure, and it remains fixed, relative to North, in all directograms in this report so the colour for each direction is constant. Effectively, all noise from HY06 predominantly light blue, HY07 dark blue and HY05 red.

The tonal noise identified radiating from each Tampen WTG in the omnidirectional recording analysis is clear in the directograms but now coloured according to source. The different rotation speeds of individual WTGs are clear, and it is notable that even systems relatively close to each other can rotate at significantly different rates at the same time, indicating a high degree of spatial variability in the wind speed across the area of the wind farm.

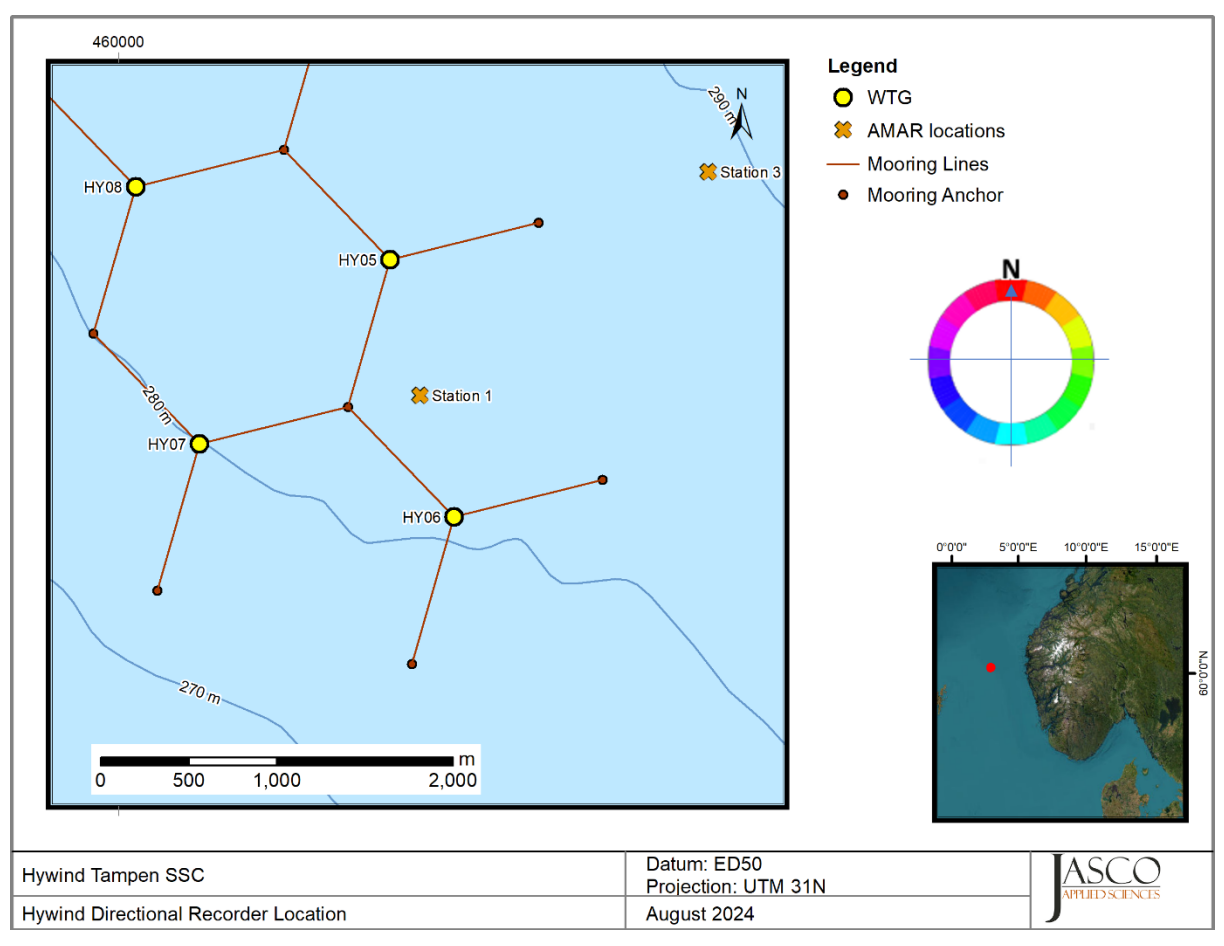


Figure 44. Relative positions of closest turbines to Station 1 and colour wheel orientation relative to North for directogram plots.

# 3.4.2. Directional Acoustic Analysis

Applying directional processing, without selecting a specific beam to display, provides colour discrimination of the direction of the source of all noise. Figure 45 shows overlapping generator fundamentals at ~25 Hz from all three of the nearest WTGs, HY05 (red), HY06 (light blue) and HY07 (dark blue) and the constantly changing colour between each of the WTG directional sectors (red, light blue and dark blue) suggests one tone is not significantly more dominant in intensity than the

others. At the rotor related tonal frequency, 75 Hz, the three different WTG inputs can also be seen but the tone from HY06 (light blue) is slightly dominant and overlies the noise from the other two systems. Some of the non-rotor related tones from the 15 Hz fundamental are faintly visible at harmonic intervals up to 180 Hz. In general, the source levels from each WTG appear to show considerable variability depending on power generation output and rotor speed, and so, even though HY07 is approximately 500m further from the recording instrument, it is unsurprising that it occasionally dominates the directional processing over HY05 and HY06.

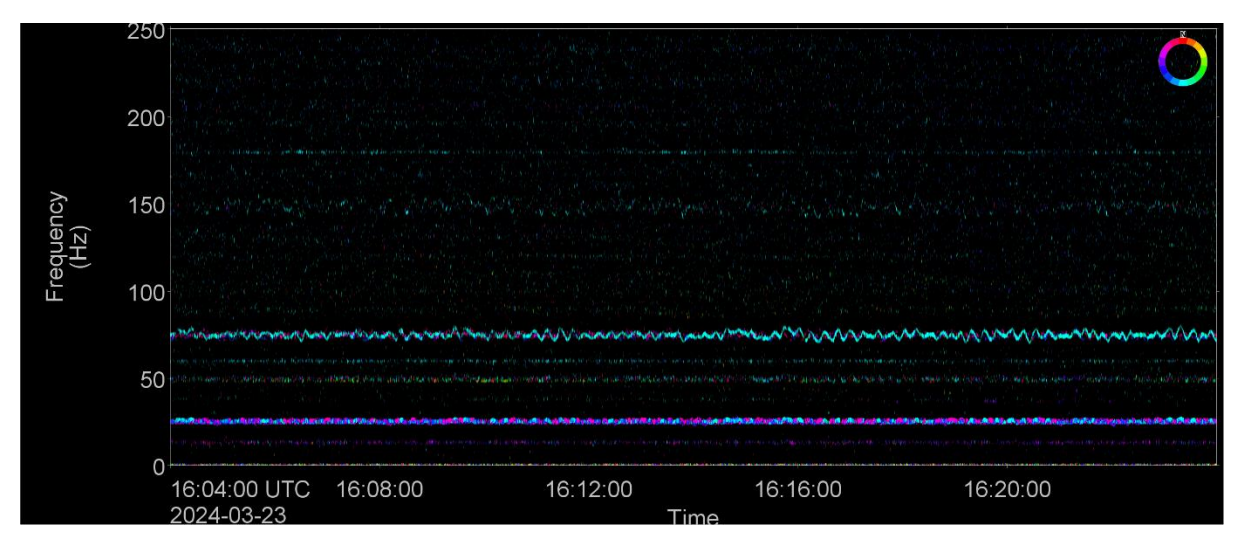


Figure 45. Overlapping generator and rotor tonals from HY05, HY06 and HY07, all at 10.5 RPM

Directional discrimination between HY05, HY06 and HY07 enables direct comparison of tonal values with the operating data for each WTG. On 8th March 2024, between 13:43 and 14:00 (UTC), analysis provides evidence that the relationship between wind speed and rotor rate is subject to a degree of variability and there is not a tight correlation. Figure 46 shows HY05 consistently operating at maximum rotor RPM (10.5) and generating the anticipated ~25 Hz generator and ~75 Hz rotor tones but the 10-minute average wind speed at that nacelle is just 11.3 kn. Conversely, during the same period, HY06 and HY07 can both be seen producing a ~18 Hz generator and ~55 Hz rotor tone (the HY06 rotor tone dominates whereas the HY07 generator tone is slightly louder) which corresponds to the operational data rotor rate of 7.5 RPM, but in a wind speed of 14.8 kn at the HY06 nacelle and 15.0 kn at the HY07 nacelle.

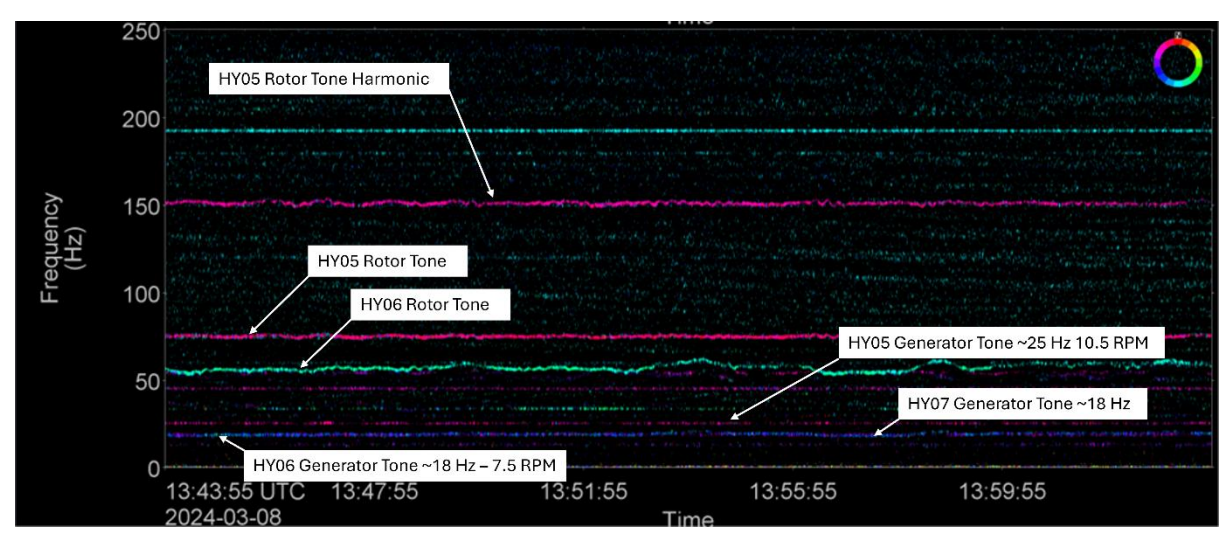


Figure 46. Directogram showing different noise outputs from three WTGs, and inconsistency of rotor rate with wind speed.

The inference from this finding is echoed in the statistical analysis in Section 3 of wind speed against rotor rates for all WTGs in the wind farm which shows a number of outlying combinations (Figure 33) where wind speeds considerably below 20 kn appear to be able to turn the rotor at its maximum 10.5 RPM rate and, conversely, the rotor rate at higher wind speeds is somewhat less than a tight, linear relationship would predict.

Focussing the directional analysis at Station1 on the direction of HY06, Figure 47 shows the primary generator tone at ~25 Hz and the rotor rate tone at ~75 Hz and fainter tones and harmonics (30 Hz and 60 Hz) from the fundamental at 15 Hz. Both loud, rotationally related tones are fractionally below the expected frequency for a rotor speed of 10.5 RPM and the operating data for HY06 for the 30-minute period around this time confirms that the RPM was, indeed, dipping slightly below the maximum limit at times.

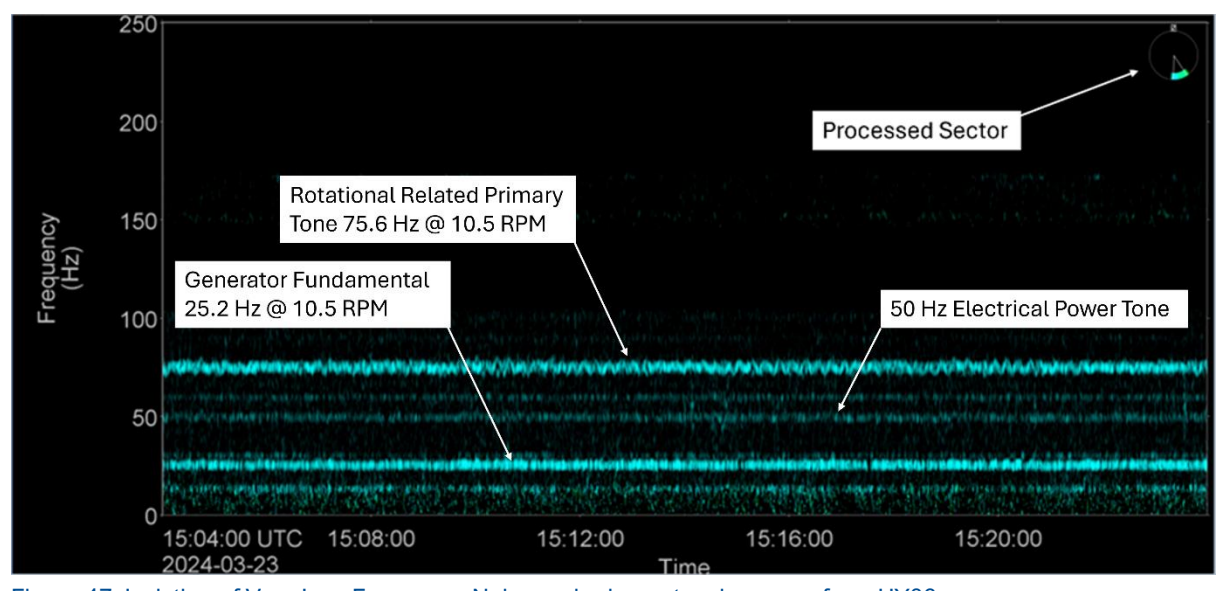


Figure 47. Isolation of Very Low Frequency Noise and primary tonal sources from HY06

# 3.4.3. Received Levels from a Single Turbine

Due to the distance of the directional recorder at Station 2 and the beamwidths achievable with the directional processing (Section 3.4.1), it was not possible to accurately isolate sound levels from the single HY06 system without contamination from nearby turbines. Received levels were therefore extracted from the recording at Station 1 only, for wind speed bins in 5 kn increments as described in Section 3.2. Directional analysis was used to ensure that only contributions from the direction of HY06 were contributing to the received level. Data were extracted in one-minute intervals and stored as power spectral densities and decidecade band levels. At higher frequencies the spectral data were extracted in millidecade bands (Martin et al. 2021); millidecades are logarithmically spaced frequency bands but have a bandwidth equal to one-thousandth of a decade rather than one-tenth for decidecades. Using millidecades reduces the size of the spectral data by a large factor without compromising the usefulness of the data.

Decidecade band levels are presented in Figure 48, while power spectral densities (PSDs) are presented in Figure 49. Levels in decidecade bands are higher than the spectral levels because the decidecade levels include the energy of all frequencies within that band. This difference becomes more exaggerated with increasing frequency as decidecade bandwidth increases. Additionally, energy contained within spectral peaks may be shared between multiple decidecade bands if, for example, the peak spans the edge of two bands. Peaks and trends observed in the spectrum may not, therefore, be directly reflected in the decidecade band levels. More information on decidecade band and spectral analysis is presented in Appendix A.2.

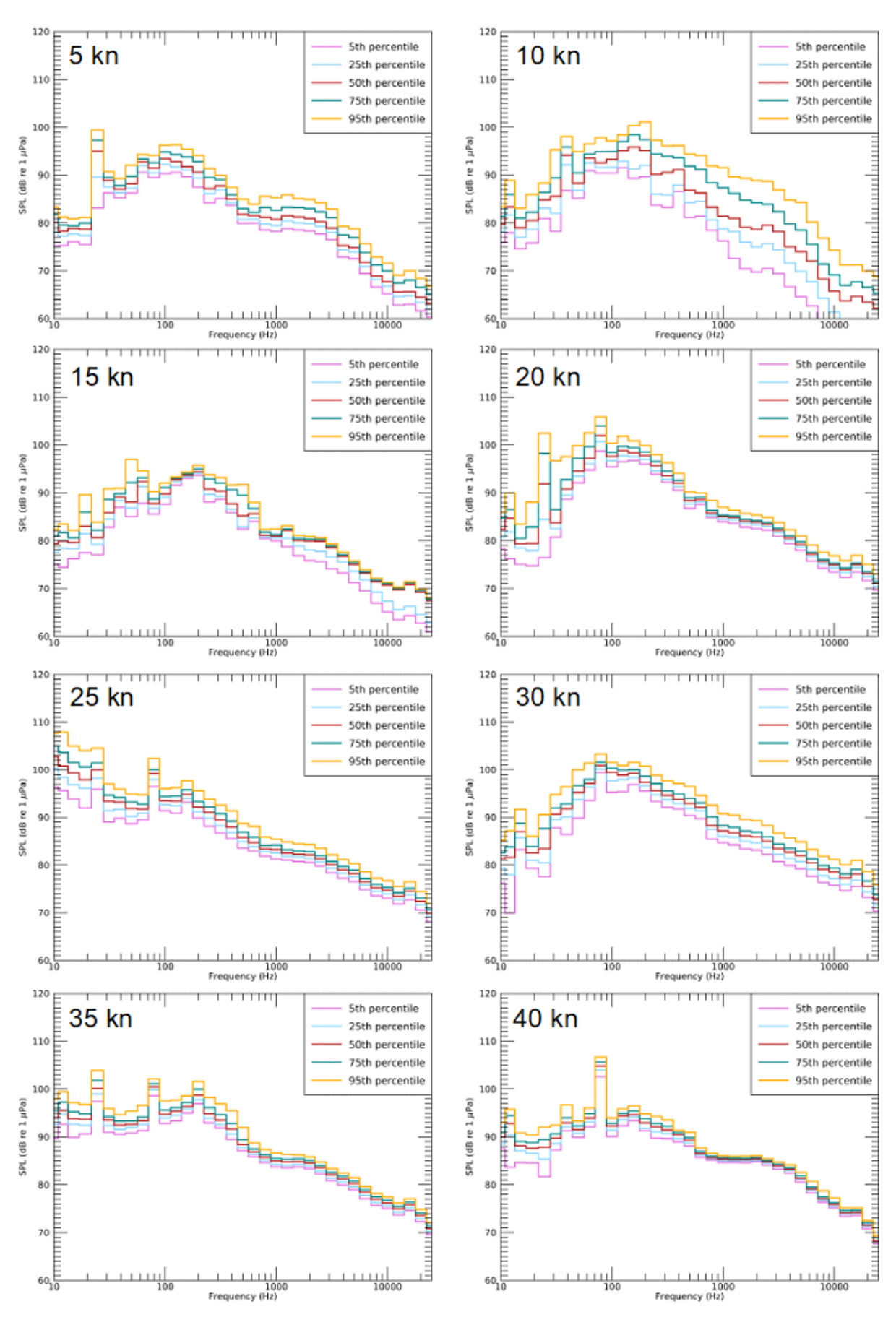


Figure 48. Received SPL at Station 1 in decade bands in the direction of HY06 for various wind speed bins. In each bin, the wind speed was ±1 kn of the stated speed.

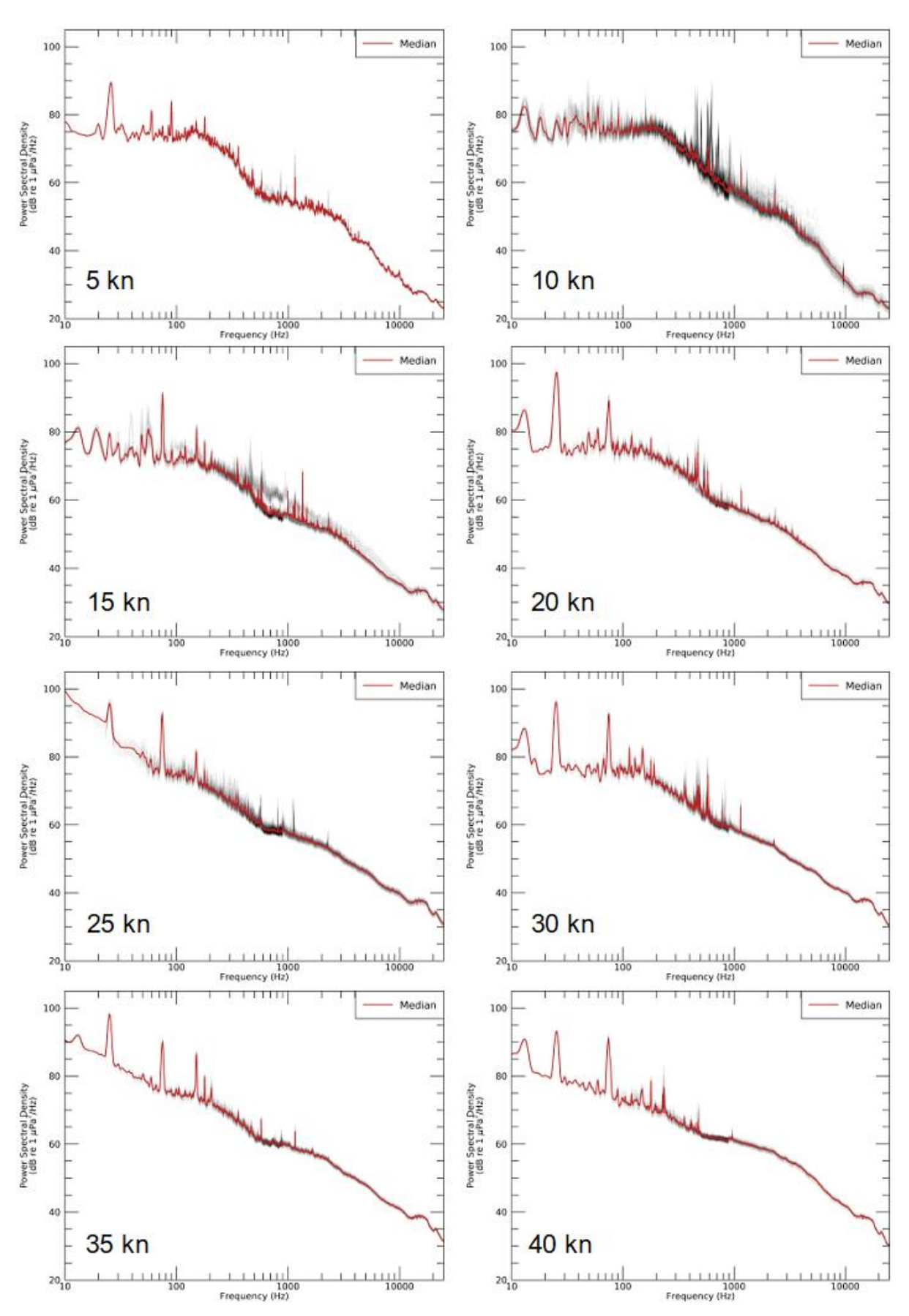


Figure 49. Median power spectral densities at Station 1 from the direction of HY06 for various wind speed bins. The black lines represent the individual spectra used to take the median. In each bin, the wind speed was  $\pm 1$  kn of the stated speed.

The plots shown in Figures 48 and 49 show similar trends for all wind speeds, with elevated levels at frequencies up to approximately 200 Hz, with a steady decline in levels above this. In some wind speed bins, for example 10 and 15 kn, the PSDs appear to vary from the median to a moderately large degree while others appear to conform better to the median for the entire duration; evidenced by the greater spread of the spectral lines in black or lack thereof. The wind speed periods for 25 and 35 kn appear to suffer from a degree of unknown low frequency contamination, hence levels are higher at frequencies below 20 Hz than for other wind speeds.

The PSDs in Figure 49 for wind speeds above 20 kn show sharp spikes around the tone at 75 Hz, which is also reflected in the decidecade spectra in Figure 48. This corresponds with the observation from Section 3.3 that levels in the 80 Hz decidecade band increase up to approximately 20 kn wind speed before reaching somewhat of a plateau. These wind speeds, along with the 5 kn spectrum, also show sharp spikes around the 25 Hz tone which appears absent from the 10 and 15 kn spectra. All the PSDs also display multiple smaller spikes between approximately 100 and 2000 Hz, which may be evidence of other machinery or electrical tones as discussed in Section 3.2.2.

### 3.4.4. Turbine Sound Field Directionality

In addition to determining sound levels from HY06, the placement and directional processing capability at Station 1 allowed for determination of levels in the direction of a second, more distant individual turbine to the southwest, HY07. A comparison of received sound levels from the two different turbine directions is considered in this section to understand whether the Hywind Tampen wind turbines display any noticeable difference in levels which may indicate a degree of horizontal directionality to the propagated sound field.

Figure 50 shows a comparison of levels in the 79 Hz decidecade band (associated with the 75 Hz tone) between the HY06 and HY07 directions. In order to compensate for the difference in propagation path length between the AMAR and the two different turbines (see Table 6), propagation loss in this band was modelled along the two source-receiver paths and levels in the direction of HY07 were increased accordingly; details of propagation loss modelling are presented in greater detail in Sections 4.1 and 4.2. Since the 75 Hz tone is only observed when the turbines are operating at maximum RPM (see Sections 3.2.1 and 3.3.2), as expected there are far greater differences between the two turbines at wind speeds below 20 kn. At wind speeds of 30 kn and above, the spread of differences is generally less pronounced, and seems to mostly be centred around 0 indicating little to no difference in levels between the two turbines for equivalent wind speeds. At 20 kn wind speed levels appeared to tend slightly higher from HY06, while at 25 kn wind speed levels were higher from HY07. This may be due to differences in operation of the two turbines at the time, or potential contamination in the respective directions from other noise sources during the time wind speed windows.

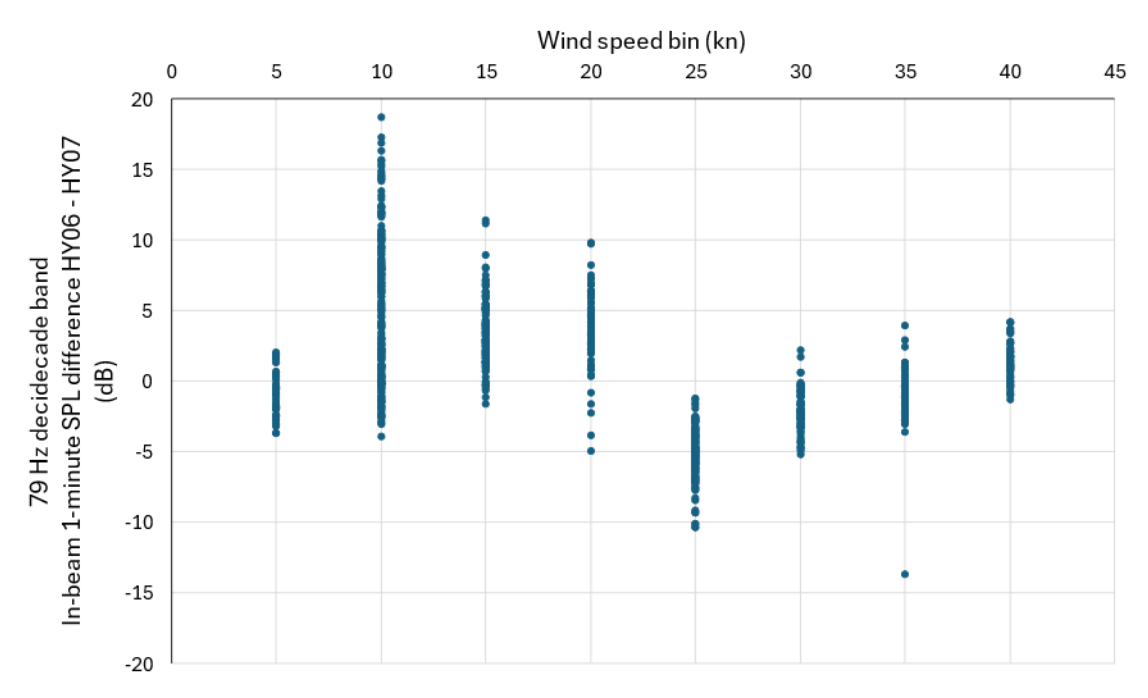


Figure 50. Difference in received levels between beam pointed towards HY06 and beam pointed towards HY07. Positive difference indicates levels in HY06 direction were greater. Received levels in direction of HY07 have been adjusted to account for difference in source-receiver distance.

## 3.5. Marine Strategy Framework Directive Descriptor 11

The Marine Framework Strategy Directive (MFSD) of the European Union employs the average sound pressure level in the 63 and 125 Hz decidecade bands as indicators of good environmental status. The data from all stations were analysed in decidecade frequency bands over one-minute analysis windows. In addition to the redacted period, data between 22 May and 25 September were excluded from this analysis due to the contamination from the apparent seismic surveys. Figure 51 shows the distribution of sound pressure levels for the two relevant decidecade bands for each of the four stations during the specified period. Median levels in both bands were similar for both Station 1 and Station 3 (within 0.3 dB difference) which reflects the proximity of the two recorders to both each other and the Tampen turbines. Median levels at Stations 2 and 4 were 0.8-1.3 dB below the other two stations in the 63 Hz band, but approximately the same in the 125 Hz band (0-0.3 dB difference). All four stations feature several outliers above the whiskers, however, their distance from the median and upper percentiles highlights how relatively infrequent these periods of elevated noise were for these two decidecade bands. Median levels in the 63 Hz band are marginally higher at all four Hywind Tampen stations than the Hywind Scotland Control station (median 101.5 dB re 1 µPa) but lower than the Hywind DEMO station (median 107.4 dB re 1 µPa). Median levels in the 125 Hz band are higher at all four Hywind Tampen stations than both the Hywind Scotland Control station (median 100.9 dB re 1  $\mu$ Pa) and Hywind station (median 102.7 dB re 1  $\mu$ Pa).

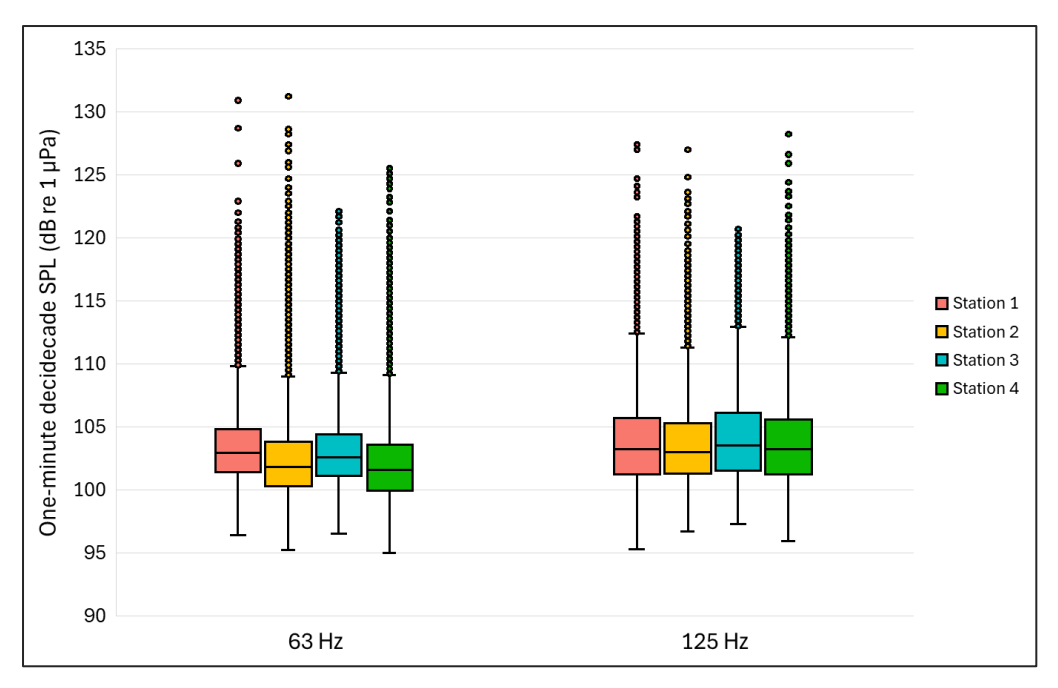


Figure 51. Distribution of one-minute decidecade SPL at Stations 1, to 4 at 63 and 125 Hz. Centre boxes represent the interquartile range (IQR) of values, while horizontal lines inside the boxes represent the median values. The range of values within above and below the quartiles are shown with vertical whiskers, and outliers beyond this span (outside 1.5 times IQR) are represented as dots.

### 3.6. Marine Mammal Exposure Levels

The potential for noise to affect animals of a given species depends on how well that animal can hear it. Noises are less likely to disturb or injure an animal if they are at frequencies that the animal cannot hear well. The perception of underwater sound depends on the hearing sensitivity of the receiving animal in the frequency bands of the sound. Hearing sensitivity in animals varies with frequency, the hearing sensitivity curve (audiogram) usually follows a U-shaped curve, where there is a central frequency band of optimal hearing sensitivity and reduced hearing sensitivity at higher and lower frequencies. The hearing sensitivity frequency range differs between species, meaning that different species will perceive underwater sound differently, depending on the frequency content of the sound.

Auditory frequency weighting functions for different functional hearing groups are applied to reflect an animal's ability to hear a sound and to de-emphasize frequencies animals do not hear well relative to the frequency band of best sensitivity (see Appendix D.2). Marine mammal hearing groups are defined for cetaceans, pinnipeds, and other marine carnivores, and further categorised based on the generalised frequency range of hearing. Figures 52 to 54 present the auditory frequency weighted daily cumulative sound exposure levels (SELs) for Stations 1, 3, and 4 respectively. Levels from Station 2 have not been presented because the duty cycle did not allow for the daily cumulative SEL to be inferred directly without extrapolation. The hearing groups presented correspond to those defined in Southall et al. (2019), namely low-frequency cetaceans, high-frequency (HF) cetaceans, very high-frequency (VHF) cetaceans, phocid seals, and otariid seals.

The assessment for impulsiveness indicated that the soundscape in the vicinity of the Hywind Tampen turbines is best characterised as non-impulsive (see Section 3.2.4). All daily cumulative SELs recorded during this study at all stations were found to lie below the thresholds for both temporary and permanent hearing threshold shifts (TTS and PTS, i.e., hearing loss) for non-impulsive sounds for all functional hearing groups (Southall et al. 2019); these thresholds are presented in Appendix D.1. A modelling assessment to predict the exact distances to these impact thresholds is presented in Section 4.5.. Unweighted daily cumulative SELs at all stations from 23rd May onwards after the

redacted period are substantially elevated compared to the earlier levels due to the nearby seismic survey airgun source, as outlined in Section 3.2.6.

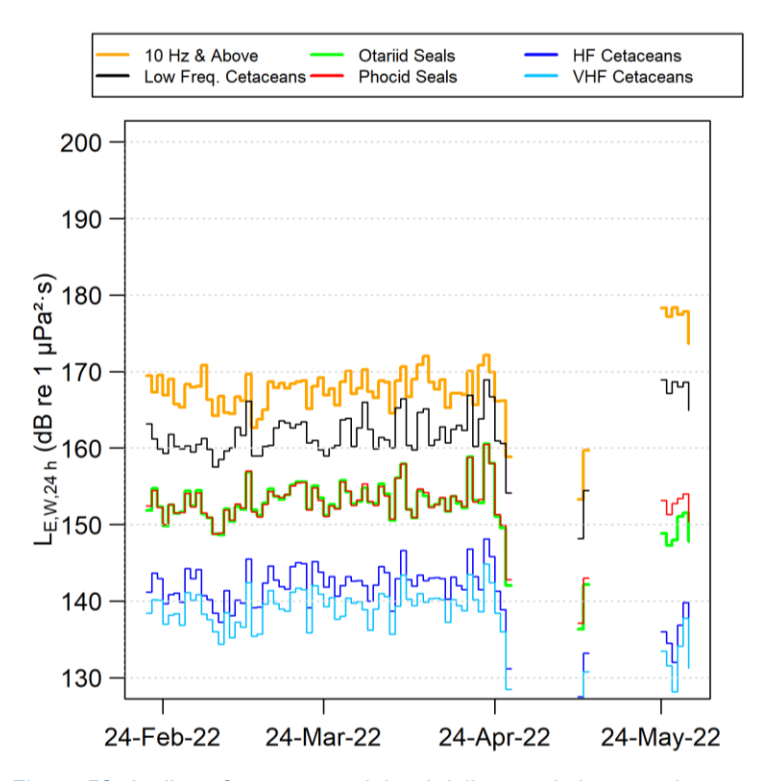


Figure 52. Auditory frequency weighted daily cumulative sound exposure levels at Station 1. The 10 Hz & Above SEL is the unweighted daily SEL.

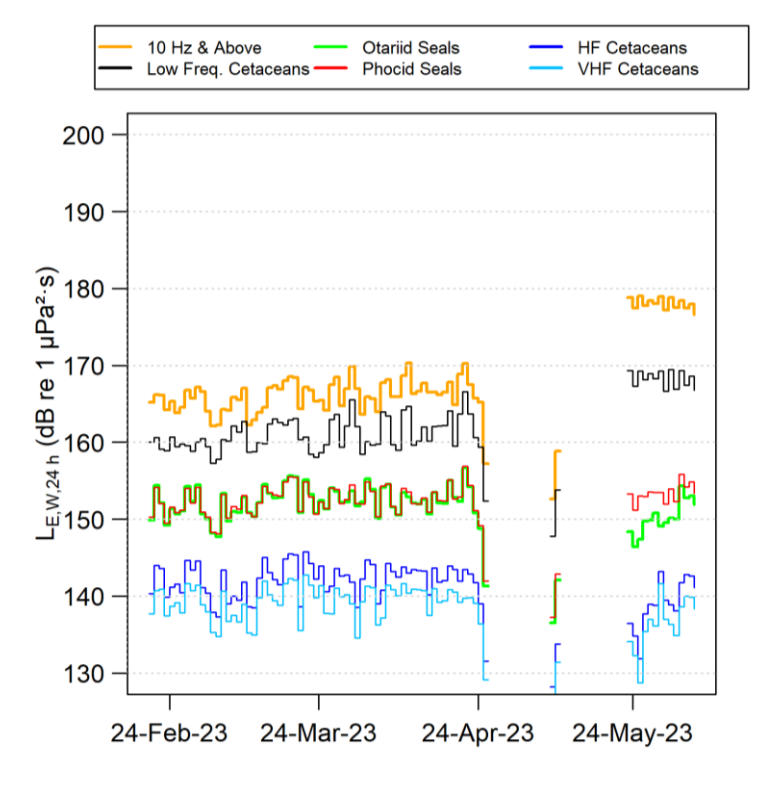


Figure 53. Auditory frequency weighted daily cumulative sound exposure levels at Station 3. The 10 Hz & Above SEL is the unweighted daily SEL.

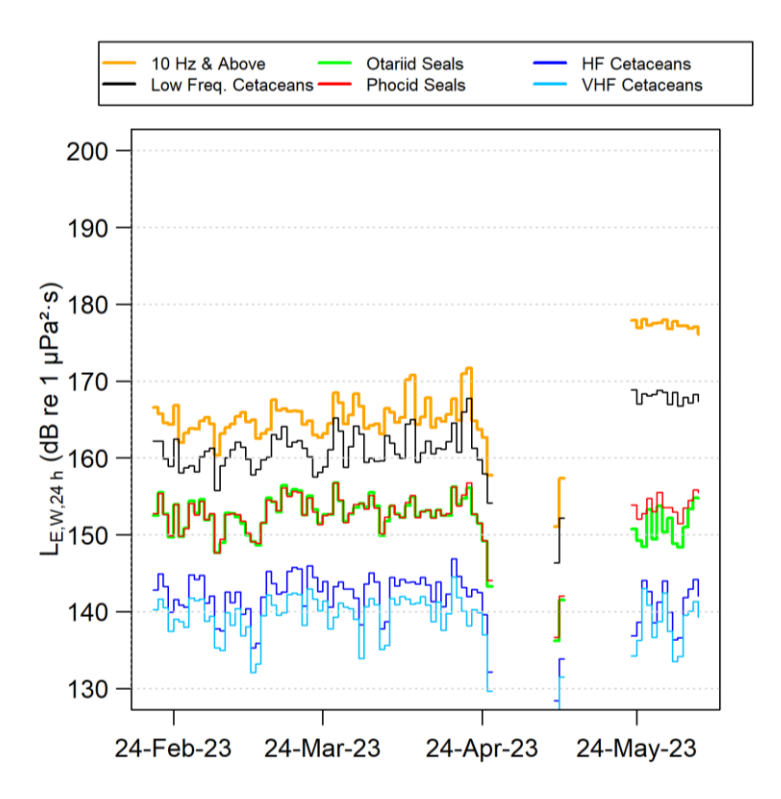


Figure 54. Auditory frequency weighted daily cumulative sound exposure levels at Station 4. The 10 Hz & Above SEL is the unweighted daily SEL.

## 4. Calculation of Monopole Source Levels

An underwater acoustic source, generating sound, radiates this acoustic energy away from the source and into the environment. The rate at which this energy, and thus sound level, decreases is characterised by the propagation loss. Geometric spreading of acoustic waves is the predominant way by which propagation loss occurs. Propagation loss also happens when the sound is absorbed and scattered by the seawater, and absorbed scattered, and reflected at the water surface and within the seabed. The propagation loss depends on the acoustic properties of the ocean and seabed and its value changes with frequency.

If the acoustic source level (SL), expressed in dB re 1  $\mu$ Pa²m², and propagation loss (PL), in units of dB, at a given frequency are known, then the received level (RL) at a receiver location can be calculated in dB re 1  $\mu$ Pa by:

$$RL = SL - PL \tag{4}$$

Similarly, when determining the source level of a monopole source, the same approach can be applied using the received level, and a prediction of propagation loss, in a process called backpropagation, i.e.,

$$SL = RL + PL \tag{5}$$

This section provides details of the backpropagation of sound from the received location to the turbine and the resulting source levels for a single turbine operating in various wind conditions. The parameterisation of the environment is detailed in Section 4.1, the sound propagation modelling is outlined in Section 4.2, the calculated band-level propagation loss is presented in Section 4.3, and the calculated source levels are presented in Section 4.4.

#### 4.1. Modelled Environmental Parameters

Sound propagation is affected by interactions with the local environment. The principal factors affecting propagation are the bathymetry, the geoacoustic profile, and the sound speed profile in the water column.

Bathymetric data for the region were taken from EMODnet (2022) (Figure 5). A single interpolated transect representing the path from Turbine HY06 to the receiver at Station 1 was extracted.

The sound speed profile is calculated from temperature and salinity profiles and vary with time of day and year. The temperature and salinity data were sourced from CMEMS (2023) for the region. The sound speed is calculated from these using formulae by Coppens (1981). Monthly averaged profiles from January through to April are similar; the profiles generated for March were used in the modelling (Figure 55).

The geoacoustic profile has been based on the lithographic description of the substrate from the 'EMODnet Geology: Seabed substrate: Multiscale - Folk 16' dataset; here, the sediment is listed as 'Muddy sand'. A depth-dependent profile is calculated using properties of 'Silty sand' from Hamilton Hamilton (1980), with shear wave properties from Holzer et al. (2005) and Buckingham (2000). Details of the generated profile are shown in Table 7.

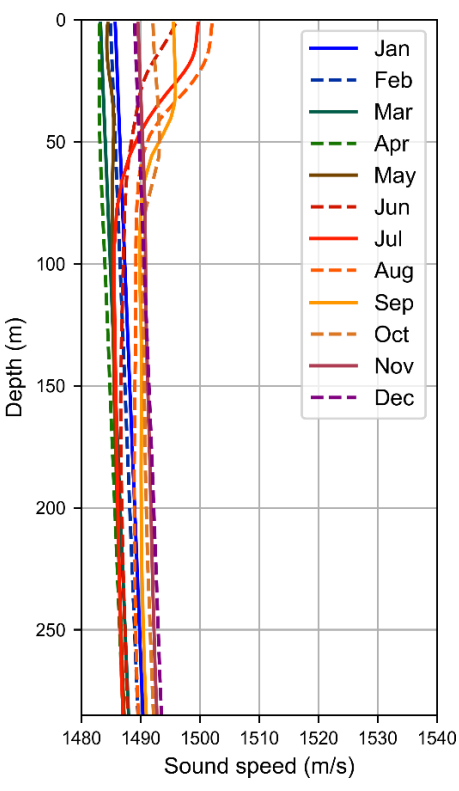


Figure 55. Monthly sound speed profiles at the Tampen site derived from salinity and temperature profiles from CMEMS.

Table 7. Geoacoustic model for Hywind Tampen, which represents increasingly consolidated muddy sand. Within each depth range, each parameter varies linearly within the stated range. The compressional wave is the primary wave. The shear wave is the secondary wave.

Depth below seafloor (m)	Material	Density	Density Compressional wave			Shear wave		
	Material	(g/cm³)	Speed (m/s)	Attenuation (dB/λ)	Speed (m/s)	Attenuation (dB/λ)		
0–20	Silty sand	1.77–1.80	1603–1629	1.07–1.22		3.65		
20–50	Silty sand	1.80-1.84	1629–1666	1.22–1.18	200			
50–100	Silty sand	1.84–1.90	1666–1726	1.18–0.88	300			
100–200	Silty sand	1.90-2.02	1726-1836	0.88-0.86	1			

# 4.2. Sound Propagation Modelling

Underwater sound propagation was predicted with JASCO's Marine Operations Noise Model (MONM) for frequencies below 100 Hz, and BELLHOP from 100 Hz to 25 kHz.

MONM computes acoustic propagation via a wide-angle parabolic equation solution to the acoustic wave equation (Collins 1993) based on a version of the US Naval Research Laboratory's Range-dependent Acoustic Model (RAM), which has been modified to account for a solid seabed (Zhang and Tindle 1995). The parabolic equation method has been extensively benchmarked and is widely employed in the underwater acoustics community (Collins et al. 1996). MONM accounts for the additional reflection loss at the seabed, which results from partial conversion of incident compressional waves to shear waves at the seabed and sub-bottom interfaces, and it includes wave attenuations in all layers. MONM incorporates the following site-specific environmental properties: a bathymetric grid of the modelled area, underwater sound speed as a function of depth, and a geoacoustic profile based on the overall stratified composition of the seafloor.

Sound propagation at higher frequencies was modelled using the BELLHOP Gaussian beam acoustic ray-trace model (Porter and Liu 1994). This model accounts for sound attenuation due to energy absorption through ion relaxation and viscosity of water in addition to acoustic attenuation due to reflection at the medium boundaries and internal layers (Fisher and Simmons 1977). The consideration of medium absorption is important for frequencies higher than 5 kHz and cannot be neglected without noticeably affecting the model results. Attenuation due to reflections from boundaries is important when considering the effects of different wind speeds and the resulting sea surface roughness: this affects increasingly lower frequencies with increasing wind speed.

#### 4.2.1. Source Considerations

The propagation models described above are both point-source models – the sound is modelled as though it emanates from a single point. In many underwater acoustic situations, the point source assumption is valid, and although the sound field close to the source is not well represented, far away from the source, there is little difference between the sound field from a distributed set of sources that is more representative of the real situation and the point source. It should be noted that the spar pillars upon which the turbines sit are understood to have a draft of approximately 90 m, which represents a considerable proportion of the water column. If used to repropagate, the calculated source levels provide an illustration of likely levels but may not accurately represent the near field close to the source.

Care must also be taken when back-propagating between single source and single receiver locations. The propagation paths may result in certain frequency bands being more or less effectively propagated. From Equation 5, it is evident that if a null occurs in the propagation at a specific frequency, then the derived source level at that frequency will be artificially elevated. To avoid this phenomenon, and to generate source levels more representative across the 90 m length of the spar, the back propagation is performed for sources from 5 to 85 m depth, with 10 m spacing. This provides a set of nine propagation loss results, which are averaged to avoid peaks and troughs in the results and thus reduce the influence of any single source depth selection.

### 4.2.2. Wind Speed Considerations

As noted above, the wind speed affects the sea surface roughness, which consequently affects the energy that reflects from the sea surface. Wind speeds were considered from 0 knots to 40 knots, in steps of 5 knots. The reflection coefficient due to surface roughness was calculated using the Schulkin equation (Hodges, 2010) and was incorporated in the propagation modelling carried out with BELLHOP.

# 4.3. Calculated Propagation Loss

Figures 56 and 57 show the propagation loss in decidecade bands between the multiple source depths at Turbine HY06 and the receiver at Station 1 for 5 knots and 40 knots wind respectively. Note, that frequencies below 100 Hz are identical as the surface roughness is not included in MONM. The spectra show the variability resulting from propagation from a single point; by taking the average, any source depth dependent peaks and troughs in the results are smoothed. Results for each modelled wind speed are shown in Appendix F.

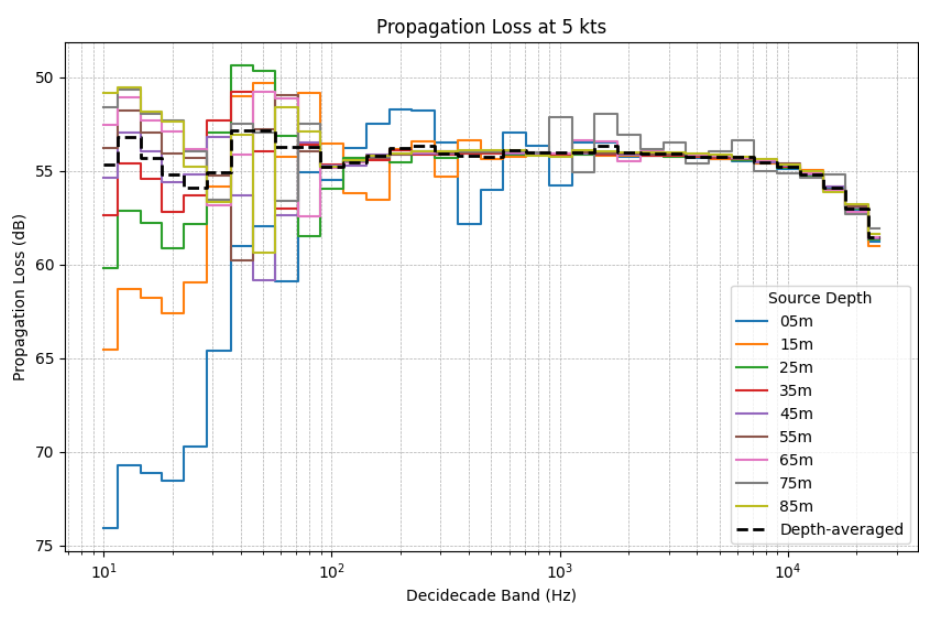


Figure 56. Propagation loss in decidecade bands between HY06 and Station 1 for 5 knots wind speed.

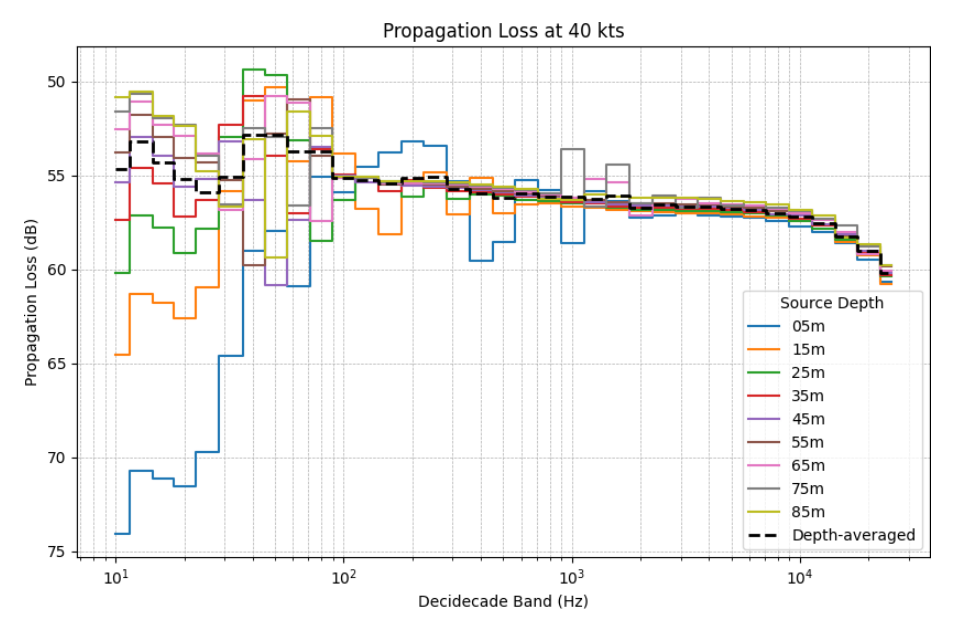


Figure 57. Propagation loss in decidecade bands between HY06 and Station 1 for 40 knots wind speed.

### 4.4. Backpropagated Source Levels

Backpropagated source levels for a single turbine were calculated by adding the modelled propagation loss in each decidecade band from Section 4.3 to the directional received levels from Section 3.4.3. Backpropagating by this method assumes that all recorded sound in the direction of HY06 originates from the turbine itself, which may not be a valid assumption in all cases but, given the relatively short distance, it is highly likely that the turbine noise is dominant across the received spectrum. However, during the analysis windows for 25 and 30 kn of wind, there appeared to be slightly elevated levels of in-beam background noise below 20 Hz from the same direction as HY06, but with no obvious contaminating source. Such low frequency sound may propagate for extended distances and is potentially related to a quite distant source. In both these cases, it is unavoidable that the total received levels below 20 Hz would be backpropagated to source, resulting in artificially elevated source level at those frequencies. While every opportunity has been taken to minimise these

types of errors, it was not possible to separate the WTG signature from contaminating noise from the same direction as it was persistent in nature.

Source levels calculated using the propagation loss curves averaged over source depth are presented in Figure 58 for the median, and Figure 59 for the 95th percentile levels. Broadband source levels are presented in Table 8.

There does not appear to be a directly linear relationship between wind speed and source level, and spectral shape also appears to change between wind speeds, however some general trends can be observed. Figures 58 and 59 show that the peaks in the spectra in the 25 and 80 Hz bands are generally higher for wind speeds greater than 20 kn, particularly the 80 Hz band relating to the 75 Hz tone. This is notable because the rotational rate of the turbine reaches a maximum in wind speeds over 20 kn (see Figure 33).

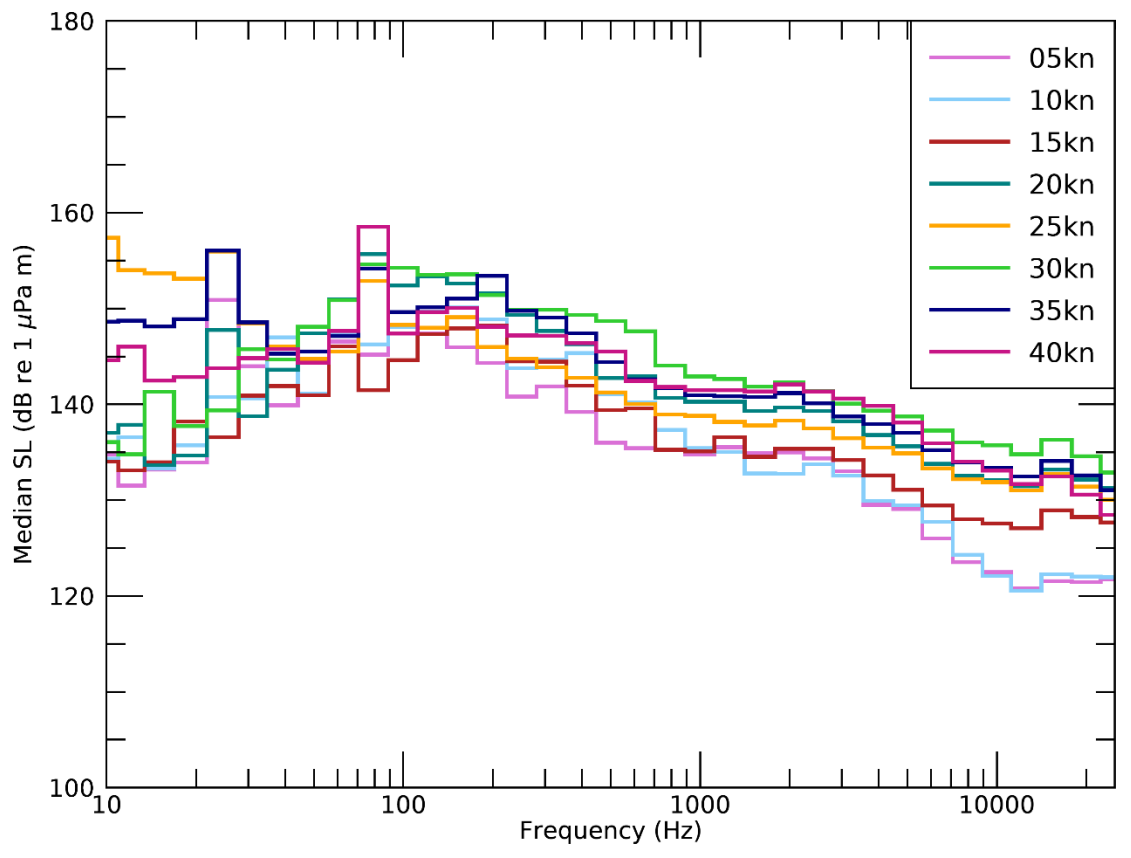


Figure 58. Median backpropagated source levels for a single turbine based on a point source assumption using propagation loss curves averaged over the modelled source depths.

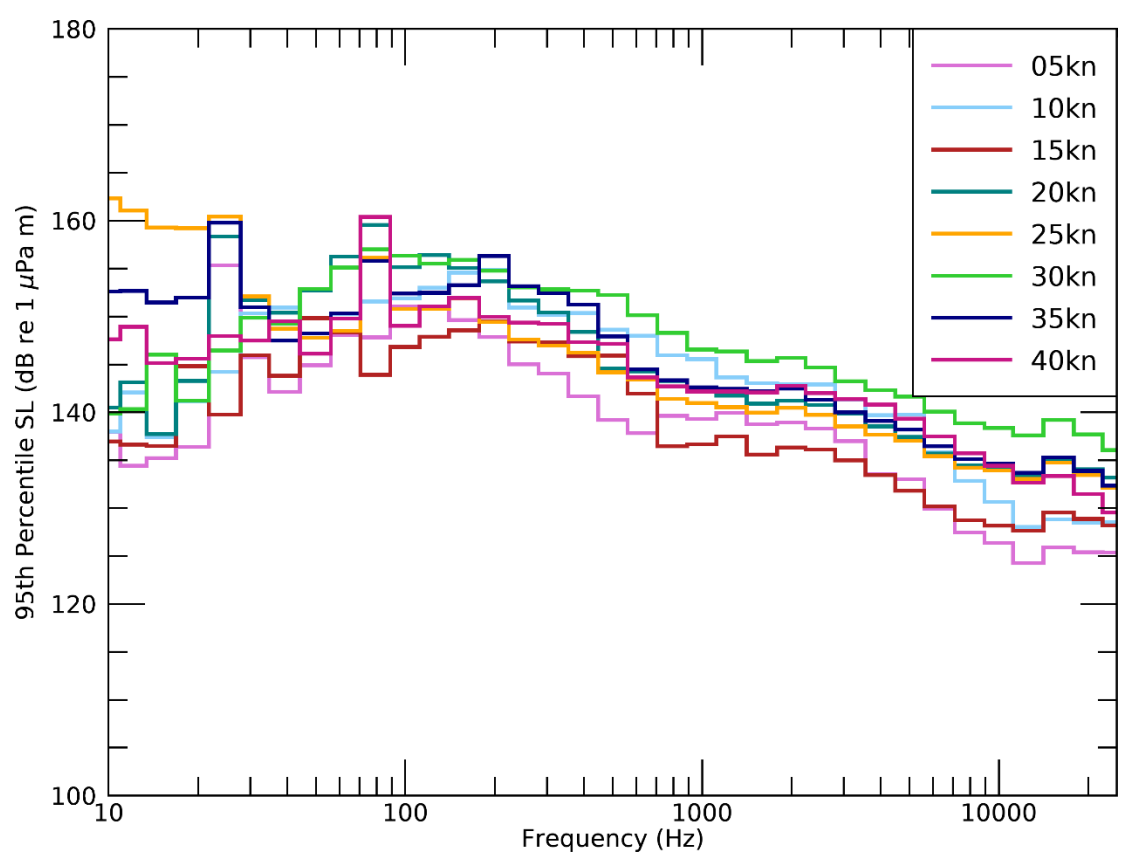


Figure 59. 95th percentile backpropagated source levels for a single turbine based on a point source assumption using propagation loss curves averaged over the modelled source depths.

Wind speed	Broadband source level (dB re 1 μPa ² m ² )								
(kn)	5 th percentile	25 th percentile	Median	75 th percentile	95 th percentile				
5	153.6	155.4	157.1	158.8	160.5				
10	153.7	155.7	158.2	160.8	163.5				
15	154.6	155.7	156.5	157.7	159.1				
20	159.9	161.1	162.3	164.0	166.4				
25	159.6	162.0	163.8	165.7	168.7				
30	160.3	162.0	163.0	164.0	166.0				
35	161.0	162.3	163.2	164.3	166.1				
40	160.1	161.3	162.1	162.9	164.1				

# 4.5. Simplified Modelled Sound Fields

An approximation of the wide area sound fields was modelled combining the source levels generated in Section 4.4 with simplified propagation loss modelling in three dimensions. Turbines were modelled as individual point sources at 45 m depth using the same propagation models and input parameters specified in Sections 4.1 and 4.2. Modelling the turbines as point sources in this way is subject to the same limitations outlined in Section 4.2.1. Sound fields were calculated in three dimensions by modelling propagation loss along 144 radials evenly spaced at 2.5° intervals with receivers spaced to cover the entire water column in a 360° swath from the source. The resulting modelled sound fields are presented in Section 4.5.1 for SPL and Section 4.5.2 for auditory frequency weighted SEL, as applied to marine mammal hearing groups. Sound fields in this section are presented as the

maximum-over-depth, i.e. the greatest level that occurs over all samples within the water column at a given range.

Results are presented for 10 and 20 kn wind speeds since analysis indicated these were the modal wind speed bins for the recording period analysed. Additionally, 10 kn represents wind speed where the rotor speed was not at maximum, while at 20 kn it was at maximum RPM.

### 4.5.1. Sound Pressure Level

Sound field maps are presented in this section representing the maximum-over-depth SPL for the entire Hywind Tampen wind farm array. Figure 60 shows the predicted sound field for 10 kn wind speed, median source levels and Figure 61 shows the predicted sound field for 20 kn wind speed, 95th percentile source levels.

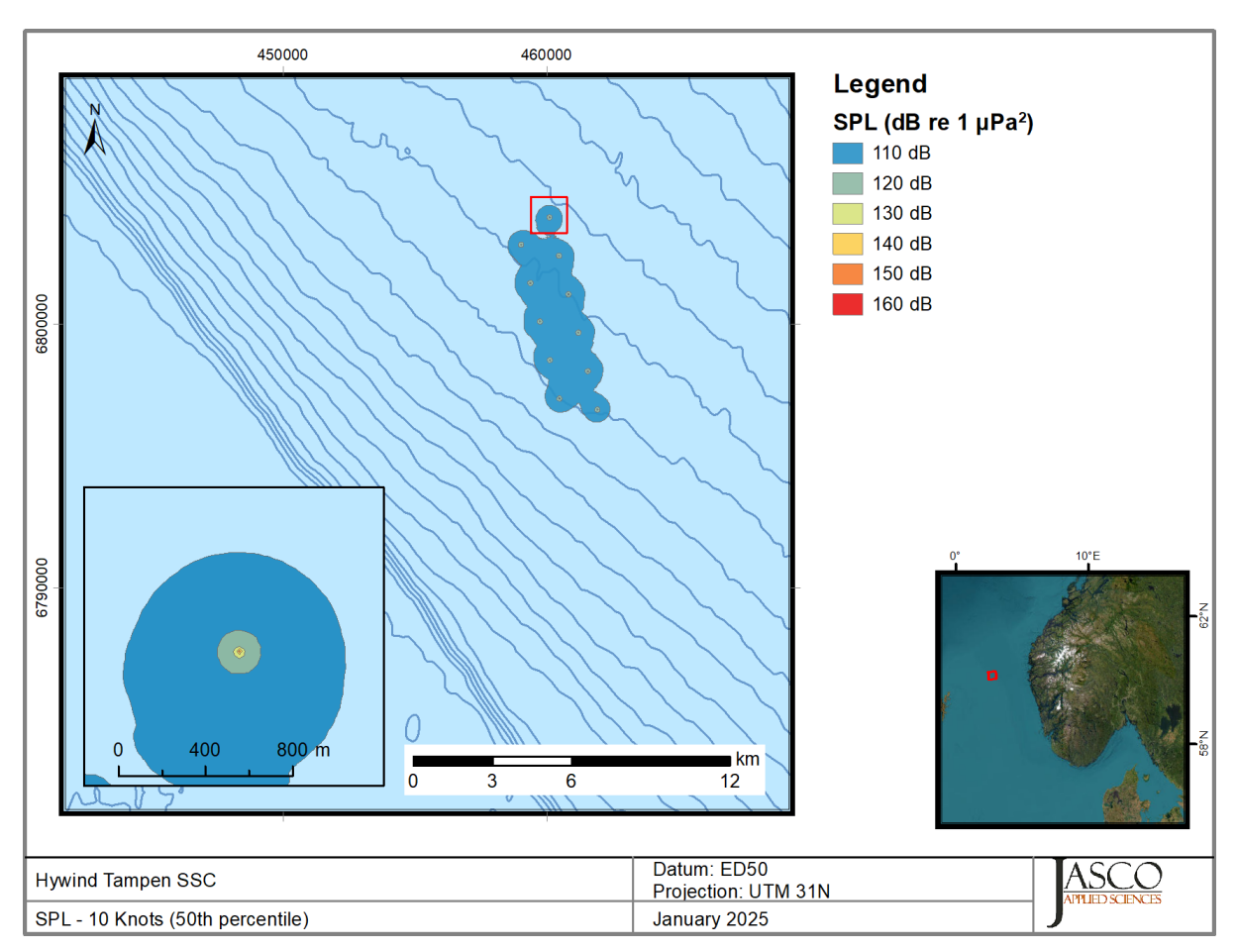


Figure 60. Modelled sound pressure level map for the Hywind Tampen wind farm assuming 50th percentile (median) source levels at a wind speed of 10 kn.

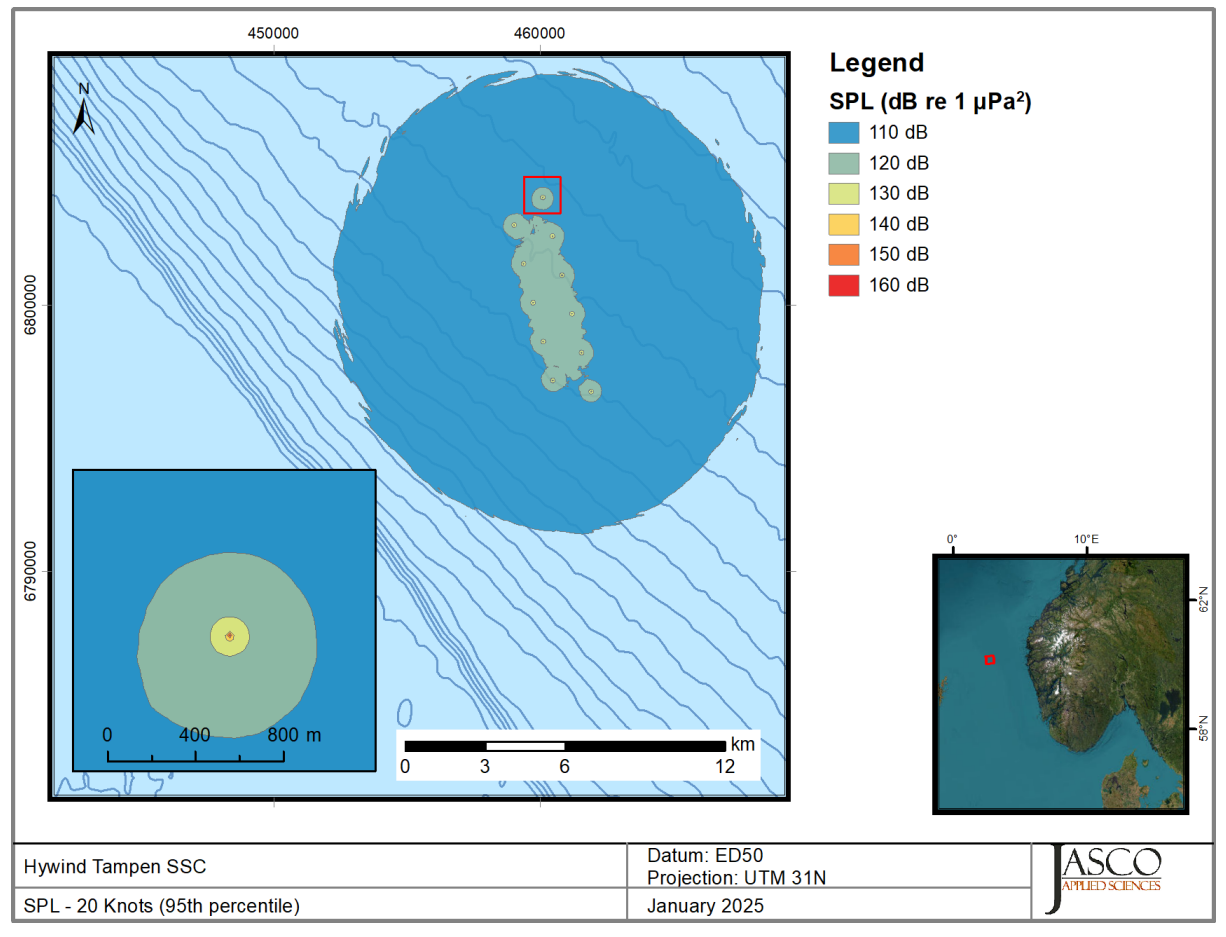


Figure 61. Modelled sound pressure level map for the Hywind Tampen wind farm assuming 95th percentile source levels at a wind speed of 20 kn.

## 4.5.2. Weighted Sound Exposure Level

Daily weighted SEL at each recorder station was presented in Section 3.6 for the considered marine mammal auditory groups. The modelled outputs allow for an estimate of sound levels over the wider area around the wind turbines. This enables a prediction of distances to the impact thresholds recommended by Southall et al. (2019), as specified in Appendix D.1, and a comparison with the recorded levels.

Table 9 presents the modelled received levels at Stations 1 and 3, the two stations closest to the wind farm array. These values can be directly compared to the results in Section 3.6. Table 10 presents the maximum distances to the TTS threshold levels from Southall et al. (2019). Levels above PTS threshold were not reached at any distance. Results in both tables are presented for 10 and 20 kn wind speeds, 50th and 95th percentile levels.

Comparing the modelled results in Table 9 with the recorded levels in Figures 52 and 53, modelled levels at the 95th percentile are at the lower end of the recorded values for low-frequency cetaceans, while for all other auditory groups modelled levels are slightly below the observed levels. This may be due to the limitations of the simplified point source modelling approach, inherent variability in the wind speed and associated source levels over the course of 24 hours, or additional sources of sound energy contributing to the weighted recorded levels not accounted for in the modelling. Predicted levels at the 95th percentile counterintuitively appear higher for 10 kn than 20 kn. This is a reflection of both the variability in the predicted source levels at 10 kn, and the difference in the spectra between the two wind speeds. Notably the frequency bands which contribute the most to the wind turbine source spectra and which displayed the greatest positive correlation with wind speed (below

approximately 200 Hz, see Section 3.3) are far below the lower frequency roll-off of the weighting function for all hearing groups except low-frequency cetaceans (see Appendix D.2). These frequencies are therefore greatly attenuated in the weighted received sound fields.

The maximum distances to the TTS threshold levels from Southall et al. (2019) presented in Table 10 represent a scenario where a receiver must remain within the stated radius for a full 24 hours at the depth where the sound level is greatest. From all modelled cases, the maximum distance to the TTS threshold is 60 m for very high-frequency cetaceans assuming conditions of 20 kn wind speed at the 95th percentile source level. Sound levels have been shown to be highly variable, and the point source modelling approach may not accurately predict the sound field close to the turbine spar buoy which spans approximately 90 m of the water column, therefore the exact distances will vary.

Table 9. Predicted received weighted 24-hour SEL at Stations 1 and 3 for the modelled wind speeds and percentiles.

	Modelled weighted received SEL _{24h} (dB re 1 μPa²s)									
	Station 1				Station 3					
Auditory group	10 kn		20 kn		10 kn		20 kn			
	50 th	95 th	50 th	95 th percentile	50 th	95 th	50 th	95 th percentile		
Low-frequency cetaceans	154.4	160.3	158.2	161.2	150.8	156.8	154.5	157.6		
High-frequency cetaceans	128.4	137.2	135.0	136.8	123.3	132.7	126.9	128.7		
Very high-frequency cetaceans	124.4	132.7	132.1	134.0	117.7	127.0	121.5	123.2		
Phocid pinnipeds	143.2	151.5	146.8	148.9	139.9	148.2	142.6	144.6		
Otariid pinnipeds	142.6	151.6	146.3	148.0	139.4	148.3	142.1	143.8		

Table 10. Modelled maximum distances to TTS threshold levels (Southall et al. 2019) for the modelled wind speeds and percentiles.

		Maximum distance to threshold (m)					
Auditory group	TTS onset level (dB re 1 μPa²s)	10	kn	20 kn			
		50 th percentile	95 th Percentile	50 th percentile	95 th Percentile		
Low-frequency cetaceans	179	20	40	40	40		
High-frequency cetaceans	178	<20	<20	<20	<20		
Very high-frequency cetaceans	153	20	40	50	60		
Phocid pinnipeds	181	<20	<20	<20	<20		
Otariid pinnipeds	199	_	<20	_	_		

A dash (—) indicates the threshold was not reached at any modelled distance from the source.

## 4.5.3. Comparison with Ambient Noise

While the modelled results in Section 4.5.1 predicted the sound footprint generated by the Tampen wind farm, this does not include information about the levels generated by the turbines relative to the ambient noise for the wider area. A degree of turbine noise was detectable at all four stations, and as such there was no true control recorder. However, by comparing the recorded spectra at all four stations and observing the frequencies where there appears to be no discernible difference this gives an impression of the ambient noise spectrum. Figure 62 shows a comparison of the median recorded spectra at all four recorders before the redacted period. The reduction in height of the primary turbine peaks at 25 and 75 Hz due to increasing distance from the turbine array is clearly visible, as well as on some of the smaller intermediate peaks. An estimate of the ambient spectrum is also presented in Figure 62 and was generated by taking the minimum level across all four spectra, manually removing and interpolating across the known turbine related spectral peaks, and smoothing the remaining

spectrum via moving average filter. As expected based on previous analysis, the distance based differences between the spectra were almost entirely in tonal peaks at frequencies below 200 Hz, with limited difference at frequencies above this.

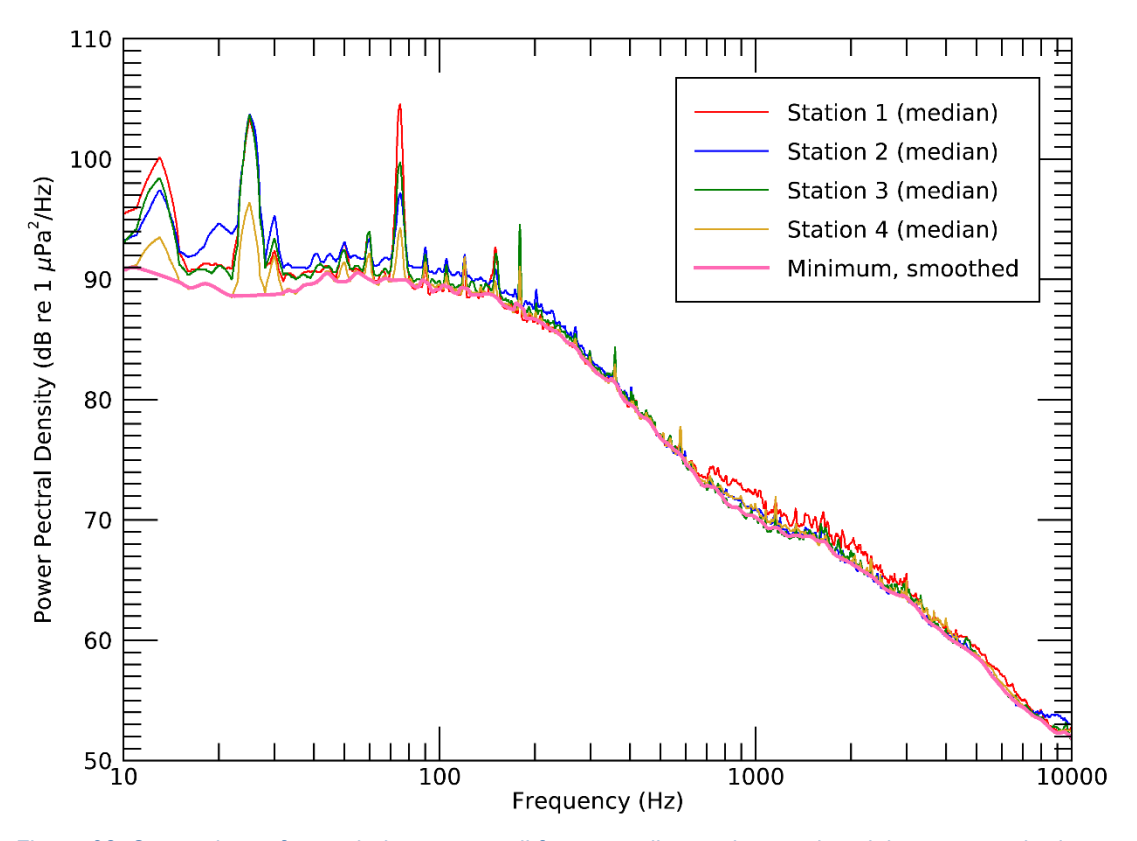


Figure 62. Comparison of recorded spectra at all four recording stations and a minimum, smoothed spectrum approximating the ambient noise levels in the wider Tampen area.

Using this smoothed spectrum, an approximation of the median broadband ambient sound level was calculated to be 113.6 dB re 1  $\mu$ Pa. Figures 63 and 64 show maps of the exceedance of modelled turbine sound pressure levels above this ambient sound level. Figure 63 shows the predicted exceedance sound field for 10 kn wind speed, median source levels and Figure 64 shows the predicted exceedance sound field for 20 kn wind speed, 95th percentile source levels. In these plots, the extent of the displayed exceedance fields represents the point that modelled turbine noise is expected to reach this broadband ambient level, i.e. 0 dB exceedance. The maximum distance from the closest single turbine to this boundary is 0.29 km for Figure 63, and 3.75 km for Figure 64. It should be noted that these maps do not infer any audibility, detectability, or lack thereof by either biological receivers or spectral analysis but serve as an approximation of the levels of turbine generated noise compared to the sound levels that may be present if turbine noise was absent.

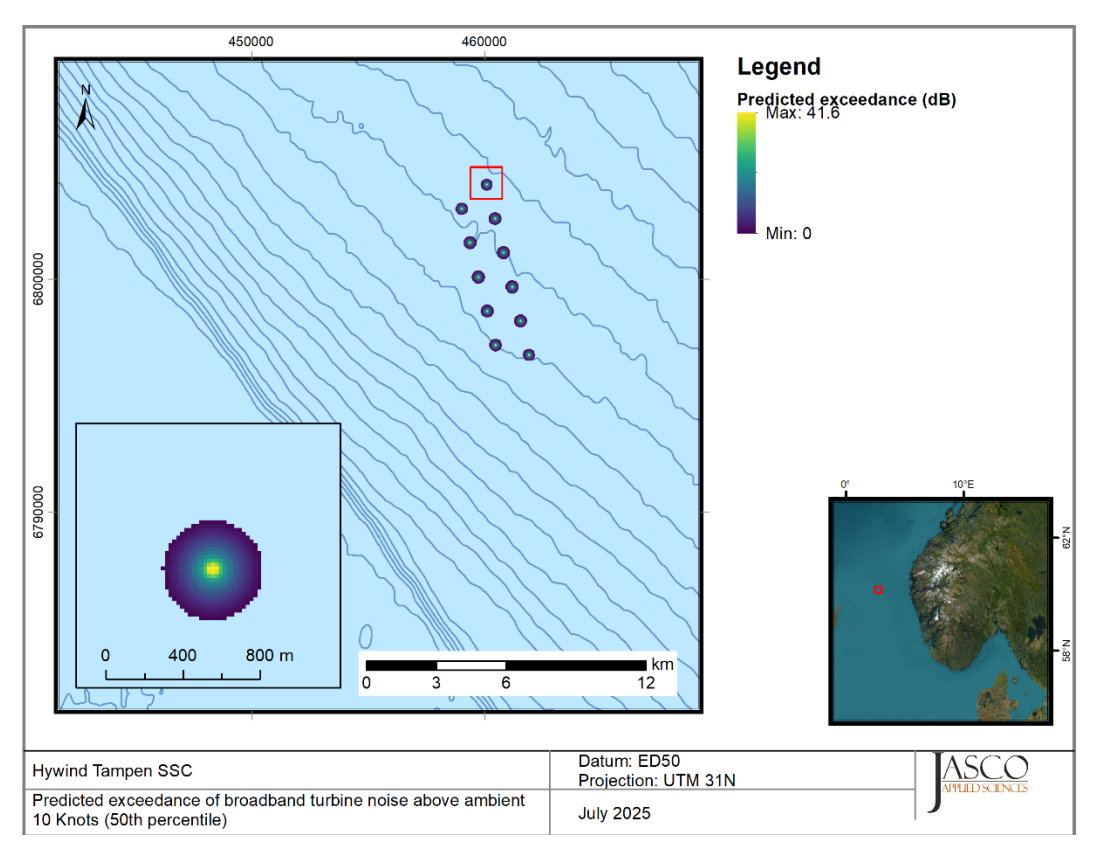


Figure 63. Map showing the difference between modelled sound pressure level from the Hywind turbines and median ambient sound levels for 50th percentile (median) source levels at a wind speed of 10 kn.

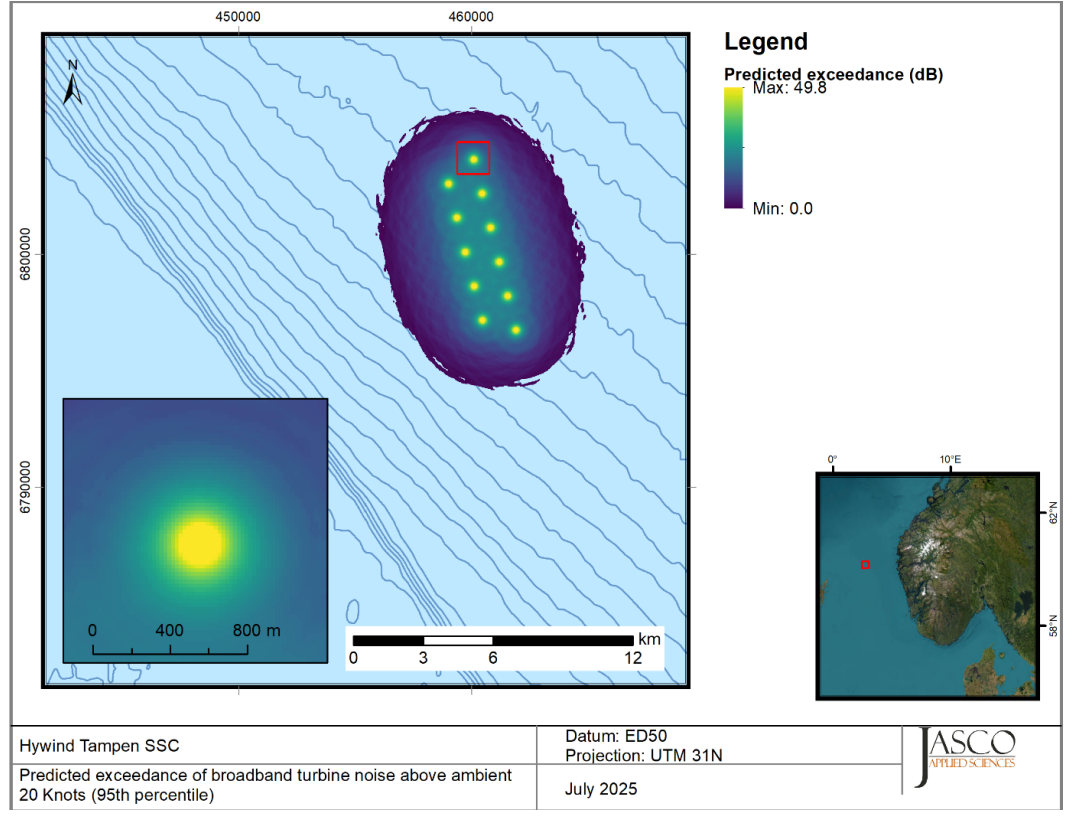


Figure 64. Map showing the difference between modelled sound pressure level from the Hywind turbines and median ambient sound levels for 95th percentile source levels at a wind speed of 20 kn.

#### 4.5.4. Comparison with Recorded Data

The analysis presented in Section 4.5.3 shows that noise from the turbines is only distinguishable above ambient noise levels at specific frequencies. It is therefore important when comparing modelled to measured received levels to consider only bands in which the measured received levels show demonstrable difference with increasing distance from the wind farm. Figures 65 and 66 show the median received levels in decidecade bands up to 1 kHz at all stations for 10 and 20 kn wind speed respectively. The only band showing a moderate degree of variation with distance from the wind farm at 10 kn wind is the 12 Hz band, while at 20 kn wind the levels in the 25 and 80 Hz bands (associated with the primary rotor tones) also monotonically decrease with distance.

Based on this, in order to compare modelled levels to those measured by the AMARs, levels for the entire wind farm were calculated from the modelled 20 kn sound fields in the 25 and 80 Hz bands at all four recorder locations. Figures 67 and 68 show the predicted modelled levels compared to the recorded levels in the 25 and 80 Hz bands respectively. In the 25 Hz band, the modelled 95th percentile levels are a good match for the recorded data at the closest stations (1, 2, and 3), while the modelled levels at Station 4 are notably below the recorded levels. In the 80 Hz band, both the median and 95th percentile modelled levels are a close match at the two closest stations (1 and 3), but the recorded levels exceed the predicted levels at greater distance from the wind farm. The gradient of the modelled propagation loss curve was 17.9-18.1 log(R) in the 25 Hz band and 18.8-19.3 log(R) in the 80 Hz band. However, care must be taken when interpreting these values since the individual turbines have a wide spatial distribution, the plotted distances are based on the distance to the closest turbine, and recorder stations were not placed along a single straight line transect. Due to these factors combined an *N* log(R) type representation of propagation loss, typically used for describing propagation loss away from a single point source, may not be appropriate.

The differences between modelled and received levels can be explained in several ways. There are likely differences in sound levels generated by individual turbines, and additionally the simplified point source model may not accurately reflect the sound field closer to the turbines. At greater distances the modelled levels only consider the predicted contribution from the Tampen turbines, while recorded levels include the band level contributions from both turbine and ambient noise. In Figures 67 and 68, the dashed grey lines represent the recorded levels in the two adjacent decidecade bands to the band under consideration: 20 and 32 Hz in the case of the 25 Hz band in Figure 67, and 63 and 100 Hz in the case of the 80 Hz band in Figure 68. The average of these levels can be considered a proxy for the ambient sound level in the band under consideration. To better understand what the influence of ambient noise may be on the modelled levels, this presumed ambient sound level was added to the modelled turbine noise levels. The resultant combined turbine and ambient noise levels are also plotted in Figures 67 and 68. In the 25 Hz band, the addition of the ambient sound levels brought both the median and 95th percentile levels far closer to the recorded levels at the two farthest stations (2 and 4). A similar effect can be seen in the 80 Hz band, where the inclusion of ambient sound corresponds near perfectly to the recorded levels at the two farthest stations. In this band both the recorded levels and the resultant modelled combined levels at distance are very similar to the presumed ambient level. Due to the logarithmic nature of sound levels reported in decibels, the increase in overall sound level when two sources are combined depends on the difference between their individual levels. If two identical sound levels (i.e., a 0 dB difference) are added, the total sound level increases by approximately 3 dB. Conversely, if one source is 12 dB quieter than the other, its contribution to the overall sound level is negligible. The similarity between recorded, ambient, and combined modelled levels in the 80 Hz band therefore indicates that, despite some potential contribution from turbine noise, ambient noise seemingly dominates at distance in this band.

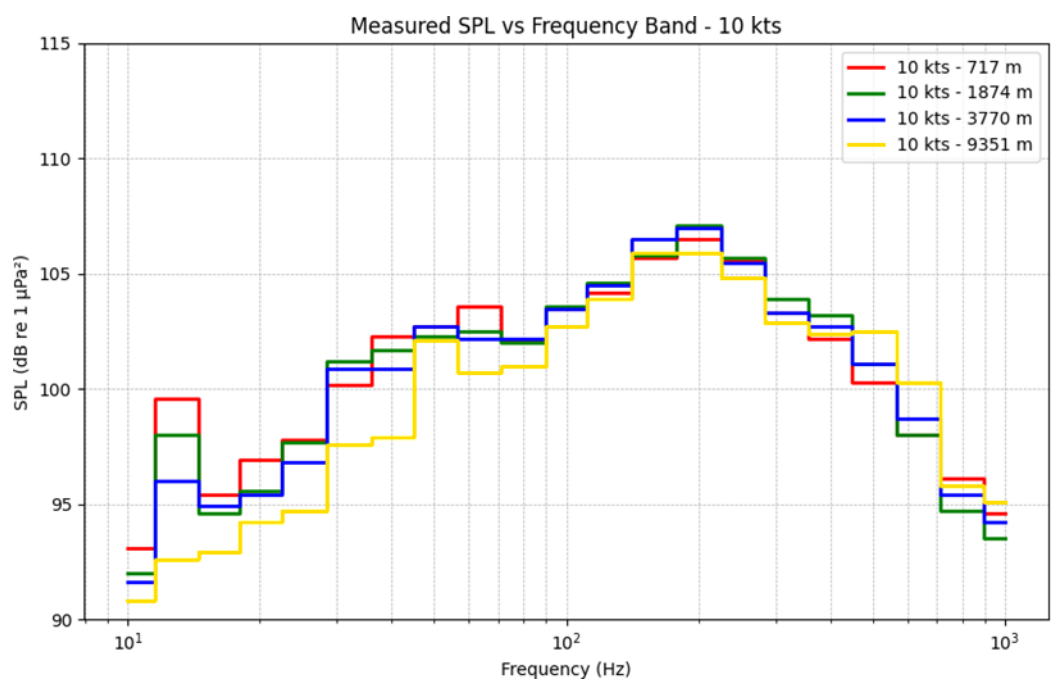


Figure 65. Median omnidirectional received levels in decidecade bands up to 1 kHz at all recorder stations for 10 kn wind speed.

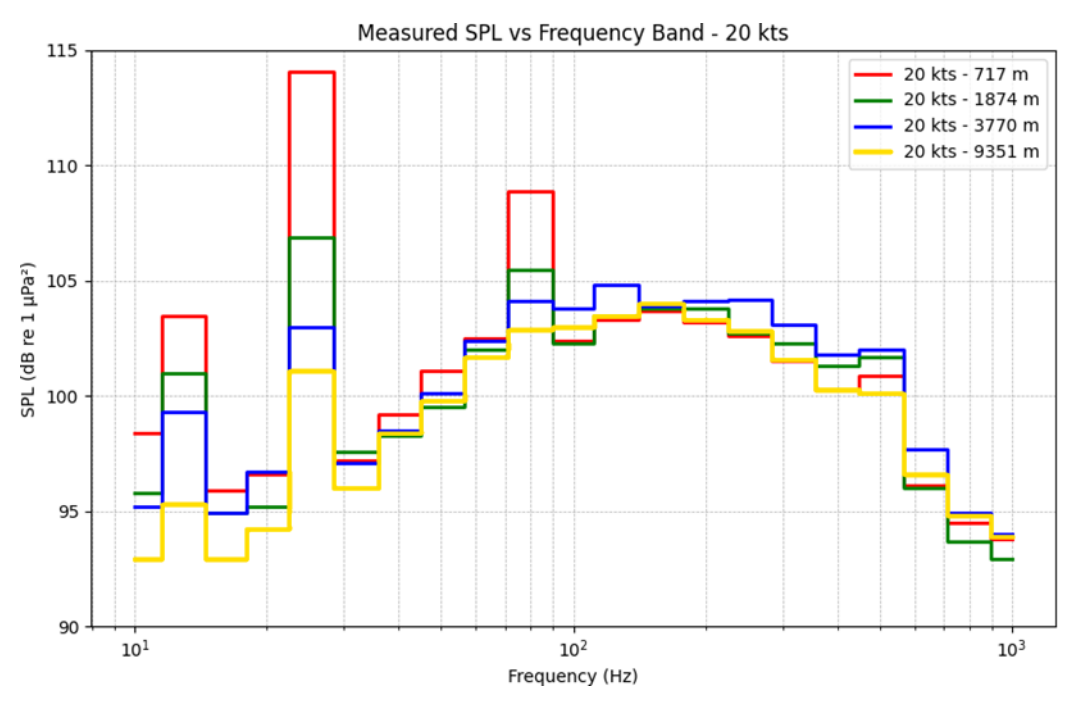


Figure 66. Median omnidirectional received levels in decidecade bands up to 1 kHz at all recorder stations for 20 kn wind speed.

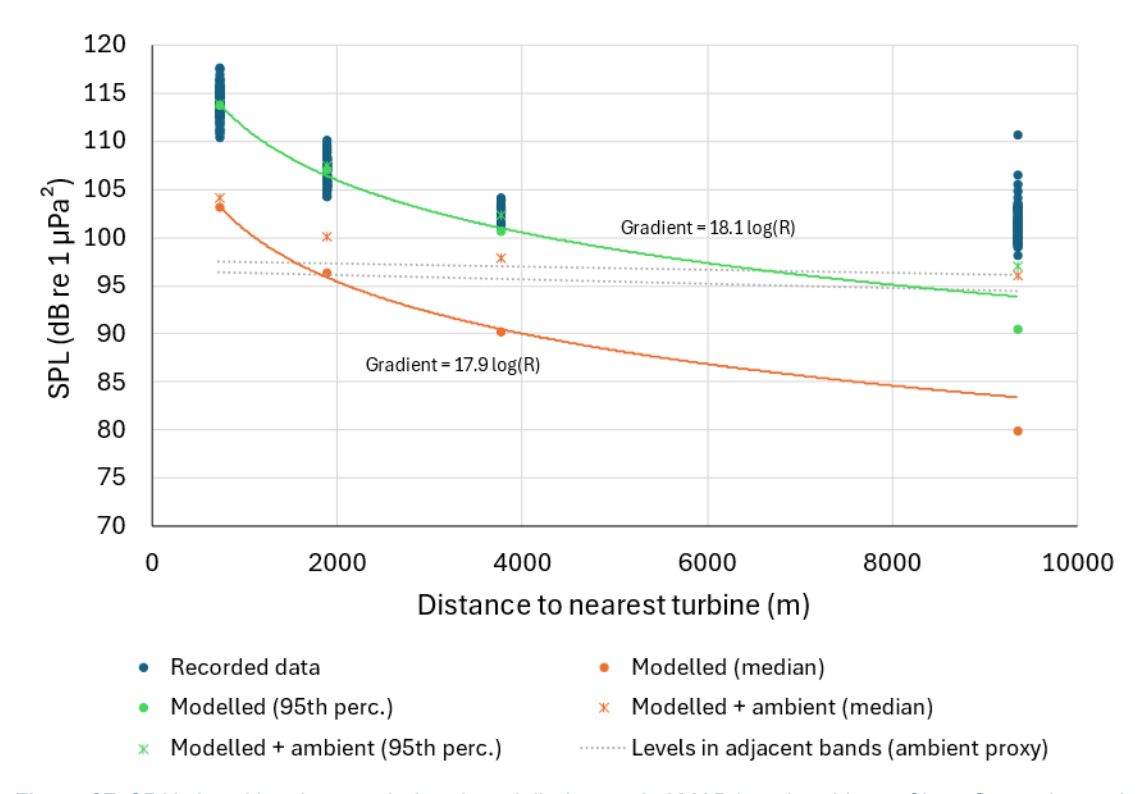


Figure 67. 25 Hz band levels recorded and modelled at each AMAR location. Lines of best fit are drawn through modelled data points only (dots). The dashed grey lines represent the recorded levels in the two adjacent decidecade bands (20 and 32 Hz), used in this instance as a proxy for the band level ambient noise.

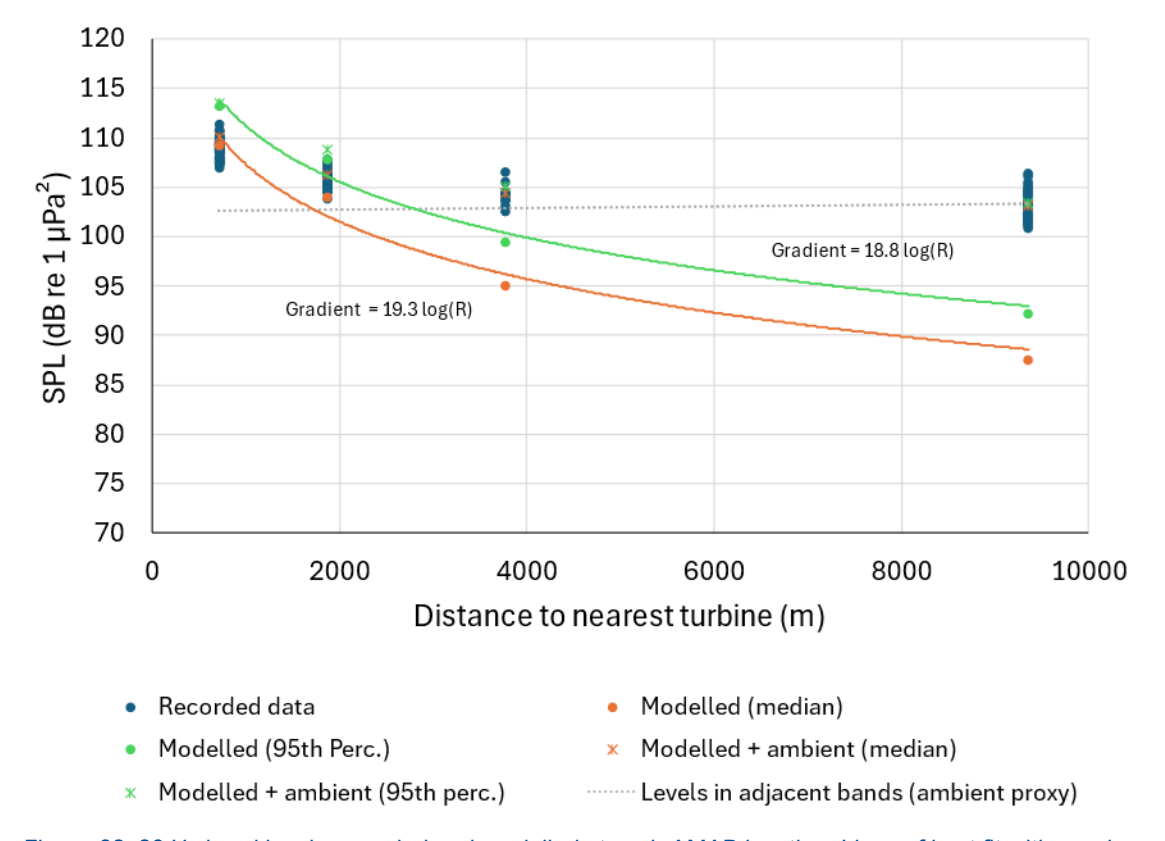


Figure 68. 80 Hz band levels recorded and modelled at each AMAR location. Lines of best fit with are drawn through modelled data points only (dots). The dashed grey lines represent the recorded levels in the two adjacent decidecade bands (63 and 100 Hz), used in this instance as a proxy for the band level ambient noise.

#### 5. Discussion and Conclusion

JASCO collected just over three continuous months of underwater sound data, and fractionally over twelve months of underwater sound data on a recording duty cycle from locations both within and around the Hywind Tampen site to 10 km to investigate the operational noise of the floating wind turbine generators. The AMAR within the Hywind site was deployed with a tetrahedral array to allow for directional discrimination of incoming sounds and was positioned specifically to isolate the most southeasterly turbine in the array (HY06). Two omnidirectional recorders were positioned to give details of the ambient soundscape. A further directional recorder was deployed for twelve months to present a longer-term impression of the overall soundscape at the Tampen site.

Total sound levels were around or above the upper bound of prevailing noise described by Wenz (1962) across the entire spectrum. Contributions to the underwater soundscape detected in the recordings were dominated by noise from the turbines, vessel activity, wind and wave noise, and seismic exploration.

The dominant sound emissions from the Hywind Tampen turbines are narrowband tones below 200 Hz. The two dominant tones contributing most to the turbine signature rise from lower frequencies and intensities to a maximum at around 25 and 75 Hz typically above ~20 kn of wind. The source of the 25 and 75 Hz tones appears to relate to the rotation of the main rotor and generator, with sound energy radiating from its sources in the nacelle down the turbine tower, through the submerged concrete spar, and into the water column. The tone at 25 Hz can be directly related to the rotational motion of the turbine (Equation 1) where a maximum rotor speed of 10.5 RPM (equivalent to 0.175 revolutions per second) with 144 generator pole pairs equates to a base frequency of 25.2 Hz. The tone at approximately 75 Hz (at 10.5 RPM) is similarly related to the rotational rate of the turbine and the number of pole pairs by a factor of three (Equation 2), though from acoustic analysis alone it is not immediately evident exactly how this tone is being generated or where the factor of three originates. At slower RPM rates, the frequency of the tones reduces, but the same relationship to the number of pole pairs is maintained.

As well as the dominant rotor related tones, other less intense and more intermittent tones are observed. The most prevalent of these is a fundamental tone at approximately 15 Hz, thought to be related to either a smaller multi-pole motor, cooling fan or other electrical system operating at a stable rate. This tone is noticeably quieter than the main generator related tones; the median spectral level at 15 Hz is 3.2 and 4.5 dB lower than the 25 and 75 Hz tones respectively across the entire recorded duration at Station 1 (Figure 12). Several other tones in the region of a few hundred to a few thousand Hz are also sporadically observed, particularly at higher wind speeds, though at a lower intensity than the main generator tones. Some display intermittent operation, with abrupt stop and start events, while others show a continuous unstable character. The stable, intermittent tones may be related to a hydraulic pump system used to maintain pressure in an accumulator which need not be in constant operation but maintains a constant rate when running. The continuous, unstable tone is more characteristic of a hydraulic actuator used to control the pitch of the blades which is reactive to fluctuations in the wind speed to maintain a constant rotor RPM.

Correlation analyses (Section 3.3) were undertaken to investigate how turbine parameters and received sound levels in different frequency bands were affected by wind speed and rotor rate. A strong positive link was found between wind speed and rotor RPM, with a near linear positive relationship up to a wind speed of approximately 20 kn where the RPM reaches a maximum of approximately 10.5 RPM for any wind speed above this. Similar positive correlations were determined between sound levels in the frequency bands containing the 25 and 75 Hz tones, though the strength of this correlation reduced with distance from the turbines. The correlation analysis showed a non-linear relationship between lower wind speeds (up to approximately 15 kn) and levels in the 20 and 25 Hz bands. This appears to be a result of both the fundamental and triplet generator tones increasing in frequency as rotor RPM increases (Figure 38). The correlation analysis for wind speed also displayed

an approximate plateau in levels in these bands, at wind speeds above 20 kn. The correlation analysis for rotor RPM indicated the change in levels in these bands with increasing rotor RPM reflected the increase in frequency of the fundamental and triplet tones exactly as expected. These trends further reflect the direct relationship between rotational rate and these tones.

The acoustic data were manually analysed for impulses associated with strain on the mooring system components. Very few transients were identified in the recordings, and those that were observed during higher wind speeds, were ultimately dismissed as possible mooring noise through directional exclusion of their source being within the Tampen site. Too few transients were discovered in the data to adequately tune an automated detector to count them. An alternative quantitative analysis of the impulsiveness of the data from all four recorders was undertaken by assessing empirical distribution function of the one-minute kurtosis (Figure 26). This analysis indicated that data from the two most distant recorders (Stations 2 and 4) was fractionally more impulsive than either of the recorders closer to the turbines, though kurtosis at all recorder locations was very low, indicating a non-impulsive soundscape. Sperm whale clicks were detected in the presence of low-level mooring noise, potentially indicating limited effect on this species of cetacean. Mooring noise is therefore not considered to be a significant acoustic component of the total Tampen noise signature.

The acoustic data were also analysed for biological noise detections. Automated detectors were used to detect marine mammal presence, and several instances of sperm whale and killer whale vocalisations were detected (Appendix D). Sperm whales and killer whales are both considered high-frequency (HF) cetaceans in Southall et al. (2019). The principle biological investigation in the analysis process was detection of the presence of spawning cod. Automated detectors were used to identify cod sounds, and a manual review of a subset of files was made to verify any potential detections. No cod grunts were confirmed during the manual review, but while acoustic detection does indicate presence, an absence of detections does not necessarily indicate an absence of cod.

Received directional noise levels, collected during relatively stable periods of wind speed, were analysed in 5 kn increments for a single turbine, HY06. Received levels from the direction of HY06 in the 79 Hz decidecade band, associated with the 75 Hz triplet tone at maximum rotor RPM, were compared to levels in the direction of a second nearby turbine, HY07. Once corrected for propagation path differences, the comparison indicated little overall difference between the levels in each direction, indicating that the sound footprint from a single turbine can be considered omnidirectional.

Received levels in each wind speed bin were backpropagated to obtain statistical decidecade source levels for a single turbine operating under multiple increasing wind conditions. The spread of broadband source levels was 153.6–161.0 dB re 1  $\mu$ Pa²m² for the 5th percentile, 156.5–163.8 dB re 1  $\mu$ Pa²m² for the median, and 159.1–168.7 dB re 1  $\mu$ Pa²m² for the 95th percentile. Generally, source levels are noticeably lower for wind speeds below 20 kn, when the generator is either in idle mode or only generating low levels of power, compared to wind speeds 20 kn and above when the rotor RPM is maximised, and significant power is being generated. On average the difference between levels above and below 20 kn is approximately 5–6 dB. This suggests that rotor rate rather than wind speed is a better predictor of sound levels and spectrum generated by a Hywind Tampen turbine, although wind speed is a suitable proxy for rotor RPM up to the system maximum.

Based on the non-impulsive characterisation of the Tampen soundscape, the daily cumulative SELs from each three-month recorder were frequency weighted and compared to the relevant marine mammal hearing groups from Southall et al. (2019); the twelve-month recorder at Station 2 was excluded from this analysis due to the duty cycle. The distances from each station to the nearest wind turbine were 717 m, 1.87 km, and 9.35 km for Stations 1, 3, and 4 respectively. All daily cumulative SELs recorded during this study at Stations 1, 3, and 4, were found to lie below the thresholds for both temporary and permanent hearing threshold shifts (i.e., hearing loss) for non-impulsive sounds for all functional hearing groups (Figures 52 to 54). To estimate the sound footprint of the entire wind farm, the backpropagated source levels for 10 and 20 kn wind speeds, 50th and 95th percentile, were repropagated assuming point sources at all eleven turbine locations. This modelling indicated a

considerable difference between the unweighted SPL sound fields for the different wind speeds, predominantly due to the increase in low frequency tonal energy with increasing wind speeds as discussed. The same modelling was used to estimate the TTS exceedance difference for the relevant marine mammal hearing groups. The largest predicted distance was 60 m for very high-frequency cetaceans, assuming an animal remains within this radius for a full 24-hour period at the depth of the greatest sound level in 20 kn wind speed for the 95th percentile level. Recorded sound levels were highly variable for a given wind speed and point source estimations of distributed sound sources such as the Hywind Tampen turbine spar may not accurately reflect the sound field close to the source. It should therefore be noted that actual distances will likely vary, though all evidence suggests there is no threat of auditory injury and low likelihood of exposure above TTS threshold with the possible exception of animals remaining in very close proximity to the turbines for 24 hours.

#### 5.1. Comparison With Hywind Scotland

One aim of this study was to compare the characteristics of the Hywind Tampen noise signature to that extracted from recordings during the Hywind Scotland sound source characterisation (Burns et al. 2022).

The shapes of the recorded spectra for both Hywind Tampen and Hywind Scotland are very similar, notably the two dominant tones at approximately 25 and 75 Hz are present in both recordings. The generators for both systems are of the same design and so have the same number of magnetic poles and operate at similar maximum operating rotational rates. Neither system is geared and so there is a complete absence of gearing tones which itself helps to minimise the overall radiated noise. Besides the two main tones seen in both locations, the Hywind Scotland also detected the stable tone with harmonic structure at 15 Hz in addition to a small number of discrete low-level peaks below 2 kHz.

The most significant difference between the two studies is the complete lack of identifiable mooring transients at the Tampen site, compared to a relative abundance of mooring related noise with a range of various audible characteristics in the Hywind Scotland recordings. In the Hywind Scotland dataset, the number of impulse detections per three hours frequently ranged from a few hundred to greater than one thousand. In one 20-minute recording from Hywind Scotland analysed in Burns et al. (2022), over 300 individual mooring transients were identified from multiple turbines. Conversely, in this study such impulsive transients were virtually non-existent. The reasons for this may be related to differences in the turbine structure and buoyancy, the mooring system, or both, rather than a difference swell and other environmental factors. The turbines at Hywind Scotland were cylindrical steel substructures individually moored by three chains in an unballasted catenary system. The Hywind Tampen turbines meanwhile are floated on a larger diameter, hollow concrete substructure connected in a honeycomb pattern by flexible cables utilising shared anchors; each turbine is connected to up to three separate turbines (see Figure 5). The exact mechanism generating the transient noises at Hywind Scotland is unknown, but this mechanism appears to no longer exist in the new substructure and mooring system utilised at Hywind Tampen.

Despite the turbines at Hywind Tampen being larger and capable of generating more power than those at Hywind Scotland, backpropagated source levels in Burns et al. (2022) were higher than in this study (see Table 11). The precise reason for this is unknown, however it is possible that the properties of the concrete substructure of the Hywind Tampen turbines has reduced the transmission path from the nacelle to the submerged section of the spar, either through mechanical damping or altering of the structural resonant frequencies, compared to the steel spar pillars used at Hywind Scotland. It is clear, though, that the noise levels in the water are less at Tampen. Another contributing factor may be the considerable transient noise from the mooring system at Hywind Scotland. It was not possible to exclude mooring noise from the received levels used to calculate the source levels in Burns et al. (2022), hence this may elevate the calculated source levels. For the same reasons, the largest modelled distance to the Southall et al. (2019) TTS thresholds was 80 m for Hywind Scotland

(15 kn, 75th percentile) compared to 60 m for Hywind Tampen (20 kn, 95th percentile), both for the very high-frequency cetacean hearing group.

Table 11. Differences between backpropagated broadband source levels at Hywind Tampen and Hywind Scotland for various wind speeds and percentiles.

Wind Speed	Median Source Levels			95 th Percentile Source Levels		
(kn)	Hywind Tampen	Hywind Scotland	Difference	Hywind Tampen	Hywind Scotland	Difference
	(dB re 1 µPa²m²)	(dB re 1 µPa²m²)	(dB)	(dB re 1 μPa²m²)	(dB re 1 µPa²m²)	(dB)
5	157.1	165.1	12.0	160.5	170.5	10.0
10	158.2	162.5	4.3	163.5	170.8	7.3
15	156.5	163.9	8.4	159.1	171.4	11.3
20	162.3	164.8	2.5	166.4	170.6	4.2
25	163.8	167.2	3.4	168.7	172.0	3.3

#### **Literature Cited**

- [ANSI] American National Standards Institute and [ASA] Acoustical Society of America. S1.1-2013. *American National Standard: Acoustical Terminology*. NY, USA. <a href="https://webstore.ansi.org/Standards/ASA/ANSIASAS12013">https://webstore.ansi.org/Standards/ASA/ANSIASAS12013</a>.
- [CMEMS] Copernicus Marine Environment Monitoring Service. 2023. Global Ocean Physics Reanalysis. <a href="https://doi.org/10.48670/moi-00021">https://doi.org/10.48670/moi-00021</a> (Accessed 2023).
- [EU] European Commision. 2022. European Marine Observation and Data Network (EMODnet) (web page). https://emodnet.ec.europa.eu/en/human-activities.
- [ISO] International Organization for Standardization. 2017a. ISO/DIS 18405.2:2017. Underwater acoustics— Terminology. Geneva. https://www.iso.org/standard/62406.html.
- [ISO] International Organization for Standardization. 2017b. *ISO 18405:2017. Underwater acoustics Terminology.* Geneva. <a href="https://www.iso.org/obp/ui/en/#!iso:std:62406:en">https://www.iso.org/obp/ui/en/#!iso:std:62406:en</a>.
- [NIOSH] National Institute for Occupational Safety and Health. 1998. *Criteria for a recommended standard: Occupational noise exposure. Revised Criteria*. Document 98-126. US Department of Health and Human Services, NIOSH, Cincinnati, OH, USA. 122 p. <a href="https://www.cdc.gov/niosh/docs/98-126/pdfs/98-126.pdf">https://www.cdc.gov/niosh/docs/98-126/pdfs/98-126.pdf</a>.
- [NMFS] National Marine Fisheries Service (US). 2018. 2018 Revision to: Technical Guidance for Assessing the Effects of Anthropogenic Sound on Marine Mammal Hearing (Version 2.0): Underwater Thresholds for Onset of Permanent and Temporary Threshold Shifts. US Department of Commerce, NOAA. NOAA Technical Memorandum NMFS-OPR-59. 167 p. <a href="https://media.fisheries.noaa.gov/dam-migration/tech_memo_acoustic_guidance_(20) (pdf)_508.pdf">https://media.fisheries.noaa.gov/dam-migration/tech_memo_acoustic_guidance_(20) (pdf)_508.pdf</a>.
- [WMO] World Meteorological Organization. 2023. *Guide to Instruments and Methods of Observation Volume I Measurement of Meteorological Variables*. WMO, Geneva. 574 p. <a href="https://library.wmo.int/idurl/4/68695">https://library.wmo.int/idurl/4/68695</a>.
- Au, W.W.L., R.A. Kastelein, T. Rippe, and N.M. Schooneman. 1999. Transmission beam pattern and echolocation signals of a harbor porpoise (*Phocoena phocoena*). *Journal of the Acoustical Society of America* 106(6): 3699-3705. https://doi.org/10.1121/1.428221.
- Buckingham, M.J. 2000. Wave propagation, stress relaxation, and grain-to-grain shearing in saturated, unconsolidated marine sediments. *Journal of the Acoustical Society of America* 108(6): 2796-2815. https://doi.org/10.1121/1.1322018.
- Burns, R.D.J., S.B. Martin, M.A. Wood, C.C. Wilson, C.E. Lumsden, and F. Pace. 2022. *HYWIND Scotland Floating Offshore Wind Farm: Sound Source Characterisation of Operational Floating Turbines*. Document 02521, Version 2.0. Technical report by JASCO Applied Sciences for Equinor Energy AS.
- Collins, M.D. 1993. A split-step Padé solution for the parabolic equation method. *Journal of the Acoustical Society of America* 93(4): 1736-1742. https://doi.org/10.1121/1.406739.
- Collins, M.D., R.J. Cederberg, D.B. King, and S. Chin-Bing. 1996. Comparison of algorithms for solving parabolic wave equations. *Journal of the Acoustical Society of America* 100(1): 178-182. <a href="https://doi.org/10.1121/1.415921">https://doi.org/10.1121/1.415921</a>.
- Coppens, A.B. 1981. Simple equations for the speed of sound in Neptunian waters. *Journal of the Acoustical Society of America* 69(3): 862-863. https://doi.org/10.1121/1.382038.
- Delarue, J.J.-Y., K.A. Kowarski, E.E. Maxner, J.T. MacDonnell, and S.B. Martin. 2018. *Acoustic Monitoring Along Canada's East Coast: August 2015 to July 2017*. Document 01279, Environmental Studies Research Funds Report Number 215, Version 1.0. Technical report by JASCO Applied Sciences for Environmental Studies Research Fund, Dartmouth, NS, Canada. 120 pp + appendices.
- Erbs, F., S.H. Elwen, and T. Gridley. 2017. Automatic classification of whistles from coastal dolphins of the southern African subregion. *Journal of the Acoustical Society of America* 141(4): 2489-2500. <a href="https://doi.org/10.1121/1.4978000">https://doi.org/10.1121/1.4978000</a>.

- Fisher, F.H. and V.P. Simmons. 1977. Sound absorption in sea water. *Journal of the Acoustical Society of America* 62(3): 558-564. https://doi.org/10.1121/1.381574.
- Hamilton, E.L. 1980. Geoacoustic modeling of the sea floor. *Journal of the Acoustical Society of America* 68(5): 1313-1340. https://doi.org/10.1121/1.385100.
- Hersbach, H., B. Bell, P. Berrisford, G. Biavati, A. Horányi, J. Muñoz Sabater, J. Nicolas, C. Peubey, R. Radu, et al. 2023. *ERA5 hourly data on single levels from 1940 to present* (webpage).
- Hodge, K.B., C.A. Muirhead, J.L. Morano, C.W. Clark, and A.N. Rice. 2015. North Atlantic right whale occurrence near wind energy areas along the mid-Atlantic US coast: Implications for management. *Endangered Species Research* 28(3): 225-234. <a href="https://doi.org/10.3354/esr00683">https://doi.org/10.3354/esr00683</a>.
- Holzer, T.L., M.J. Bennett, T.E. Noce, and J.C. Tinsley, III. 2005. Shear-Wave Velocity of Surficial Geologic Sediments in Northern California: Statistical Distributions and Depth Dependence. *Earthquake Spectra* 21(1): 161-177. <a href="https://doi.org/10.1193/1.1852561">https://doi.org/10.1193/1.1852561</a>.
- Kowarski, K.A., J.J.-Y. Delarue, B.J. Gaudet, and S.B. Martin. 2021. Automatic data selection for validation: A method to determine cetacean occurrence in large acoustic data sets. *JASA Express Letters* 1: 051201. https://doi.org/10.1121/10.0004851.
- Martin, B., J. MacDonnell, J. Vallarta, E. Lumsden, and R.D.J. Burns. 2011. HYWIND Acoustics Measurements Report. Ambient Levels and HYWIND SIgnature. Ver 1.3. Document 00229. JASCO Applied Sciences (UK) Ltd.

  <a href="https://static1.squarespace.com/static/52aa2773e4b0f29916f46675/t/5fda3a9324291a0a8b1d0a25/1608137377245/Equinor-Hywind-Acoustic-Measurement-Report-JASCO-00229-December-2011.pdf">https://static1.squarespace.com/static/52aa2773e4b0f29916f46675/t/5fda3a9324291a0a8b1d0a25/1608137377245/Equinor-Hywind-Acoustic-Measurement-Report-JASCO-00229-December-2011.pdf</a>.
- Martin, S.B., K. Lucke, and D.R. Barclay. 2020. Techniques for distinguishing between impulsive and non-impulsive sound in the context of regulating sound exposure for marine mammals. *Journal of the Acoustical Society of America* 147(4): 2159-2176. https://doi.org/10.1121/10.0000971.
- Martin, S.B., B.J. Gaudet, H. Klinck, P.J. Dugan, J.L. Miksis-Olds, D.K. Mellinger, D.A. Mann, O. Boebel, C.C. Wilson, et al. 2021. Hybrid millidecade spectra: A practical format for exchange of long-term ambient sound data. *JASA Express Letters* 1(1), https://doi.org/10.1121/10.0003324.
- Merchant, N.D., T.R. Barton, P.M. Thompson, E. Pirotta, D.T. Dakin, and J. Dorocicz. 2013. Spectral probability density as a tool for ambient noise analysis. *Journal of the Acoustical Society of America* 133(4): EL262-EL267. https://doi.org/10.1121/1.4794934.
- Møhl, B., M. Wahlberg, P.T. Madsen, L.A. Miller, and A. Surlykke. 2000. Sperm whale clicks: Directionality and source level revisited. *Journal of the Acoustical Society of America* 107(1): 638-648. <a href="https://doi.org/10.1121/1.428329">https://doi.org/10.1121/1.428329</a>.
- Mouy, X., S.K. Archer, S. Dosso, S. Dudas, P. English, C. Foord, W. Halliday, F. Juanes, D. Lancaster, et al. 2024. Automatic detection of unidentified fish sounds: A comparison of traditional machine learning with deep learning. *Frontiers in Remote Sensing* 5. <a href="https://www.frontiersin.org/journals/remote-sensing/articles/10.3389/frsen.2024.1439995">https://www.frontiersin.org/journals/remote-sensing/articles/10.3389/frsen.2024.1439995</a>.
- Porter, M.B. and Y.C. Liu. 1994. Finite-element ray tracing. *In*: Lee, D. and M.H. Schultz (eds.). *International Conference on Theoretical and Computational Acoustics*. Volume 2. World Scientific Publishing Co. pp. 947-956.
- Širović, A., A. Rice, E. Chou, J.A. Hildebrand, S.M. Wiggins, and M.A. Roch. 2015. Seven years of blue and fin whale call abundance in the Southern California Bight. *Endangered Species Research* 28(1): 61-76. https://doi.org/10.3354/esr00676.
- Southall, B.L., J.J. Finneran, C.J. Reichmuth, P.E. Nachtigall, D.R. Ketten, A.E. Bowles, W.T. Ellison, D.P. Nowacek, and P.L. Tyack. 2019. Marine Mammal Noise Exposure Criteria: Updated Scientific Recommendations for Residual Hearing Effects. *Aquatic Mammals* 45(2): 125-232. https://doi.org/10.1578/AM.45.2.2019.125.

- Thode, A.M., T. Sakai, J. Michalec, S. Rankin, M.S. Soldevilla, S.B. Martin, and K.H. Kim. 2019. Displaying bioacoustic directional information from sonobuoys using "azigrams". *Journal of the Acoustical Society of America* 146(1): 95-102. <a href="https://doi.org/10.1121/1.5114810">https://doi.org/10.1121/1.5114810</a>.
- Urazghildiiev, I.R. and D.E. Hannay. 2017. Maximum likelihood estimators and Cramér–Rao bound for estimating azimuth and elevation angles using compact arrays. *Journal of the Acoustical Society of America* 141(4): 2548-2555. https://doi.org/10.1121/1.4979792.
- van den Berg, G.P. 2005. The beat is getting stronger: The effect of atmospheric stability on low frequency modulated sound of wind turbines. *Journal of low frequency noise vibration and active control* 24(1): 1-23.
- Wenz, G.M. 1962. Acoustic Ambient Noise in the Ocean: Spectra and Sources. *Journal of the Acoustical Society of America* 34(12): 1936-1956. https://doi.org/10.1121/1.1909155.
- Zhang, Z.Y. and C.T. Tindle. 1995. Improved equivalent fluid approximations for a low shear speed ocean bottom. *Journal of the Acoustical Society of America* 98(6): 3391-3396. https://doi.org/10.1121/1.413789.

## **Appendix A. Acoustic Data Analysis Methods**

#### A.1. Total Ambient Sound Levels

Underwater sound pressure amplitude is quantified in decibels (dB) relative to a fixed reference pressure of  $p_0$  = 1 µPa. Because the perceived loudness of sound is not necessarily proportional to the instantaneous acoustic pressure, several sound level metrics are commonly used to evaluate sound and its effects on marine life. Here we provide specific definitions of relevant metrics used in this report. Where possible, we follow International Organization for Standardization definitions and symbols for sound metrics (e.g., ISO 18405:2017b, ANSI S1.1-2013).

The zero-to-peak pressure level, or peak pressure level (PK or  $L_{p,pk}$ ; dB re 1  $\mu$ Pa), is the decibel level of the maximum instantaneous sound pressure level in a stated frequency band attained by an acoustic pressure signal, p(t):

$$L_{\rm pk} = 10 \log_{10} \frac{p_{\rm pk}^2}{p_0^2} = 20 \log_{10} \frac{p_{\rm pk}}{p_0} = 20 \log_{10} \frac{\max|p(t)|}{p_0} \,. \tag{A-1}$$

PK is often included as criterion for assessing whether a sound is potentially injurious; however, because it does not account for the duration of a noise event, it is generally a poor indicator of perceived loudness.

The sound pressure level (SPL or  $L_p$ ; dB re 1  $\mu$ Pa) is the decibel level of the root-mean-square (rms) pressure in a stated frequency band over a specified time window (T; s) containing the acoustic event of interest. It is important to note that SPL always refers to a rms pressure level and therefore not instantaneous pressure:

$$SPL = L_p = 10 \log_{10} \left[ \frac{1}{T} \int_{T} p^2(t) dt / p_0^2 \right]$$
 (A-2)

The SPL represents a nominal effective continuous sound over the duration of an acoustic event, such as the emission of one acoustic pulse, a marine mammal vocalization, the passage of a vessel, or over a fixed duration. Because the window length, T, is the divisor, events with similar sound exposure level (SEL), but more spread out in time have a lower SPL.

The sound exposure level (SEL or  $L_E$ ; dB re 1  $\mu$ Pa² s) is the time-integral of the squared acoustic pressure over a duration (T):

$$L_E = 10 \log_{10} \left( \int_T p^2(t) dt / T_0 p_0^2 \right) dB$$
, (A-3)

where  $T_0$  is a reference time interval of 1 s. SEL continues to increase with time when non-zero pressure signals are present. It is a dose-type measurement, so the integration time applied must be carefully considered for its relevance to impact to the exposed recipients. SEL can be calculated over a fixed duration, such as the time of a single event or a period with multiple acoustic events.

SEL can be calculated over periods with multiple events or over a fixed duration. For a fixed duration, the square pressure is integrated over the duration of interest. For multiple events, the SEL can be computed by summing (in linear units) the SEL of the *N* individual events:

$$L_{E,N} = 10 \log_{10} \sum_{i=1}^{N} 10^{\frac{L_{E,i}}{10}}$$
(A-4)

Because the SPL and SEL are both computed from the integral of square pressure, these metrics are related numerically by the following expression, which depends only on the duration of the time window T:

$$L_p = L_E - 10\log_{10}(T) \tag{A-5}$$

Energy equivalent SPL ( $L_{eq}$ ; dB re 1  $\mu$ Pa) denotes the SPL of a stationary (constant amplitude) sound that generates the same SEL as the signal being examined, p(t), over the same period, T:

$$L_{\rm eq} = 10 \log_{10} \left[ \frac{1}{T} \int_{T} p^{2}(t) dt / p_{0}^{2} \right]$$
 (A-6)

The equations for SPL and the energy-equivalent SPL are numerically identical. Conceptually, the difference between the two metrics is that the former is typically computed over short periods (typically of 1 s or less) and tracks the fluctuations of a non-steady acoustic signal, whereas the latter reflects the average SPL of an acoustic signal over times typically of 1 min to several hours.

#### A.2. Decidecade Band Analysis

The distribution of a sound's power with frequency is described by the sound's spectrum. The sound spectrum can be split into a series of adjacent frequency bands. Splitting a spectrum into 1 Hz wide bands, called passbands, yields the power spectral density of the sound. These values directly compare to the Wenz curves, which represent typical deep ocean sound levels (Wenz 1962). This splitting of the spectrum into passbands of a constant width of 1 Hz, however, does not represent how animals perceive sound.

Because animals perceive exponential increases in frequency rather than linear increases, analysing a sound spectrum with passbands that increase exponentially in size better approximates real-world scenarios. In underwater acoustics, a spectrum is commonly split into decidecade bands, which are one tenth of a decade wide. A decidecade is sometimes referred to as a "third-octave" because one tenth of a decade is approximately equal to one third of an octave. Each decade represents a factor 10 in sound frequency. Each octave represents a factor 2 in sound frequency. The centre frequency of the ith band,  $f_c(i)$ , is defined as:

$$f_{\rm c}(i) = 10^{\frac{i}{10}} \,\mathrm{kHz}$$
 (A-7)

and the low  $(f_{lo})$  and high  $(f_{hi})$  frequency limits of the ith decade band are defined as:

$$f_{\text{lo},i} = 10^{\frac{-1}{20}} f_{\text{c}}(i) \text{ and } f_{\text{hi},i} = 10^{\frac{1}{20}} f_{\text{c}}(i)$$
 (A-8)

The decidecade bands become wider with increasing frequency, and on a logarithmic scale the bands appear equally spaced (Figure A-1). Decade and decidecade band centre frequencies and limits are presented in Tables A-1 and A-2 respectively.

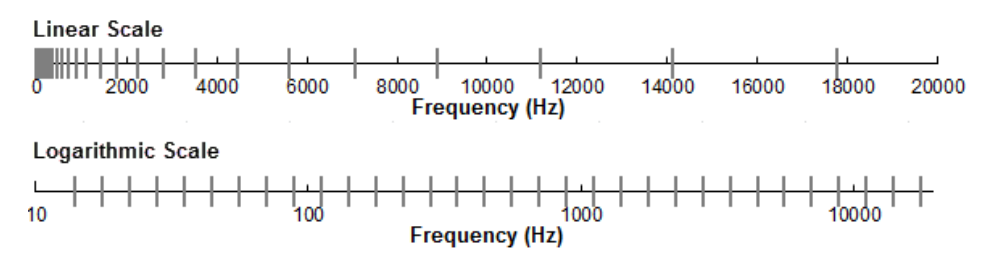


Figure A-1. Decidecade frequency bands (vertical lines) shown on a linear frequency scale and a logarithmic scale.

The sound pressure level in the *i*th band ( $L_{p,i}$ ) is computed from the spectrum S(f) between  $f_{lo,i}$  and  $f_{hi,i}$ :

$$L_{p,i} = 10 \log_{10} \int_{f_{lo,i}}^{f_{hi,i}} S(f) df dB,$$
 (A-9)

summing the sound pressure level of all the bands yields the broadband sound pressure level:

Broadband SPL = 
$$10 \log_{10} \sum_{i} 10^{\frac{L_{p,i}}{10}} \text{ dB}$$
. (A-10)

Figure A-2 shows an example of how the decidecade band sound pressure levels compare to the sound pressure spectral density levels of an ambient sound signal. Because the decidecade bands are wider than 1 Hz, the decidecade band SPL is higher than the spectral levels at higher frequencies. Decidecade band analysis is applied to continuous and impulsive noise sources. For impulsive sources, the decidecade band SEL is typically reported.

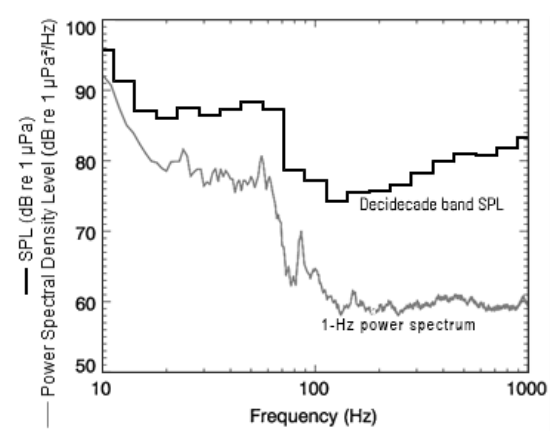


Figure A-2. Sound pressure spectral density levels and the corresponding decidecade band sound pressure levels of example ambient sound shown on a logarithmic frequency scale. Because the decidecade bands are wider with increasing frequency, the third-octave-band SPL is higher than the power spectrum which is based on bands with a constant width of 1 Hz.

Table A-1. Decade-band frequencies (Hz).

Decade band	Lower frequency	Nominal centre frequency	Upper frequency
1	8.9	28.2	89.1
2	89.1	281.8	891
3	891	2819	8913
4	8913	28185	89130¹

¹ Above the upper frequency limit of the Hywind Tampen recorders.

Table A-2. Decidecade-band frequencies (Hz).

Band	Lower frequency	Nominal centre frequency	Upper frequency
10	8.9	10.0	11.2
11	11.2	12.6	14.1
12	14.1	15.8	17.8
13	17.8	20.0	22.4
14	22.4	25.1	28.2
15	28.2	31.6	35.5
16	35.5	39.8	44.7
17	44.7	50.1	56.2
18	56.2	63.1	70.8
19	70.8	79.4	89.1
20	89.1	100.0	112.2
21	112	126	141
22	141	158	178
23	178	200	224
24	224	251	282
25	282	316	355
26	355	398	447
27	447	501	562
28	562	631	708
29	708	794	891
30	891	1000	1122
31	1122	1259	1413
32	1413	1585	1778
33	1778	1995	2239
34	2239	2512	2818
35	2818	3162	3548
36	3548	3981	4467
37	4467	5012	5623
38	5623	6310	7079
39	7079	7943	8913
40	8913	10000	11220
41	11220	12589	14125

## **Appendix B. Ambient Noise Analysis Results**

## **B.1. PSD Plots for All Four Hydrophone Channels at Station 1**

Power Spectral Density spectrograms and Decidecade band SPL and power spectral densities with percentiles plots are provided below for all four recording channels at Station 1.

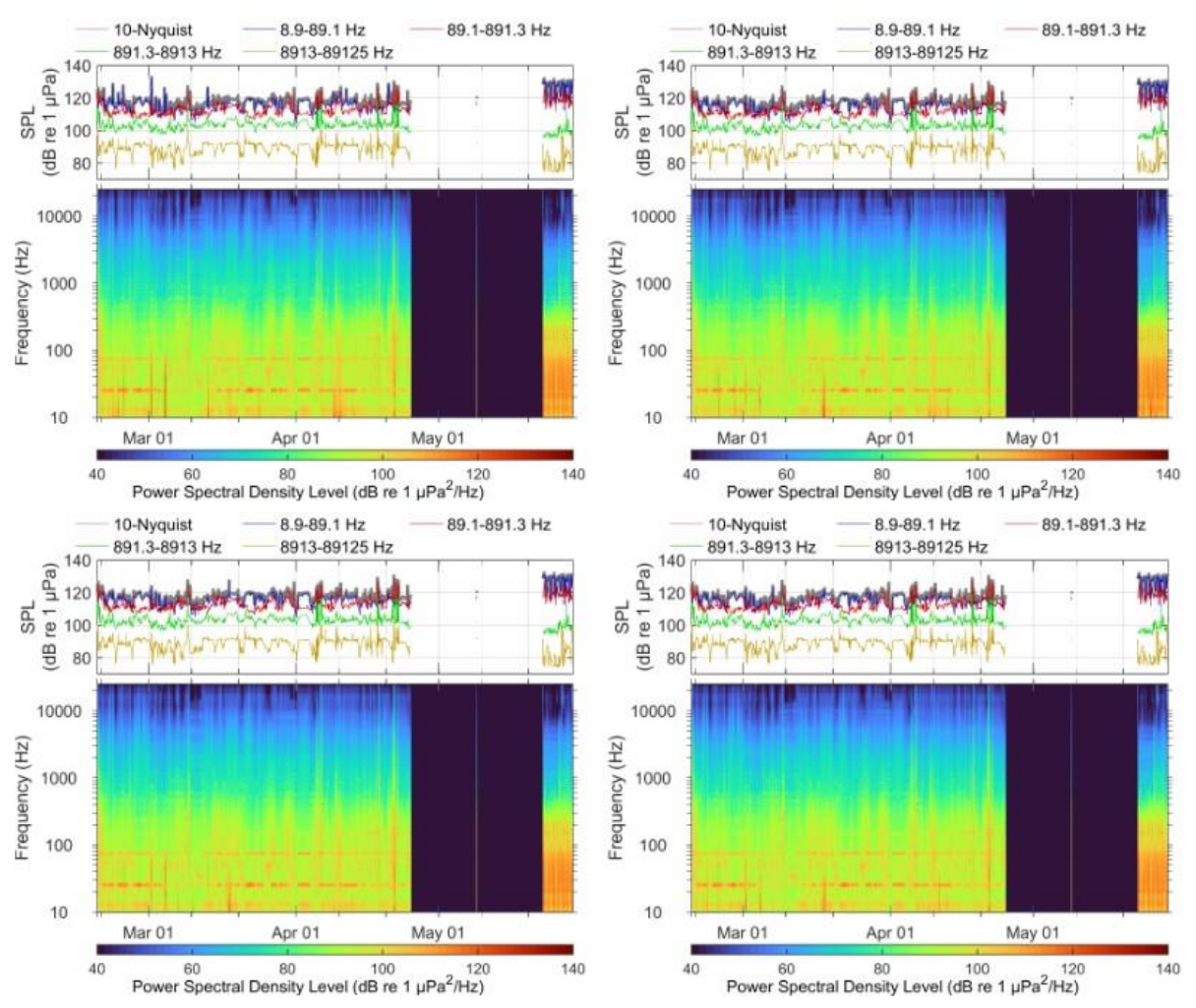


Figure B-1. Acoustic summary of the recorder at Station 1 for channels A (upper left), B (upper right), C (lower left), and D (lower right).

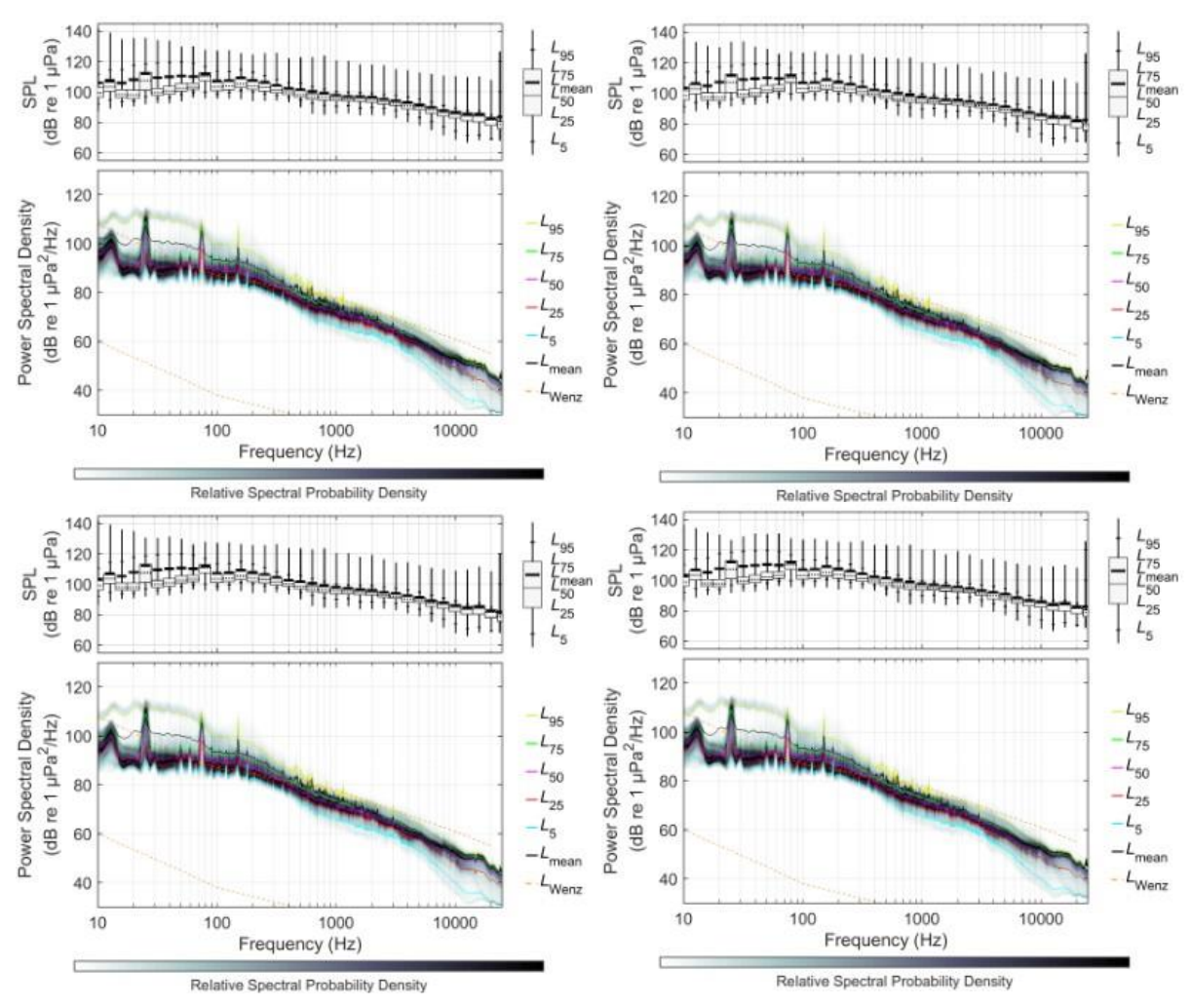


Figure B-2. Decidecade band SPL and power spectral densities with percentiles for the recorder at Station 1 for channels A (upper left), B (upper right), C (lower left), and D (lower right).

## **B.2. PSD Plots for All Four Hydrophone Channels at Station 2**

Power Spectral Density spectrograms and Decidecade band SPL and power spectral densities with percentiles plots are provided below for all four recording channels at Station 2.

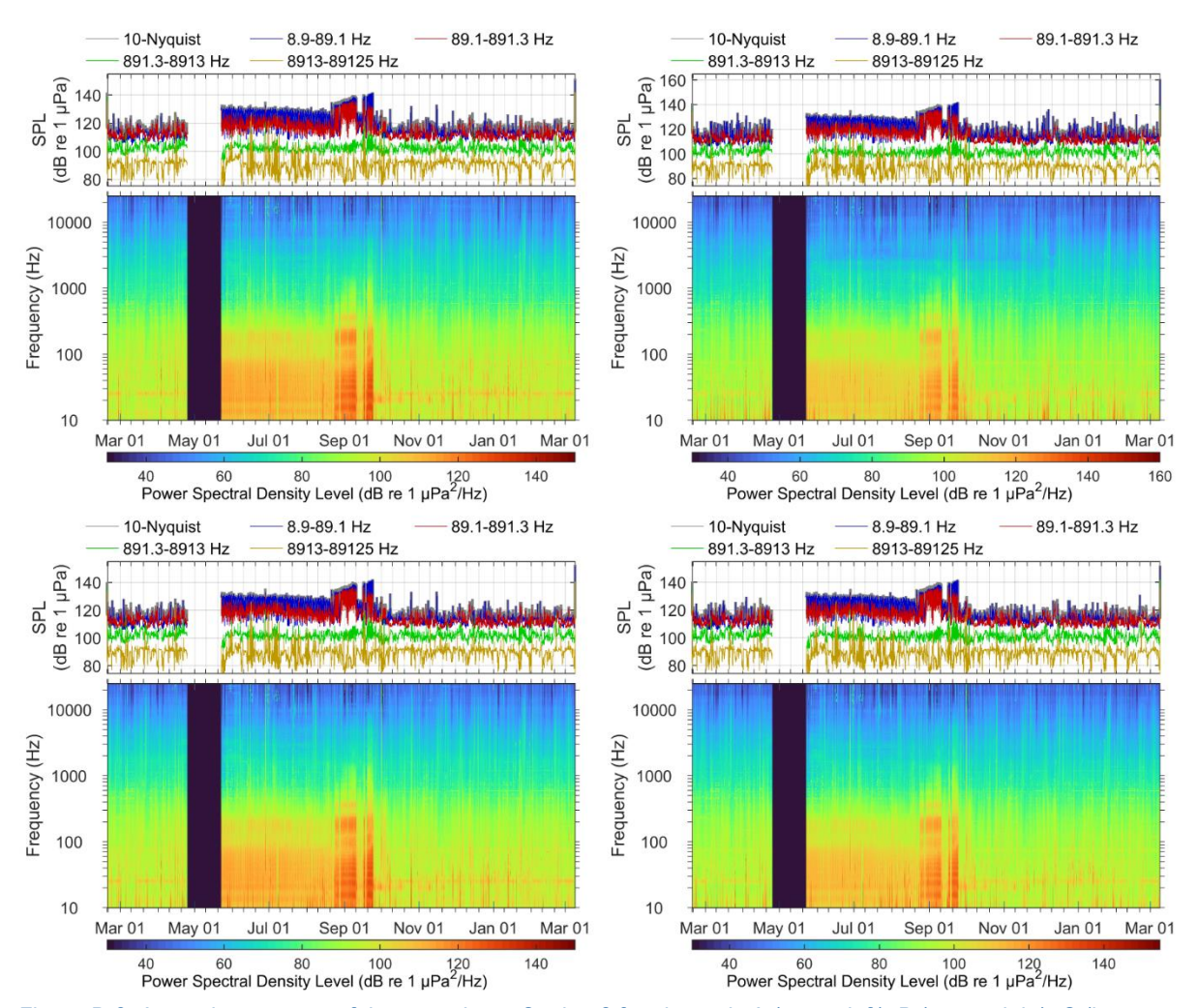


Figure B-3. Acoustic summary of the recorder at Station 2 for channels A (upper left), B (upper right), C (lower left), and D (lower right).

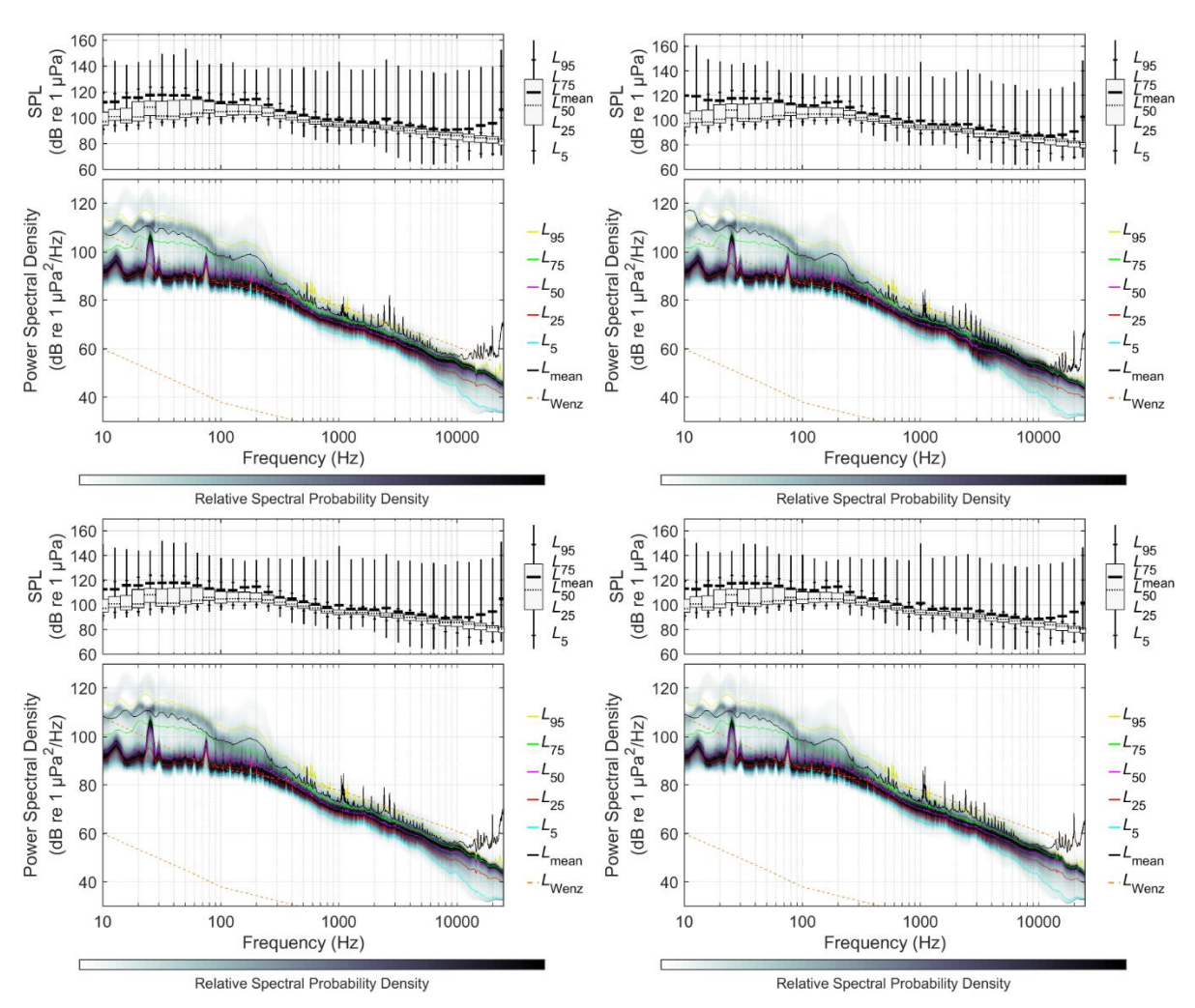


Figure B-4. Decidecade band SPL and power spectral densities with percentiles for the recorder at Station 1 for channels A (upper left), B (upper right), C (lower left), and D (lower right).

## **Appendix C. Directional Analysis**

#### C.1. Orthogonal Arrays of Omnidirectional Hydrophones

The analysis was performed using a maximum likelihood estimation (MLE) beamformer (Urazghildiiev and Hannay 2017). For each beam, the time delay of arrival between hydrophones are computed assuming that plane wave arrives from that direction. The ability of the MLE beamformer to determine the direction of arrival depends on the time delay between hydrophones. When the delay is greater than the time required for one half of a wavelength to travel between the hydrophones, the results become increasingly ambiguous, which sets an upper limit on the frequencies that may be analysed. If the delay, which equates to a phase change, is not long enough, then there is not enough information to determine the direction of arrival, which sets a lower limit on the frequencies that can be analysed as a function of the spacing between the hydrophones. This is manifested by an increase in the bearing estimation error that increases as the frequency decreases. It also depends on the signal-tonoise ratio (SNR) between the signal of interest and the background. The error can be reduced by increasing the spacing between hydrophones, however, that also lowers the maximum usable frequency.

During deployment preparations the distances between the tips of each hydrophone pair were measured. These distances, along with the nominal hydrophone locations, were then used in a least-squares regression to find the precise hydrophone locations relative to the reference hydrophone. For the array deployed at Station 1, the nominal hydrophone spacing was approximately 0.5 m (Table C-1), and therefore the upper cut-off frequency at the speed of sound is approximately 750 Hz. For frequencies above the 750 Hz cut-off, broadband direction of arrivals becomes ambiguous when applying a beamformer. Instead, the time delay of arrival of a transient signal on each of the hydrophones may be used to determine the direction.

For simplicity and power savings, the AMARs with arrays of multiple omnidirectional hydrophones did not include a compass sensor. Orientation of the array was determined using three separate methods; baseplate placement and orientation using the compass of the deployment ROV, matching the received sound levels from the deploying vessel after deployment to the AIS vessel track, and matching received tonals to known turbine bearings.

The arrays are formed from standard omnidirectional hydrophones. Each hydrophone is calibrated through normal processes before deployment and on retrieval, which provides assurance of system operations.

Location	Channel A	Channel B	Channel C	Channel D
Х	0	0.470	0	0
Υ	0	0	0	0.480

-0.595

Table C-1. Offsets (in meters) of the Station 1 hydrophones. Channel A is the top hydrophone.

-0.595

### C.2. Visualizing the Direction of Arrival of Broadband Data

Spectrograms that use an intensity gradient (e.g., grayscale) or a colour gradient (e.g., colour map) to communicate the differences in received sound levels as a function of frequency and time. However, it is also possible to use colour to represent direction. If intensity is not included in the mapping, then the result is an azigram (Thode et al. 2019). However, by including intensity the background noise is reduced, which improves a user's understanding of the data, which is referred to as a 'directogram'. This type of representation has also been used in airborne and naval sonar systems for several

-0.595

0

decades. The colour-direction-intensity was implemented using the HSV colour map for direction since it 'rotates' from red-to-red, and the 'alpha' channel is used to encode intensity.

## **Appendix D. Marine Mammal Impact Criteria**

#### D.1. Auditory injury and Temporary Threshold Shift (TTS)

Impact criteria for assessing onset of auditory injury and TTS from acoustic exposure in marine mammals from Southall et al. (2019) are specified as SEL_{24h} thresholds; the subscript '24h' refers to the accumulation period for calculating SEL. The auditory impact thresholds for non-impulsive sound as applied in this study are presented in Table D-1.

Table D-1. Sound exposure level (SEL) thresholds for auditory injury (PTS onset), and TTS onset in marine mammals for non-impulsive sounds, as recommended by Southall et al. (2019).

Auditon: Croup	Weighted SEL _{24h} (dB re 1 μPa ² s)				
Auditory Group	Auditory injury (PTS)	TTS			
Low-frequency cetaceans	199	179			
High-frequency cetaceans	198	178			
Very high-frequency cetaceans	173	153			
Phocid pinnipeds	201	181			
Otariid pinnipeds	219	199			

#### **D.2. Auditory Frequency Weighting Functions**

The potential for noise to affect animals of a given species depends on how well that animal can hear it. The importance of sound components at particular frequencies can be scaled by frequency weighting relevant to an animal's sensitivity to those frequencies.

In 2015, a US Navy technical report by Finneran (2015) recommended auditory weighting functions. The auditory weighting functions for marine mammals are applied in a similar way as A-weighting for noise level assessments for humans. These frequency-weighting functions are expressed as:

$$G(f) = K + 10 \log_{10} \left\{ \frac{(f/f_1)^{2a}}{[1 + (f/f_1)^2]^a [1 + (f/f_2)^2]^b} \right\}.$$
 (D-1)

Finneran (2015) proposed five functional hearing groups for marine mammals in water: low-, mid- and high-frequency cetaceans (LF, MF, and HF cetaceans, respectively), phocid pinnipeds, and otariid pinnipeds. The parameters for these frequency-weighting functions were further modified the following year (Finneran 2016) and were adopted in NOAA's technical guidance that assesses acoustic impacts on marine mammals (NMFS 2018), and in the guidance by Southall et al. (2019).

The various updates did not affect the content related to either the definitions of frequency-weighting functions or the threshold values, although the names of the groups and some of the species they apply to vary somewhat between publications. Table D-2 lists the frequency-weighting parameters for the Southall et al. (2019) hearing groups, and Figure D-1 shows the resulting frequency-weighting curves.

Table D-2. Parameters for the auditory weighting functions recommended by Southall et al. (2019).

Functional hearing group	а	b	$f_1$ (Hz)	$f_2$ (Hz)	<i>K</i> ¹ (dB)
Low-frequency cetaceans	1.0	2	200	19,000	0.13
High-frequency cetaceans	1.6	2	8,800	110,000	1.20
Very high-frequency cetaceans	1.8	2	12,000	140,000	1.36
Phocid carnivores in water	1.0	2	1,900	30,000	0.75
Other marine carnivores in water	2.0	2	940	25,000	0.64

¹ In Southall et al. (2019), this constant is symbolized by C.

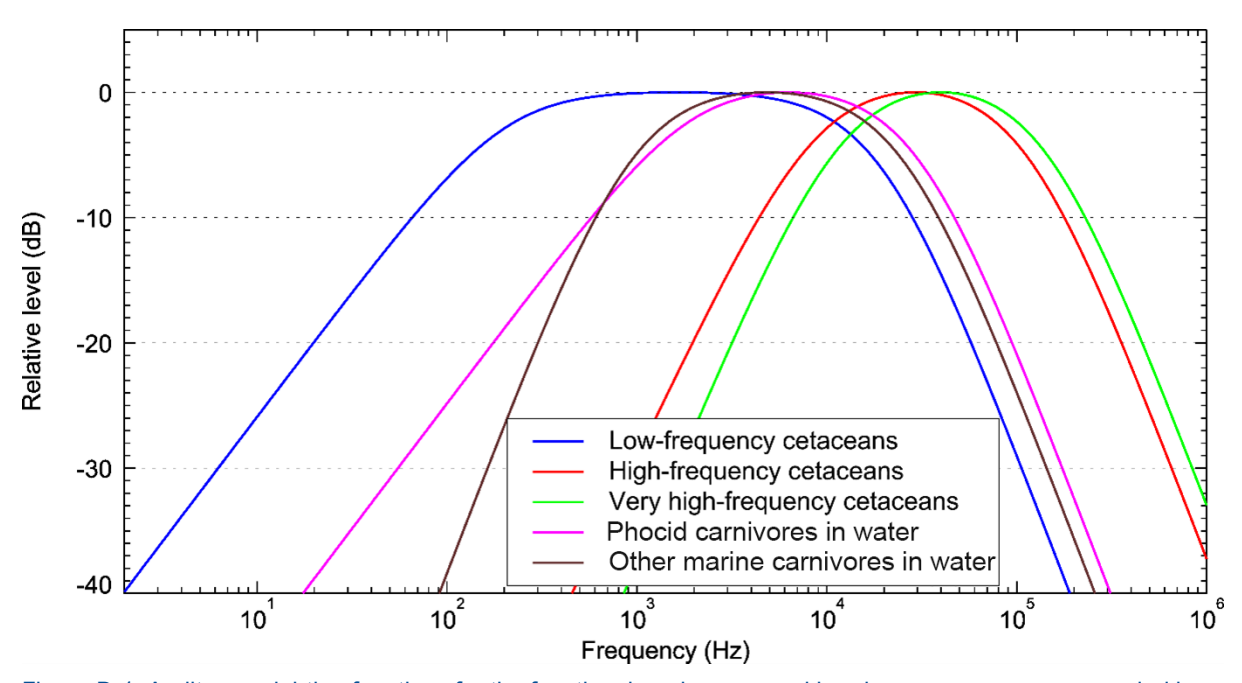


Figure D-1. Auditory weighting functions for the functional marine mammal hearing groups as recommended by Southall et al. (2019).

## **Appendix E. Marine Mammal Detections**

In addition to processing of the data through JASCO's cod grunt detector, outlined in Section 3.2.5, a number of JASCO's automated detector/classifiers were also applied to the data to detect marine mammal clicks and vocalisations.

Odontocete clicks are high-frequency impulses ranging from 1 to over 150 kHz (Au et al. 1999, Møhl et al. 2000). An automated click detector was applied to identify clicks from various odontocetes. This automated detector is based on zero-crossings in the acoustic time series. Zero-crossings are the rapid oscillations of a click's pressure waveform above and below the signal's normal level. Zero-crossing-based features of automatically detected events are then compared to templates of known clicks for classification. Flowcharts of the automated click and click train detector/classifier processes are shown in Figures D-1 and D-2 respectively.

Tonal signals are narrowband, often frequency-modulated, signals produced by many species across a range of taxa (e.g., baleen whale moans, delphinids whistles). The automated tonal signal detector identified continuous contours of elevated energy (see Figure D-3) and classified them against a library of marine mammal signals. JASCO's suite of tonal automated detectors includes species/signal-specific detectors and those that are more generic, capturing signals from potentially more than one species that overlap in spectral characteristics.

A brief manual validation confirmed the presence of sperm whale and killer whale vocalisations in the data, spectrograms are presented in Sections E.1 and E.2. No baleen whales were manually confirmed in the data, though an absence of confirmed detections does not necessarily indicate absence.

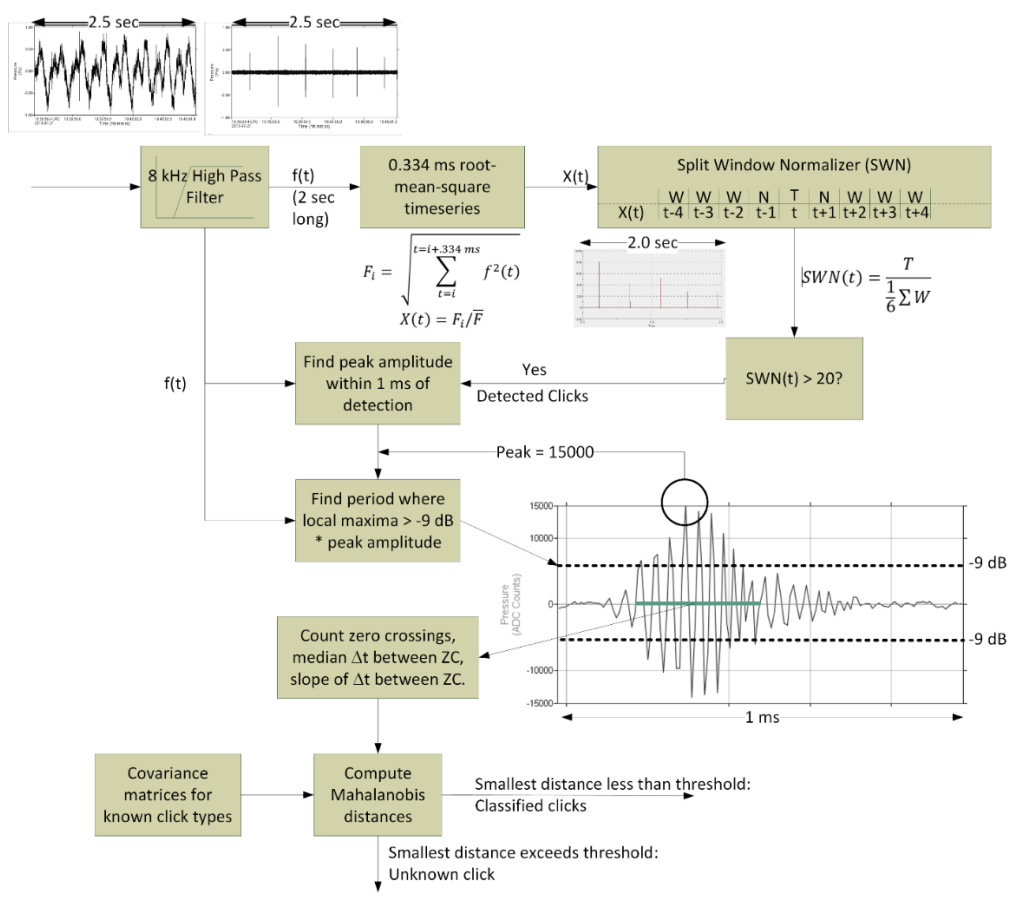


Figure E-1. Flowchart of the automated click detector/classifier process.

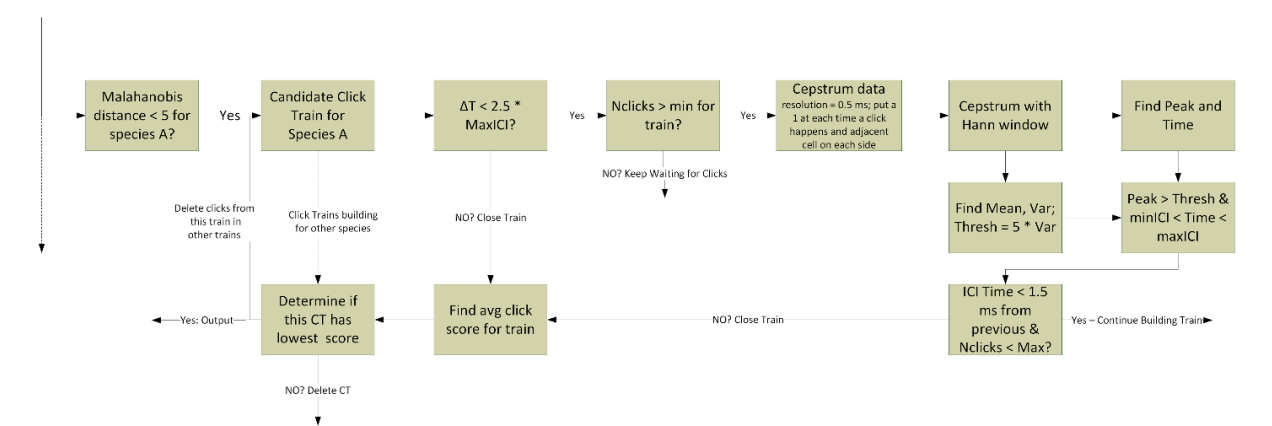


Figure E-2. Flowchart of the click train automated detector/classifier process.

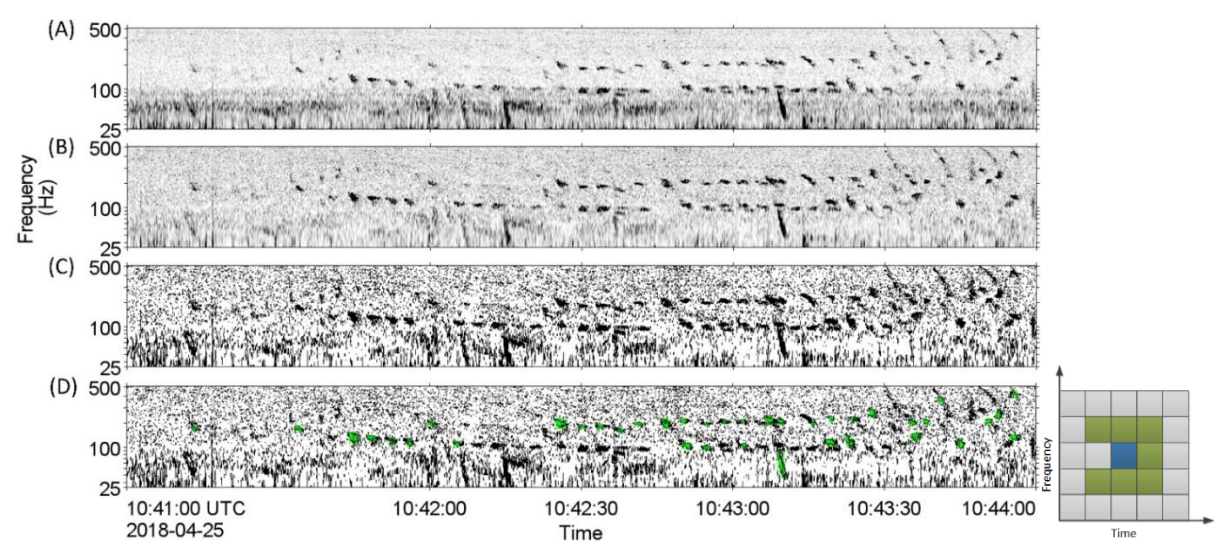


Figure E-3. Illustration of the contour detection process. (A) A spectrogram is generated at the frequency and time resolutions appropriate for the tonal calls of interest. (B) A median normalizer is applied at each frequency. (C) The data are turned into a binary representation by setting all normalized values less than the threshold to 0 and all values greater than the threshold to 1. (D) The regions that are '1' in the binary spectrogram are connected to create contours, which are then sorted to detect signals of interest, shown here as green overlays. Bins are connected according to the adjacent plot, where the blue square represents a bin of the binary spectrogram equalling 1, and the green squares represent the potential bins it could be connected to. The algorithm advances from left to right, so grey cells left of the test cell need not be checked.

#### E.1. Sperm Whales

A spectrogram showing an extended sperm whale click train from Station 1 is shown in Figure D-4. As well as the high amplitude sperm whale clicks which are visible in both the spectrogram and the pressure signal, there are faint signals which may potentially be noises from the mooring system (see Section 3.2.4) as well as strong low frequency tonal signals related to rotation/power generation of the turbines.

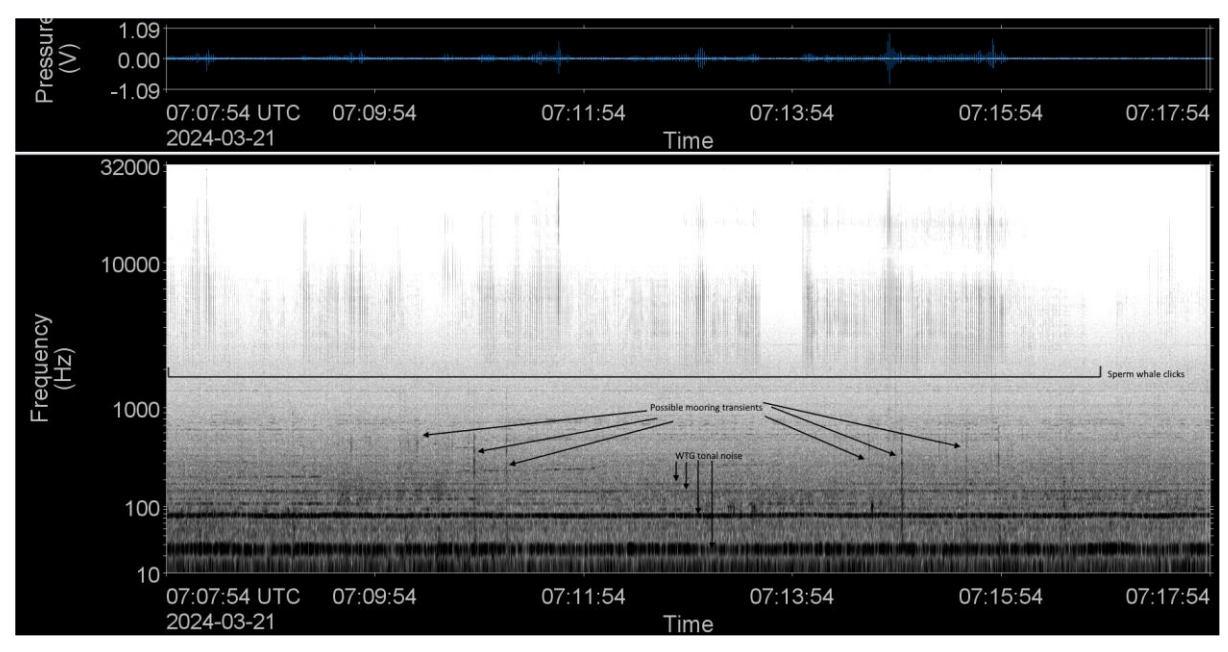


Figure E-4. Spectrogram showing sperm whale clicks in a recording from Station 1 among possible mooring transients and tonal noise from the WTGs.

#### E.2. Killer Whales

A spectrogram showing detected killer whale vocalisations from Station 4 is shown in Figure D-5. Echolocation clicks and click trains are visible as sharp vertical lines in the spectrogram, while tonal whistles are visible as stacked horizontal lines typically rising in frequency. It should be noted that despite the visible evidence of killer whale activity in the spectrogram, remarkably little is visible in the pressure signal. This section of recording was dominated by seismic survey noise, which can be seen in the repetitive pattern in the pressure signal but is not visible in the spectrogram due to the very low frequency nature of seismic noise being below the displayed frequency range.

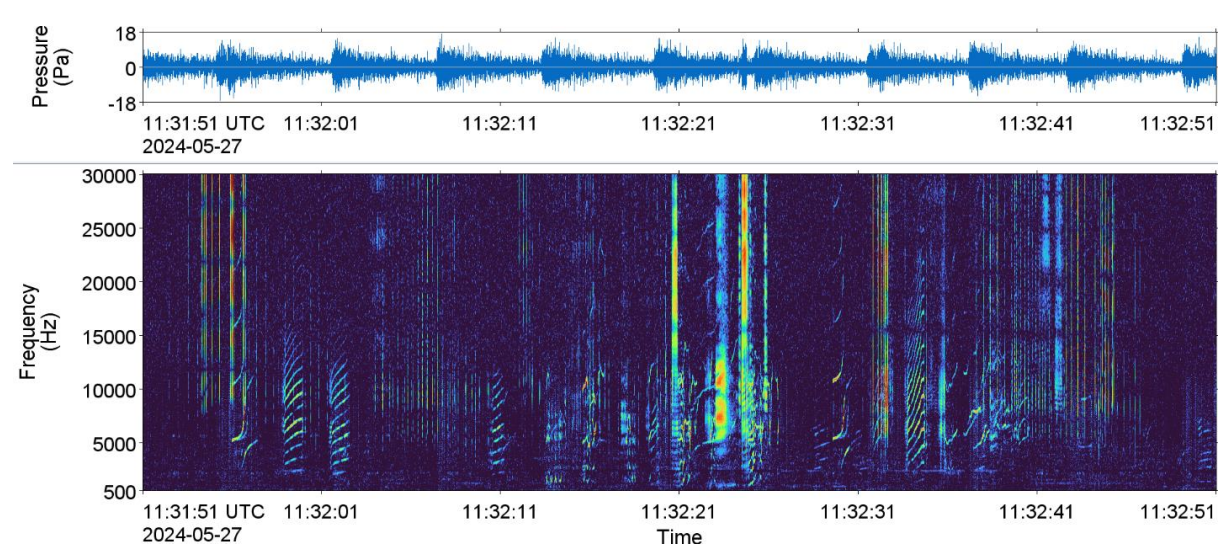


Figure E-5. Spectrogram showing killer whale echolocation clicks and whistles in a recording from Station 4.

#### E.3. Sperm Whales & Killer Whales

Figure D-6 shows a spectrogram of a period of simultaneous sperm whale and killer whale clicks and vocalisations recorded at Station 4. The sperm whale clicks can be differentiated by their lower frequency range and wider temporal spacing compared to the killer whale clicks. As in Figure D-5, the pressure signal is dominated by a seismic survey which does not appear in the spectrogram because of the displayed frequency range.

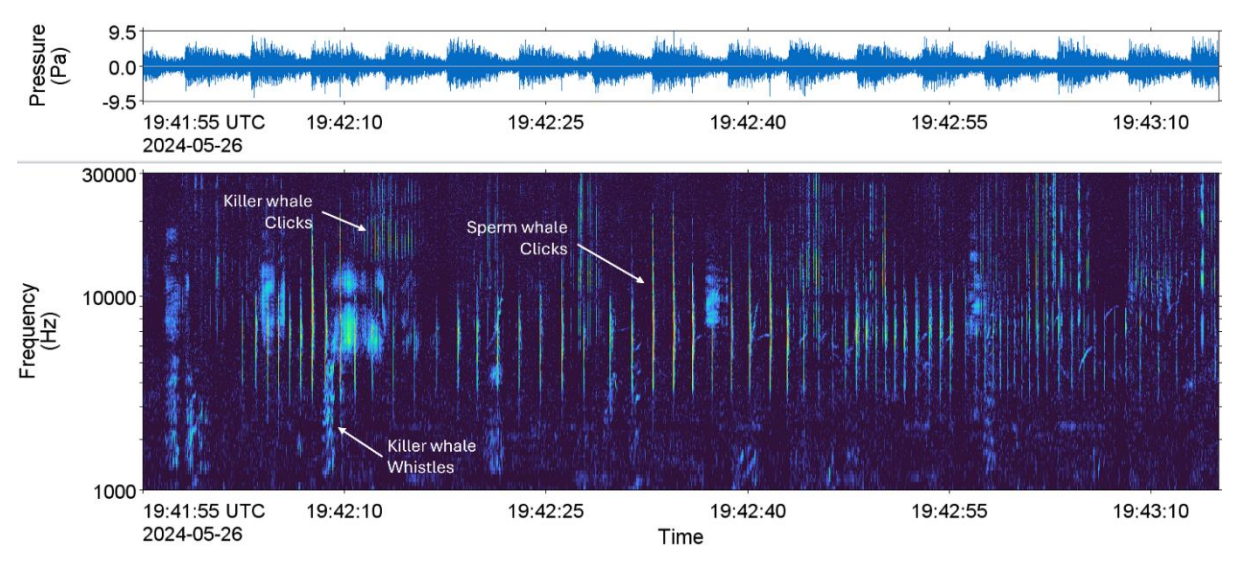


Figure E-6. Spectrogram showing simultaneous sperm whale clicks, killer whale clicks, and killer whale whistles in a recording from Station 4.

# **Appendix F. Broadband Received Levels**

#### F.1. Received Levels from Box Plots

Table F-1. Broadband received levels used in box plots. Stated minimums and maximums exclude outliers displayed in Section 3.3.

W		Broadband sound pressure level (dB re 1 µPa)					
Wind speed (kn)	Station	Minimum	Lower Quartile	Median	Upper Quartile	Maximum	
	1	109.7	112.6	113.9	115.3	121.3	
5	2	110.8	112.2	113.8	115.0	119.9	
5	3	109.5	112.5	113.6	115.5	122.9	
	4	109.4	112.0	113.3	115.5	124.9	
	1	111.0	113.3	115.1	116.7	126.4	
40	2	109.7	112.6	114.4	116.1	125.6	
10	3	110.1	112.8	114.6	116.5	125.7	
	4	108.3	111.7	113.7	116.3	128.2	
	1	110.6	113.4	115.2	116.8	124.6	
45	2	110.2	112.8	114.3	115.7	123.2	
15	3	110.1	112.8	114.2	116.2	123.8	
	4	108.3	111.8	113.7	115.5	126.3	
	1	112.3	115.4	116.3	117.6	123.5	
00	2	110.8	113.2	114.5	115.8	123.1	
20	3	111.2	114.0	115.1	116.7	124.3	
	4	109.6	112.4	113.7	115.5	124.0	
	1	113.1	116.1	117.4	119.0	125.1	
0.5	2	111.1	113.2	114.9	117.6	124.8	
25	3	111.9	114.5	115.7	118.1	124.5	
	4	109.9	112.3	113.9	116.5	127.9	
	1	113.6	115.9	117.1	118.0	123.9	
00	2	112.5	113.6	114.2	115.6	121.1	
30	3	112.2	114.7	115.5	116.5	121.7	
	4	111.1	112.6	113.8	115.1	122.4	
	1	114.1	116.3	117.2	118.2	123.5	
0.5	2	112.6	113.8	114.6	115.3	119.1	
35	3	113.1	115.1	115.6	116.1	119.0	
	4	111.2	112.7	114.1	115.1	120.4	
	1	115.1	116.7	118.0	118.3	119.3	
46	2	113.2	114.3	115.4	117.0	118.3	
40	3	113.9	115.3	116.2	117.9	119.0	
	4	112.1	113.5	114.7	116.0	118.9	

# **Appendix G. Propagation Loss Modelling Results**

## **G.1. Propagation Loss at Multiple Wind Speeds**

This section presents plots of the modelled propagation loss in decidecade bands, for the different modelled source depths, for increasing wind speeds between 0 and 40 kn.

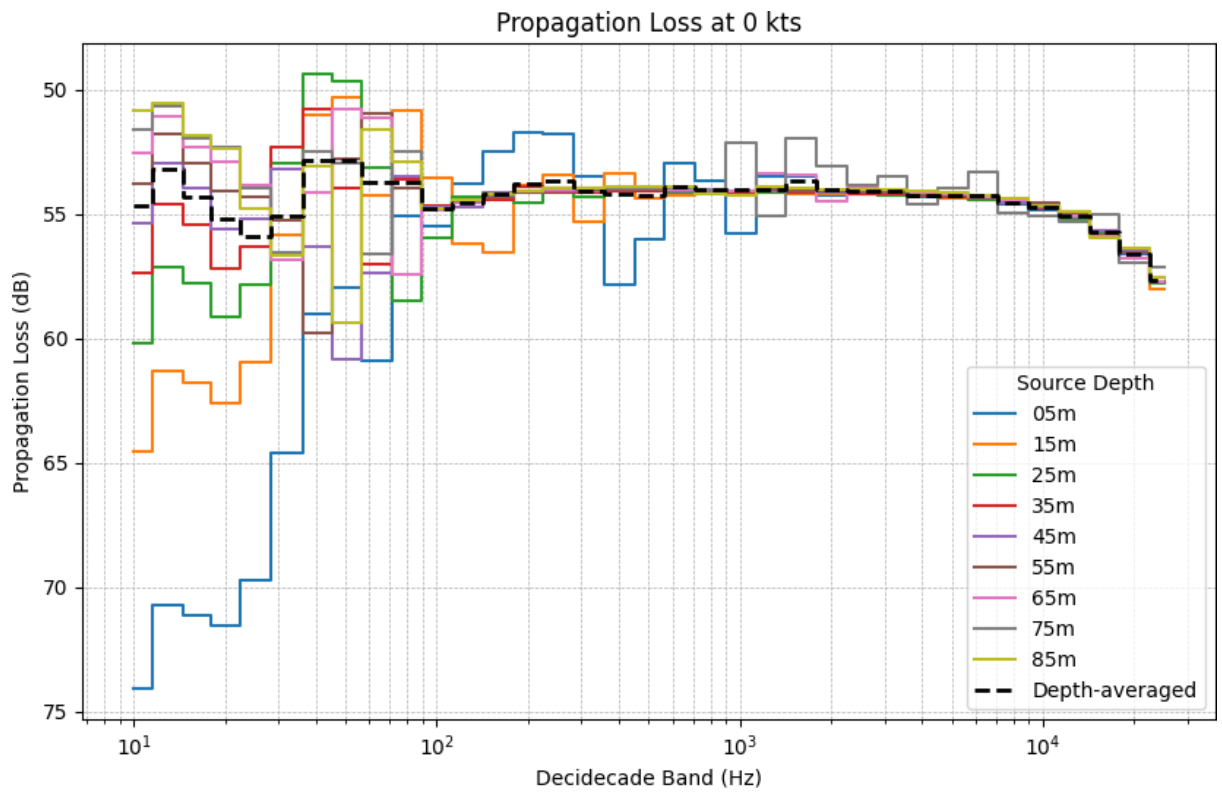


Figure G-1. Propagation loss in decidecade bands between HY06 and Station 1 for 0 knots wind speed.

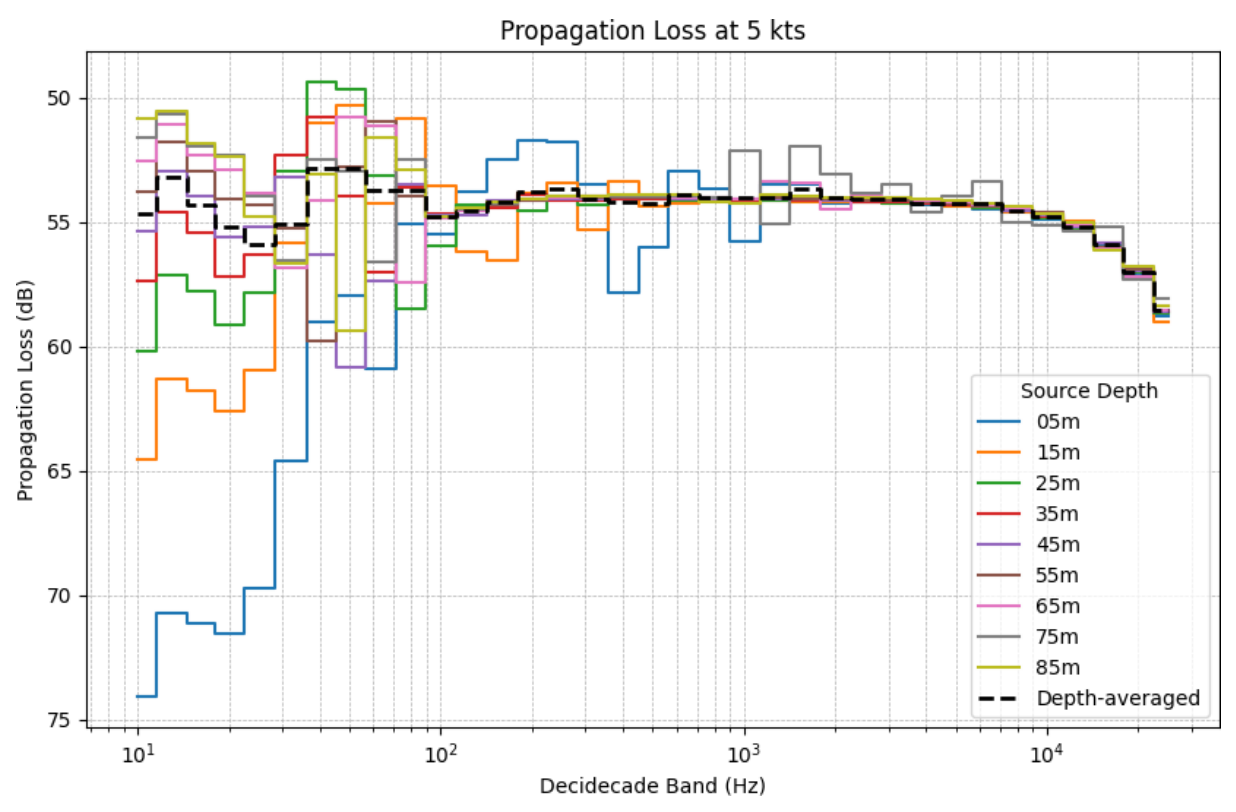


Figure G-2. Propagation loss in decidecade bands between HY06 and Station 1 for 5 knots wind speed.

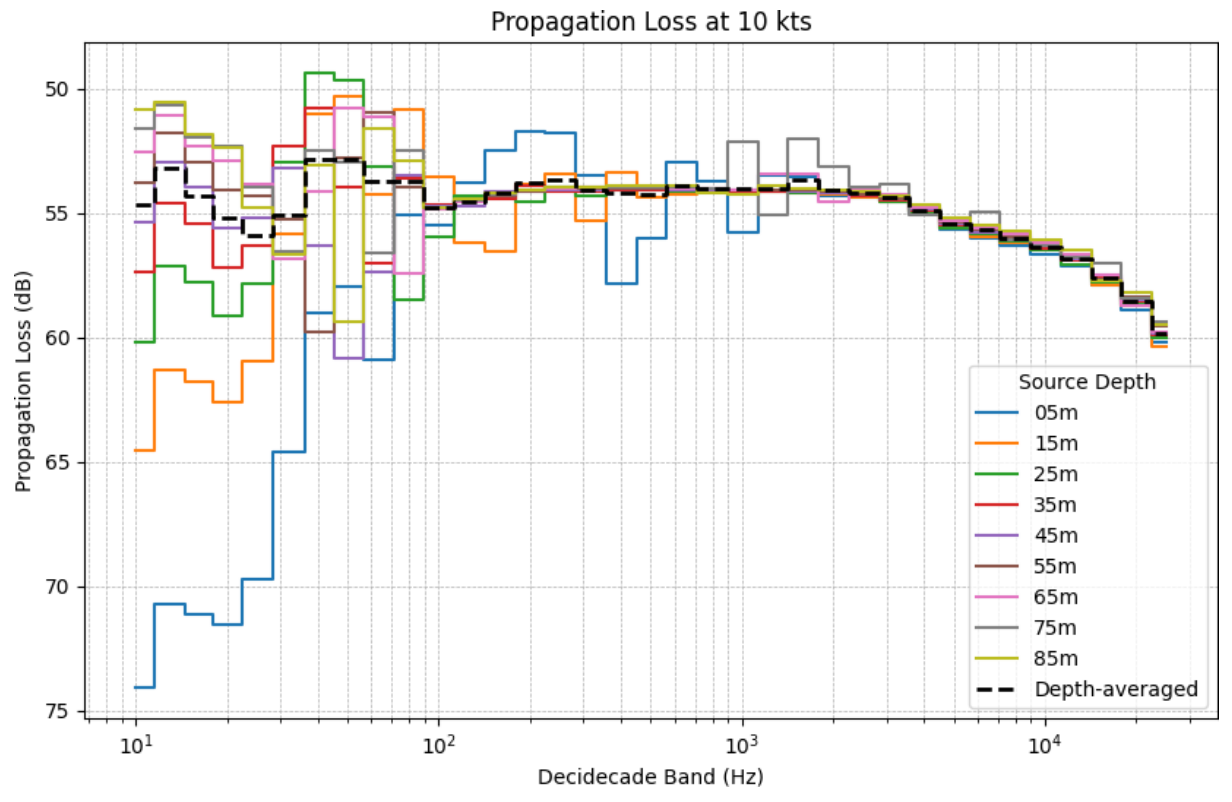


Figure G-3. Propagation loss in decidecade bands between HY06 and Station 1 for 10 knots wind speed.

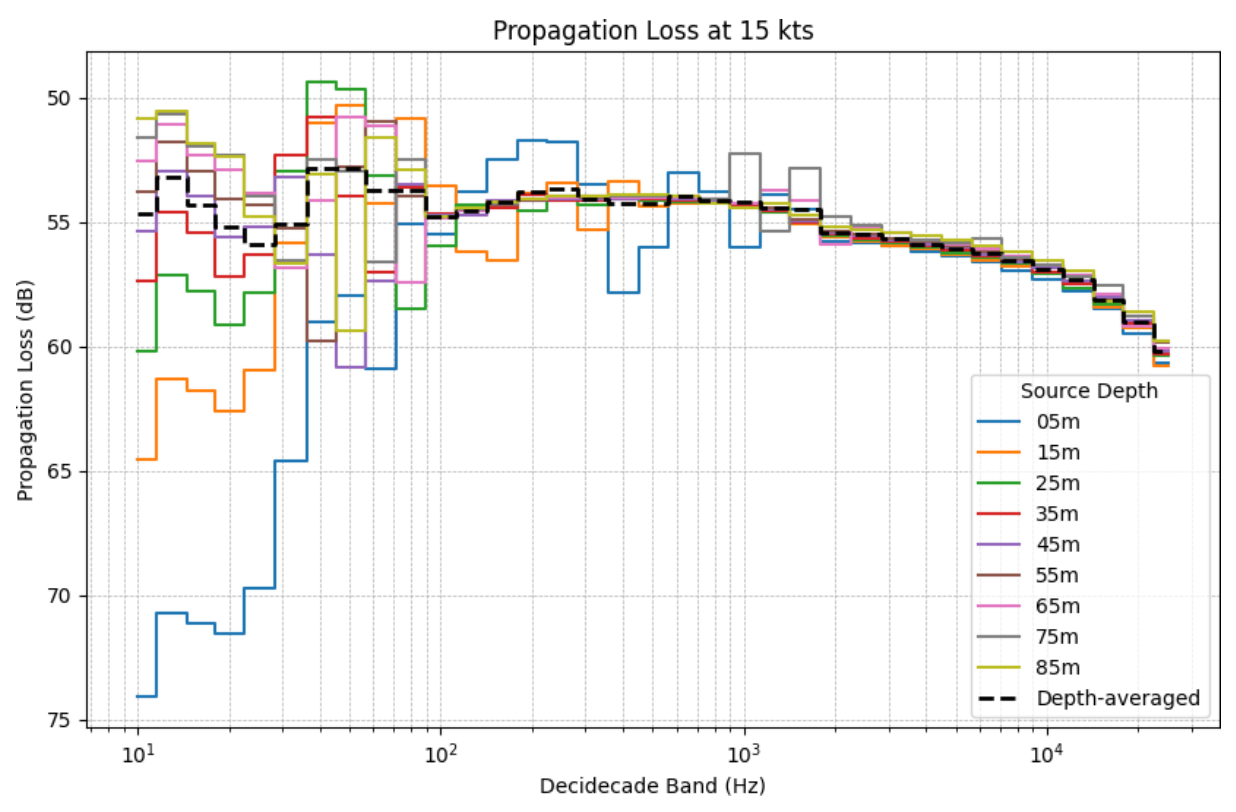


Figure G-4. Propagation loss in decidecade bands between HY06 and Station 1 for 15 knots wind speed.

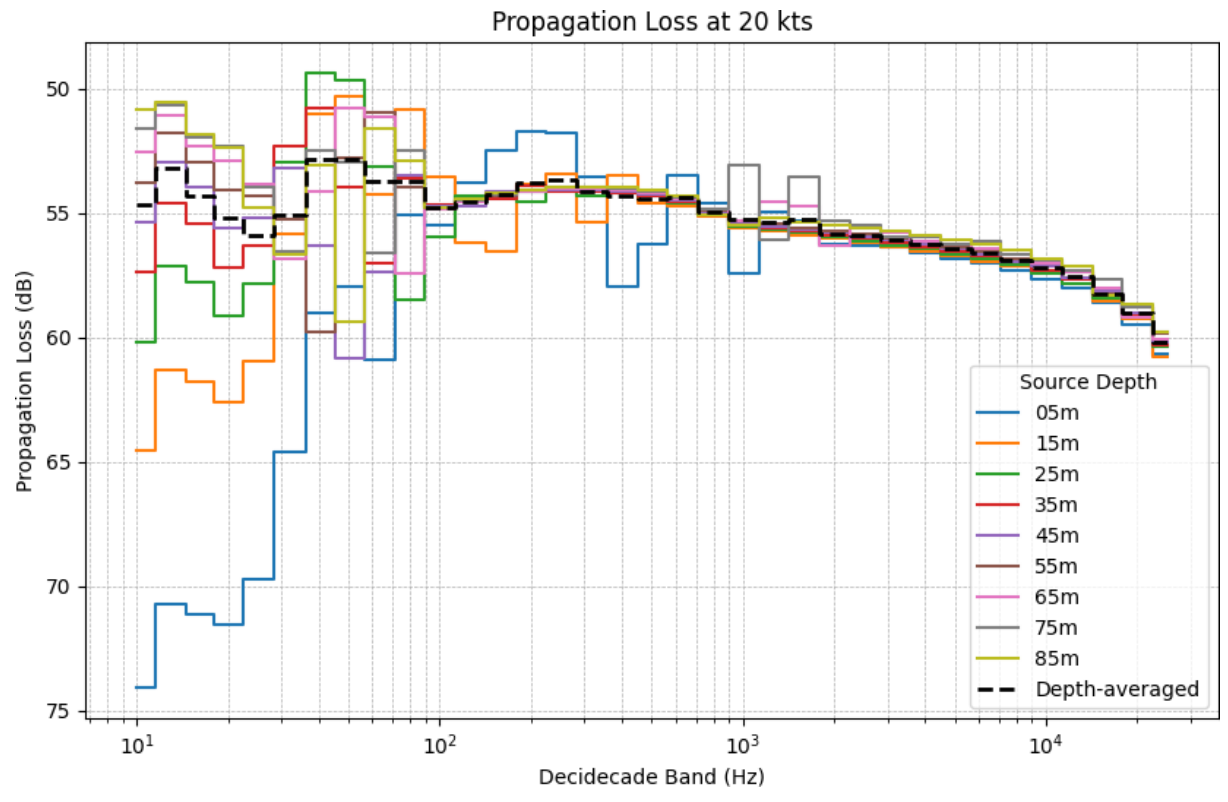


Figure G-5. Propagation loss in decidecade bands between HY06 and Station 1 for 20 knots wind speed.

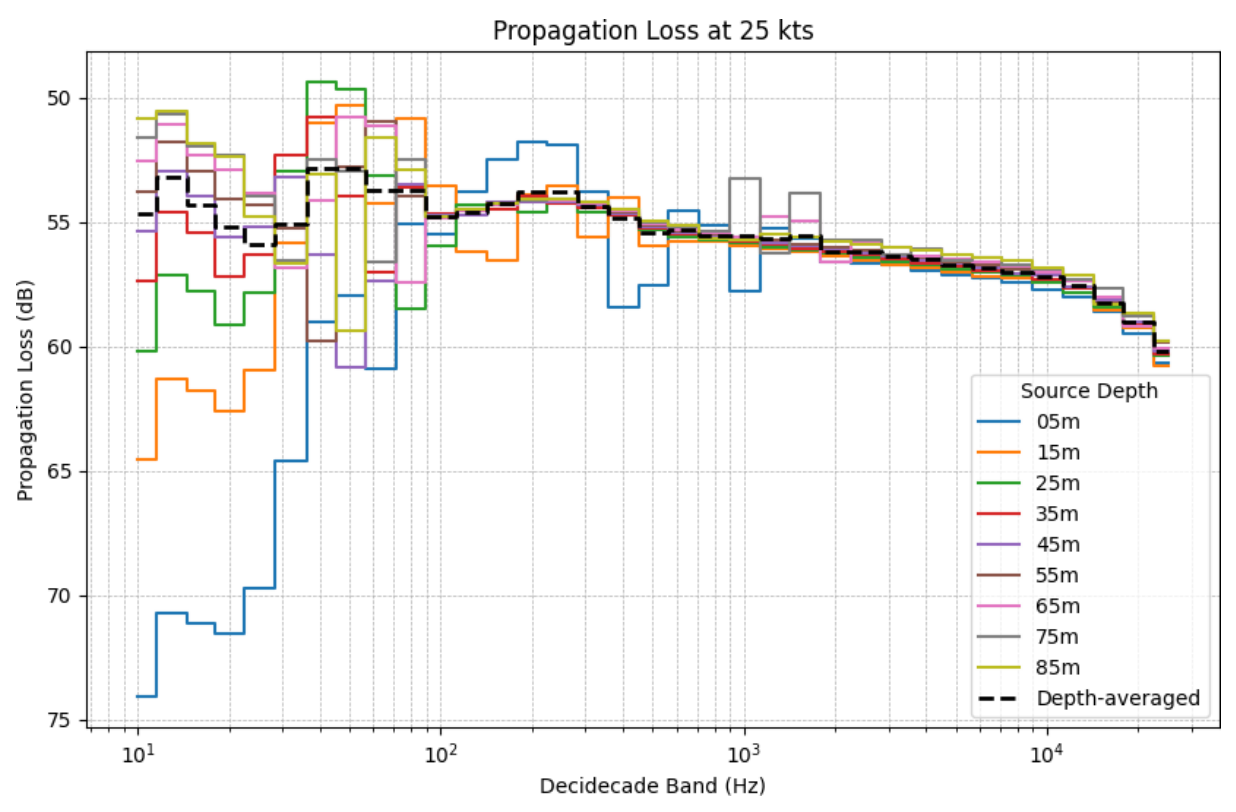


Figure G-6. Propagation loss in decidecade bands between HY06 and Station 1 for 25 knots wind speed.

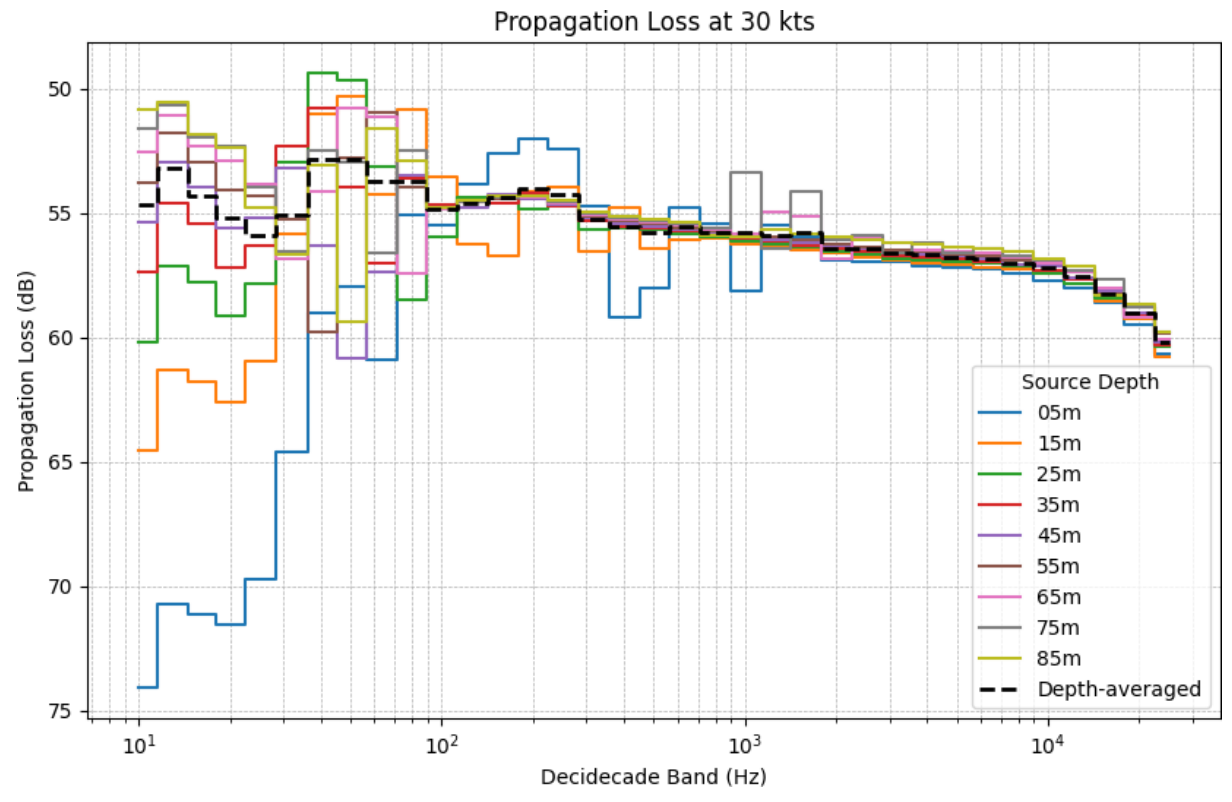


Figure G-7. Propagation loss in decidecade bands between HY06 and Station 1 for 30 knots wind speed.

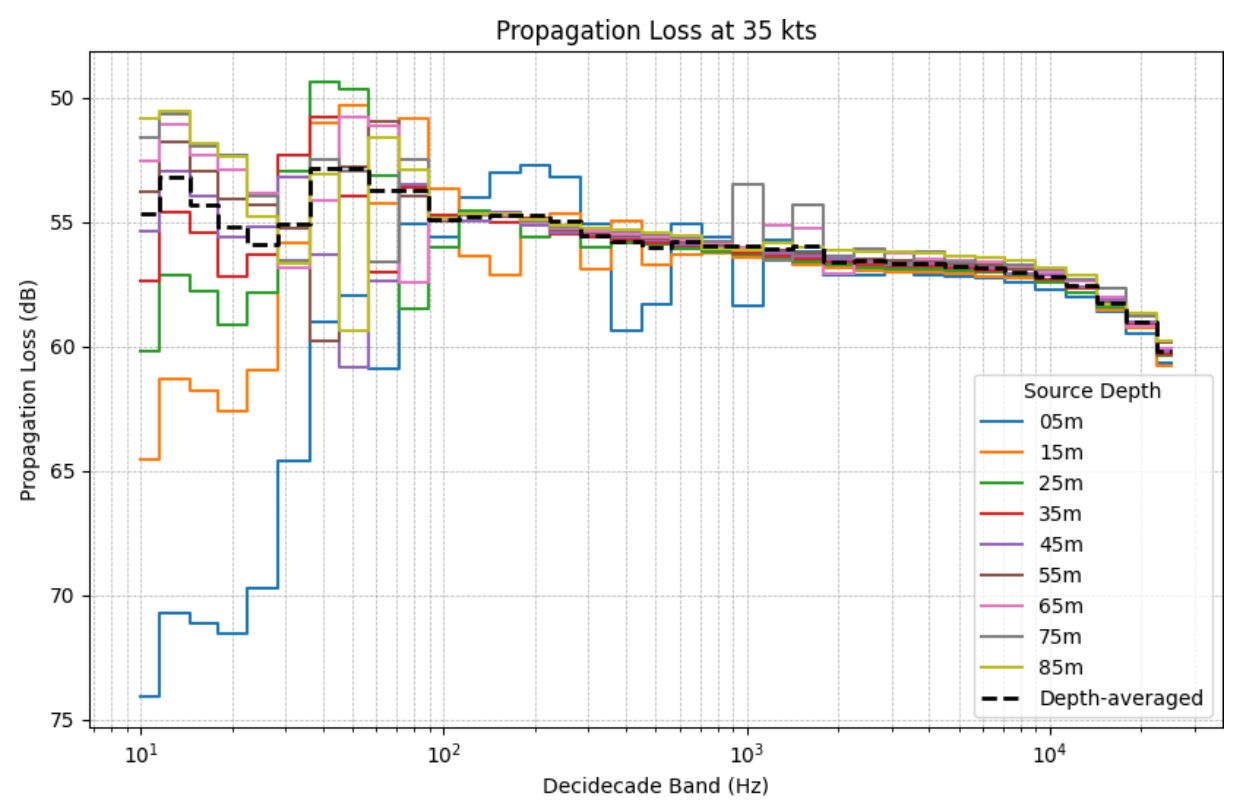


Figure G-8. Propagation loss in decidecade bands between HY06 and Station 1 for 35 knots wind speed.

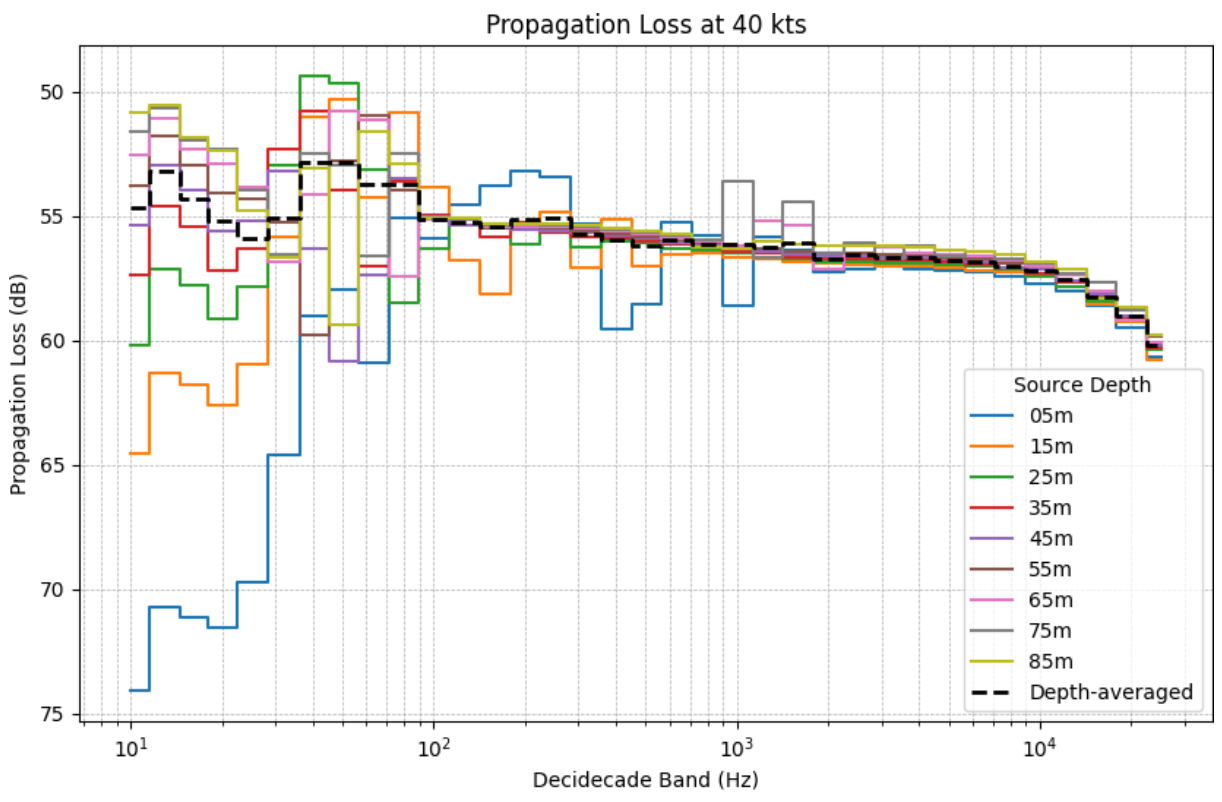


Figure G-9. Propagation loss in decidecade bands between HY06 and Station 1 for 40 knots wind speed.

# **Appendix H. Backpropagated Source Levels**

#### H.1. Modelled Percentile Source Levels

This section presents source levels calculated for increasing wind speeds as calculated by the methodology outlined in Section 4.

Table H-1. Backpropagated decidecade band source levels for a single turbine operating in 5 kn wind speed.

	Source Level (dB re 1 μPa²m²)					
Decidecade band			Percentile			
centre frequency (Hz)	5 th	25 th	50 th (median)	75 th	95 th	
10	129.8	132.9	134.8	136.4	138.0	
12	128.5	130.5	131.5	132.8	134.4	
15	130.4	132.0	133.2	133.7	135.2	
19	130.7	132.6	133.9	135.2	136.4	
25	139.0	145.5	150.9	153.2	155.4	
31	141.3	142.6	144.0	144.6	145.8	
39	138.1	139.2	139.9	140.7	142.1	
50	139.1	140.2	141.1	142.6	144.9	
63	144.3	145.7	146.5	147.1	148.1	
79	143.2	144.2	145.2	146.3	147.8	
100	145.1	147.1	148.2	149.7	151.1	
125	145.1	146.2	147.4	148.9	150.9	
158	143.9	145.3	146.0	148.0	149.6	
199	141.3	143.2	144.3	146.6	147.9	
251	137.8	139.8	140.8	143.2	145.0	
316	139.2	141.0	141.9	143.1	144.0	
398	137.9	138.4	139.2	140.2	141.7	
501	134.2	135.0	136.0	137.3	139.2	
630	133.9	134.7	135.4	136.1	137.8	
794	132.5	133.8	135.2	137.3	139.6	
1000	132.2	133.5	134.8	136.7	139.3	
1250	132.9	134.5	135.5	137.3	139.9	
1600	132.2	133.7	134.9	136.9	138.8	
2000	132.4	133.9	135.0	137.1	138.9	
2500	131.8	133.4	134.3	136.4	138.3	
3150	130.6	132.1	133.0	135.2	137.0	
4000	127.2	128.6	129.5	131.8	133.6	
5000	126.8	128.2	129.1	131.2	133.0	
6300	123.7	125.2	126.0	128.1	130.0	
8000	121.2	122.8	123.5	125.8	127.5	
10000	120.0	121.6	122.5	124.7	126.4	
12500	118.0	119.8	120.8	122.7	124.3	
16000	118.9	120.7	121.6	123.9	125.9	
20000	118.6	120.4	121.5	123.6	125.4	
25000	118.9	120.6	121.8	123.8	125.4	

Table H-2. Backpropagated decidecade band source levels for a single turbine operating in 10 kn wind speed.

	Source Level (dB re 1 µPa²m²)					
Decidecade band centre frequency			Percentile			
(Hz)	5 th	25 th	50 th (median)	75 th	95 th	
10	130.5	132.9	134.3	136.0	138.0	
12	131.1	134.8	136.6	139.2	142.1	
15	128.9	131.3	133.3	135.4	137.4	
19	131.0	133.9	135.7	137.4	141.2	
25	136.8	139.0	140.8	142.3	144.2	
31	133.3	137.1	140.6	144.5	150.3	
39	139.6	144.9	147.0	148.7	150.9	
50	138.0	139.7	141.1	143.3	147.8	
63	144.7	146.3	147.3	148.2	150.3	
79	144.1	145.3	146.3	148.6	151.6	
100	145.2	146.4	148.1	149.7	151.9	
125	146.1	147.5	149.7	151.6	153.0	
158	143.6	145.5	150.1	152.7	154.6	
199	143.4	145.8	148.9	151.2	154.9	
251	137.3	139.7	143.8	148.1	150.9	
316	137.4	140.0	144.6	148.0	150.2	
398	140.8	142.2	145.4	147.8	150.4	
501	135.4	138.5	141.1	146.1	148.6	
630	135.3	138.4	140.2	145.1	148.0	
794	132.5	134.7	137.3	142.4	146.0	
1000	130.3	132.8	135.4	141.4	145.6	
1250	126.6	132.2	135.0	140.2	143.7	
1600	124.1	129.7	132.8	138.5	143.0	
2000	123.8	129.1	132.8	138.3	142.9	
2500	124.7	129.9	133.7	138.1	142.9	
3150	123.8	128.7	132.5	136.7	141.3	
4000	121.5	126.5	129.9	134.7	139.7	
5000	120.0	125.3	129.5	134.0	139.8	
6300	118.3	123.4	127.7	131.2	135.8	
8000	115.6	120.3	124.3	127.4	132.8	
10000	113.0	117.7	122.1	125.5	130.7	
12500	110.8	115.8	120.6	123.8	128.0	
16000	112.3	117.5	122.2	125.3	128.8	
20000	112.0	117.1	122.0	125.1	128.5	
25000	112.2	117.2	122.0	125.2	128.5	

Table H-3. Backpropagated decidecade band source levels for a single turbine operating in 15 kn wind speed.

	Source Level (dB re 1 μPa²m²)						
Decidecade band centre frequency	Percentile						
(Hz)	5 th	25 th	50 th (median)	75 th	95 th		
10	129.7	132.2	134.0	135.6	137.0		
12	127.7	131.6	133.1	134.9	136.6		
15	130.6	132.6	134.0	134.9	136.5		
19	132.7	136.7	138.2	141.2	144.8		
25	133.0	135.1	136.6	138.1	139.8		
31	137.9	139.6	140.9	143.6	145.9		
39	139.8	141.2	141.9	142.6	143.8		
50	137.9	139.7	140.9	145.0	149.8		
63	141.6	145.1	146.1	146.9	148.4		
79	139.3	140.4	141.5	142.4	143.9		
100	142.4	143.8	144.6	145.9	146.8		
125	146.2	146.9	147.3	147.6	147.9		
158	147.3	147.6	147.9	148.2	148.6		
199	147.4	147.9	148.2	148.8	149.5		
251	141.7	143.3	144.5	146.6	147.4		
316	142.7	143.4	144.5	146.1	147.3		
398	140.1	140.7	142.0	144.9	145.9		
501	136.6	137.1	139.4	143.8	145.9		
630	138.0	138.7	139.6	140.6	142.0		
794	134.5	134.9	135.3	135.9	136.5		
1000	134.1	134.8	135.1	135.4	136.7		
1250	133.1	134.9	136.6	136.9	137.5		
1600	131.3	133.4	134.5	135.0	135.6		
2000	131.3	133.5	135.4	135.7	136.3		
2500	131.1	133.3	135.4	135.8	136.1		
3150	129.8	132.3	134.2	134.6	135.0		
4000	129.1	131.5	132.6	133.0	133.4		
5000	127.3	129.6	131.1	131.4	131.8		
6300	125.8	128.0	129.4	129.7	130.2		
8000	123.5	125.8	128.0	128.4	128.7		
10000	122.0	124.3	127.6	127.9	128.2		
12500	120.8	122.9	127.1	127.4	127.6		
16000	122.5	124.4	129.0	129.3	129.5		
20000	121.8	123.6	128.3	128.6	128.9		
25000	121.1	123.0	127.7	128.0	128.2		

Table H-4. Backpropagated decidecade band source levels for a single turbine operating in 20 kn wind speed.

	Source Level (dB re 1 µPa²m²)					
Decidecade band centre frequency			Percentile			
(Hz)	5 th	25 th	50 th (median)	75 th	95 th	
10	132.9	135.3	137.0	139.3	140.5	
12	129.4	135.0	137.9	139.7	143.1	
15	129.3	132.7	133.7	134.8	137.7	
19	129.9	133.1	134.6	138.1	143.3	
25	132.3	140.4	147.8	154.1	158.3	
31	135.8	137.6	138.8	141.5	151.7	
39	141.4	142.3	143.6	145.6	150.4	
50	144.9	146.4	147.4	150.1	152.7	
63	148.5	149.8	151.0	153.4	156.3	
79	152.4	154.4	155.7	157.7	159.5	
100	150.2	151.5	152.4	153.2	155.1	
125	151.1	152.3	153.4	154.3	156.4	
158	151.0	151.8	152.6	153.7	155.1	
199	149.7	150.7	151.6	152.3	153.7	
251	147.6	148.2	149.3	150.2	151.7	
316	146.3	147.0	147.7	148.7	150.4	
398	144.8	145.6	146.3	146.9	148.4	
501	141.2	142.1	142.8	143.4	144.6	
630	142.0	142.5	142.9	143.4	144.3	
794	139.8	140.3	140.7	141.2	143.3	
1000	139.2	139.8	140.3	140.6	142.2	
1250	139.0	139.8	140.3	140.5	141.8	
1600	138.1	138.8	139.3	139.7	140.9	
2000	138.4	139.2	139.7	140.0	141.2	
2500	138.1	138.8	139.3	139.7	140.8	
3150	137.0	137.8	138.2	138.7	139.9	
4000	135.6	136.3	136.8	137.2	138.5	
5000	134.4	135.1	135.6	136.1	137.4	
6300	132.4	133.2	133.8	134.2	135.7	
8000	131.1	132.1	132.6	132.9	134.5	
10000	130.6	131.5	132.1	132.4	134.0	
12500	129.9	130.8	131.5	131.8	133.3	
16000	131.7	132.6	133.2	133.5	135.1	
20000	130.7	131.5	132.1	132.5	134.0	
25000	129.8	130.7	131.2	131.6	133.2	

Table H-5. Backpropagated decidecade band source levels for a single turbine operating in 25 kn wind speed.

	Source Level (dB re 1 μPa²m²)					
Decidecade band centre frequency			Percentile			
(Hz)	5 th	25 th	50 th (median)	75 th	95 th	
10	151.1	154.9	157.4	159.7	162.3	
12	148.8	151.6	154.0	156.8	161.1	
15	148.2	151.2	153.7	155.8	159.3	
19	147.2	151.3	153.1	155.8	159.2	
25	151.8	154.2	155.9	157.4	160.4	
31	144.1	146.5	148.5	149.7	152.1	
39	142.6	144.5	146.0	147.0	148.7	
50	141.6	143.1	144.8	146.1	147.8	
63	143.2	144.6	145.5	146.5	148.5	
79	150.2	151.7	152.9	153.7	156.1	
100	146.2	147.4	148.3	149.2	150.8	
125	145.4	147.0	148.0	149.0	150.8	
158	147.4	148.3	149.1	150.0	151.9	
199	143.7	145.0	146.0	147.1	149.4	
251	141.9	143.6	144.8	146.0	147.6	
316	141.1	142.7	143.9	145.2	147.0	
398	140.4	141.7	142.8	144.0	146.2	
501	139.0	140.3	141.2	142.3	144.2	
630	138.2	139.1	140.0	141.2	143.4	
794	137.4	138.3	138.9	139.7	141.4	
1000	136.8	138.1	138.8	139.7	141.0	
1250	136.7	137.6	138.2	138.9	140.5	
1600	136.3	137.3	137.8	138.5	140.0	
2000	136.7	137.6	138.3	138.9	140.5	
2500	136.0	136.8	137.5	138.2	139.7	
3150	134.8	135.7	136.5	137.2	138.5	
4000	133.7	134.8	135.5	136.2	137.7	
5000	133.2	134.2	134.9	135.7	137.0	
6300	131.7	132.6	133.3	134.0	135.4	
8000	130.6	131.5	132.2	132.9	134.2	
10000	130.2	131.1	131.9	132.5	133.9	
12500	129.4	130.3	131.0	131.7	133.1	
16000	130.9	132.1	132.7	133.3	134.8	
20000	129.6	130.7	131.4	132.1	133.5	
25000	128.3	129.4	130.1	130.8	132.1	

Table H-6. Backpropagated decidecade band source levels for a single turbine operating in 30 kn wind speed.

	Source Level (dB re 1 μPa²m²)					
Decidecade band	Percentile					
centre frequency (Hz)	5 th	25 th	50 th (median)	75 th	95 th	
10	130.9	134.1	136.1	137.2	139.9	
12	123.1	131.1	134.8	137.0	140.3	
15	137.5	140.1	141.3	143.1	146.0	
19	134.5	136.2	137.7	139.1	141.2	
25	133.4	136.4	139.4	143.5	146.5	
31	142.8	144.6	145.8	147.0	149.9	
39	139.2	142.9	144.7	145.7	149.3	
50	142.7	146.6	148.1	149.5	152.9	
63	147.3	150.1	150.9	151.7	155.1	
79	153.1	153.8	154.6	155.3	157.0	
100	150.1	152.5	154.2	155.1	156.3	
125	150.0	152.6	153.5	154.5	155.5	
158	151.2	152.7	153.6	154.3	155.9	
199	149.6	150.6	151.4	152.7	154.8	
251	147.6	149.0	149.8	151.3	153.1	
316	147.3	148.9	149.9	150.8	152.8	
398	147.4	148.4	149.3	150.5	152.7	
501	146.2	147.7	148.7	149.8	152.2	
630	145.2	146.9	147.6	148.5	150.1	
794	141.2	143.2	144.0	145.9	148.3	
1000	140.5	141.8	142.9	144.1	146.5	
1250	140.1	141.7	142.7	143.8	146.4	
1600	139.2	140.7	141.9	142.9	145.3	
2000	139.5	141.1	142.3	143.3	145.7	
2500	138.6	140.1	141.4	142.3	144.7	
3150	137.3	138.8	140.1	141.0	143.3	
4000	136.6	138.0	139.3	140.2	142.3	
5000	136.0	137.4	138.7	139.6	141.6	
6300	134.4	135.9	137.3	138.1	140.1	
8000	133.3	134.7	136.0	136.9	138.9	
10000	132.9	134.3	135.7	136.6	138.4	
12500	132.2	133.5	134.8	135.6	137.6	
16000	133.7	135.1	136.3	137.3	139.2	
20000	132.3	133.4	134.6	135.7	137.7	
25000	130.5	131.7	132.9	134.0	136.1	

Table H-7. Backpropagated decidecade band source levels for a single turbine operating in 35 kn wind speed.

		Source Level (dB re 1 μPa²m²)		
Percentile				
5 th	25 th	50 th (median)	75 th	95 th
144.3	147.2	148.6	150.2	152.6
145.9	147.9	148.7	150.4	152.7
144.2	147.0	148.1	149.6	151.5
145.8	147.7	148.9	150.0	152.0
153.3	154.9	156.1	157.7	159.8
146.1	147.4	148.6	149.3	151.0
143.4	144.4	145.3	146.1	147.5
143.7	144.8	145.5	146.2	148.2
145.1	146.4	147.1	147.9	150.3
152.3	153.6	154.2	154.8	155.8
147.7	148.8	149.6	150.5	152.4
148.1	149.3	150.1	150.9	152.5
149.7	150.5	151.0	151.9	153.3
151.6	152.5	153.4	154.7	156.3
147.9	148.8	149.8	151.1	153.2
147.4	148.2	149.1	150.2	152.4
145.3	146.4	147.4	148.6	151.2
143.1	143.8	144.4	145.5	147.9
141.6	142.1	142.6	143.2	144.5
140.6	141.1	141.7	142.2	143.4
139.7	140.3	140.9	141.4	142.6
139.6	140.2	140.8	141.4	142.4
139.7	140.2	140.8	141.4	142.2
140.0	140.5	141.2	141.7	142.5
138.8	139.4	140.1	140.6	141.3
137.5	138.0	138.7	139.3	140.0
136.6	137.2	137.9	138.4	139.1
135.7	136.4	137.0	137.6	138.2
133.9	134.6	135.2	135.7	136.5
132.7	133.3	134.0	134.5	135.1
132.2	132.8	133.4	133.9	134.6
131.2	131.8	132.5	133.0	133.7
132.8	133.4	134.1	134.6	135.3
131.3	131.9	132.6	133.1	133.9
129.8	130.4	131.1	131.6	132.3
	144.3 145.9 144.2 145.8 153.3 146.1 143.4 143.7 145.1 152.3 147.7 148.1 149.7 151.6 147.9 147.4 145.3 143.1 141.6 139.7 139.6 139.7 140.0 138.8 137.5 136.6 135.7 132.2 131.2 132.8 131.3	144.3       147.2         145.9       147.9         144.2       147.0         145.8       147.7         153.3       154.9         146.1       147.4         143.4       144.4         143.7       144.8         145.1       146.4         152.3       153.6         147.7       148.8         148.1       149.3         149.7       150.5         151.6       152.5         147.9       148.8         147.4       148.2         145.3       146.4         143.1       143.8         141.6       142.1         140.6       141.1         139.7       140.3         139.6       140.2         139.7       140.2         140.0       140.5         138.8       139.4         137.5       138.0         136.6       137.2         135.7       136.4         132.7       133.3         132.2       132.8         131.2       131.8         132.8       133.4         131.3       131.9	5m         25m         (median)           144.3         147.2         148.6           145.9         147.9         148.7           144.2         147.0         148.1           145.8         147.7         148.9           153.3         154.9         156.1           146.1         147.4         148.6           143.4         144.4         145.3           143.7         144.8         145.5           145.1         146.4         147.1           152.3         153.6         154.2           147.7         148.8         149.6           148.1         149.3         150.1           149.7         150.5         151.0           151.6         152.5         153.4           147.9         148.8         149.8           147.4         148.2         149.1           145.3         146.4         147.4           143.1         143.8         144.4           141.3         143.8         144.4           141.6         142.1         142.6           140.6         141.1         141.7           139.7         140.2         140.8           1	5m         25m         (median)         75m           144.3         147.2         148.6         150.2           145.9         147.9         148.7         150.4           144.2         147.0         148.1         149.6           145.8         147.7         148.9         150.0           153.3         154.9         156.1         157.7           146.1         147.4         148.6         149.3           143.4         144.4         145.3         146.1           143.7         144.8         145.5         146.2           145.1         146.4         147.1         147.9           152.3         153.6         154.2         154.8           147.7         148.8         149.6         150.5           148.1         149.3         150.1         150.9           149.7         150.5         151.0         151.9           151.6         152.5         153.4         154.7           147.9         148.8         149.8         151.1           147.4         148.2         149.1         150.2           145.3         146.4         147.4         148.6           143.1         143.8<

Table H-8. Backpropagated decidecade band source levels for a single turbine operating in 40 kn wind speed.

	Source Level (dB re 1 μPa²m²)				
Decidecade band centre frequency	Percentile				
(Hz)	5 th	25 th	50 th (median)	75 th	95 th
10	142.2	143.1	144.6	145.6	147.6
12	136.8	143.6	146.0	147.7	148.9
15	139.0	141.4	142.5	143.3	145.2
19	139.8	141.7	142.8	144.0	145.6
25	137.6	141.2	143.8	145.4	148.0
31	142.3	143.6	144.8	145.7	147.5
39	144.1	144.9	145.8	146.8	149.5
50	142.7	143.6	144.3	145.2	146.1
63	145.8	146.9	147.6	148.6	149.8
79	156.3	157.6	158.5	159.3	160.4
100	145.2	146.5	147.4	147.9	149.0
125	147.5	148.7	149.6	150.2	151.1
158	148.9	149.6	150.1	150.8	151.9
199	146.4	146.9	148.1	148.9	150.0
251	144.8	146.2	147.2	147.9	149.4
316	145.4	146.5	147.2	148.0	149.2
398	144.9	145.5	146.4	146.9	147.3
501	144.3	144.9	145.5	146.0	147.2
630	141.7	142.2	142.4	142.8	143.7
794	141.3	141.6	141.8	142.1	142.7
1000	140.8	141.2	141.5	141.8	142.2
1250	140.9	141.2	141.5	141.8	142.2
1600	140.7	141.1	141.4	141.6	142.1
2000	141.5	141.8	142.1	142.4	142.8
2500	140.7	141.1	141.3	141.6	142.0
3150	139.9	140.4	140.6	140.9	141.4
4000	139.1	139.6	139.8	140.1	140.8
5000	137.3	137.9	138.1	138.6	139.3
6300	135.1	135.6	135.9	136.3	137.5
8000	133.3	133.7	134.0	134.5	135.7
10000	132.3	132.7	133.1	133.4	134.4
12500	131.0	131.5	131.7	132.1	132.6
16000	131.8	132.3	132.5	132.9	133.3
20000	129.9	130.4	130.6	131.1	131.5
25000	127.9	128.2	128.5	129.1	129.5

# **Appendix I. Hydrophone Technical Specifications**



#### GeoSpectrum Technologies Inc. Customizing Detection

#### M36-100

The M36-100 is a wide-band omni-directional hydrophone designed for marine observation. It comes with a pre-amplified output of 0 to 35 dB (selectable on order) with current or voltage signalling.



Characteristics	
Nominal Voltage Sensitivity (without preamp)	-200 dBV re 1 μPa @ 20°C
Size	7.8" length, 1.3" max OD
Depth Rating	2500 m
Storage and Operating Temperatures	-40 to +70°C
Acceleration Sensitivity	<1.5 mbar/g, in air, any axis
Labelling	Calibration parameters, serial number, date
Connector	MCBH-8M
Pre-Amplifier	
Preamp signalling	Current, single ended voltage or, differential voltage (selectable on order)
Gain	0 - 35 dB (selectable on order)
Input Voltage	6.8 VDC nominal 4.5 – 30 VDC operating range
Band Pass	5 Hz HPF, no LPF installed (unless otherwise specified)
IRN	<140 nV/√Hz @10 Hz <4 nV/√Hz @1 kHz
Current Draw	1.3 mA (at 6.8 VDC) 4.2 mA with current signalling preamp

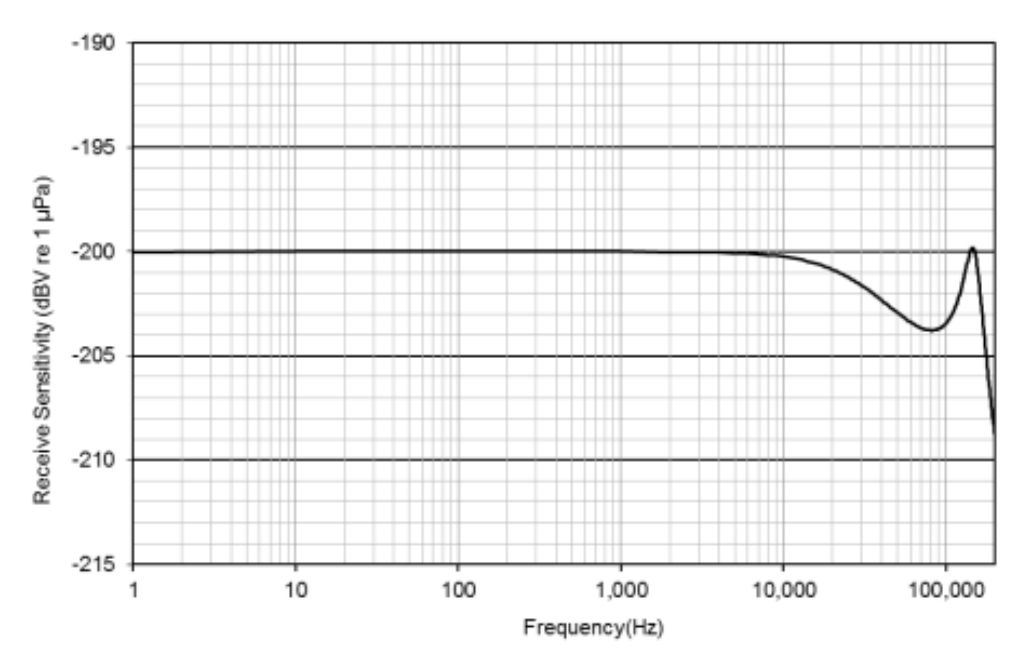
ADDRESS: 10 Akerley Blyd., Unit 19 Durtmouth, NS Canada B3B 134

M36-100-07-18-v4

Phone: 902.406.4111 Fax: 902.435.8987 website: www.geospectrum.ca e-mail: sales@geospectrum.ca



# GeoSpectrum Technologies Inc. Customizing Detection



M36 Frequency Response (without preamp)